Title

Control and Dynamic Manipulability of a Dual-Arm/Hand Robotic Exoskeleton System (EXO-UL8) for Rehabilitation Training in Virtual Reality

Author

Shen, Yang

Publication Date

2019

Peer reviewed|Thesis/dissertation

UNIVERSITY OF CALIFORNIA
Los Angeles

Control and Dynamic Manipulability of a Dual-Arm/Hand Robotic Exoskeleton System (EXO-UL8) for Rehabilitation Training in Virtual Reality

A dissertation submitted in partial satisfaction
of the requirements for the degree
Doctor of Philosophy in Mechanical Engineering

by

Yang Shen

2019

ABSTRACT OF THE DISSERTATION

Control and Dynamic Manipulability of a Dual-Arm/Hand Robotic Exoskeleton System (EXO-UL8) for Rehabilitation Training in Virtual Reality

by

Yang Shen
Doctor of Philosophy in Mechanical Engineering
University of California, Los Angeles, 2019
Professor Jacob Rosen, Chair

Every year there are about 800,000 new stroke patients in the US, and many of them suffer from upper limb neuromuscular disabilities including but not limited to: weakness, spasticity and abnormal synergy. Patients usually have the potential to rehabilitate (to some extent) based on neuroplasticity, and physical therapy intervention helps accelerate the recovery. However, many patients could not afford the expensive physical therapy after the onset of stroke, and miss the opportunity to get recovered. Robot-assisted rehabilitation thus might be the solution, with the following unparalleled advantages: (1) 24/7 capability of human arm gravity compensation; (2) multi-joint movement coordination/correction, which could not be easily done by human physical therapists; (3) dual-arm training, either coupled in joint space or task space; (4) quantitative platform for giving instructions, providing assistance, exerting resistance, and collecting real-time data in kinematics, dynamics and biomechanics; (5) potential training protocol personalization; etc.

However, in the rehabilitation robotics field, there are still many open problems. I am especially interested in: (1) compliant control, in high-dimensional multi-joint coordination condition; (2) assist-as-needed (AAN) control, in quantitative model-based approach and model-free approach; (3) dual-arm training, in both symmetric and asymmetric modes; (4) system integration, e.g., virtual reality (VR) serious games and graphical user interfaces (GUIs) design and development.

Our dual-arm/hand robotic exoskeleton system, EXO-UL8, is in its 4th generation, with seven

(7) arm degrees-of-freedom (DOFs) and one (1) DOF hand gripper enabling hand opening and closing on each side. While developing features on this research platform, I contributed to the robotics research field in the following aspects:

(1) I designed and developed a series of eighteen (18) serious VR games and GUIs that could be used for interactive post-stroke rehabilitation training. The VR environment, together with the exoskeleton robot, provides patients and physical therapists a quantitative rehabilitation training platform with capability in real-time human performance data collection and analysis.

(2) To provide better compliant control, my colleagues and I proposed and implemented two new admittance controllers, based on the work done by previous research group alumni. Both the hyper parameter-based and Kalman Filter-based admittance controllers have satisfactory heuristic performance, and the latter is more promising in future adaptation. Unlike many other upper-limb exoskeletons, our current system utilizes force and torque (F/T) sensors and position encoders only, no surface electromyography (sEMG) signals are used. It brings convenience to practical use, as well as technical challenges.

(3) To provide better AAN control, which is still not well understood in the academia, I worked out a redundant version of modified dynamic manipulability ellipsoid (DME) model to propose an Arm Postural Stability Index (APSI) to quantify the difficulty heterogeneity of the 3D Cartesian workspace. The theoretical framework could be used to teach the exoskeleton where and when to provide assistance, and to guide the virtual reality where to add new minimal challenges to stroke patients. To the best of my knowledge, it is also for the first time that human arm redundancy resolution was investigated when arm gravity is considered.

(4) For the first time, my colleagues and I have done a pilot study on asymmetric dual-arm training using the exoskeleton system on one (1) post-stroke patient. The exoskeleton on the healthy side could trigger assistance for that on the affected side, and validates that the current mechanism/control is eligible for asymmetric dual-arm training.

(5) Other works of mine include: activities of daily living (ADLs) data visualization for VR game difficulty design; human arm synergy modeling; dual-arm manipulation taxonomy classification (on-going work).

The dissertation of Yang Shen is approved.

Fabien Scalzo

Tsu-Chin Tsao

Tetsuya Iwasaki

Jacob Rosen, Committee Chair

University of California, Los Angeles

2019

To my grandfather, who reminds me of the "Philosophy" in this degree

To my parents, who encourage me to explore the unknowns

To my lady, who has the brightest smile in the world

TABLE OF CONTENTS

LIST OF FIGURES

LIST OF TABLES

ACKNOWLEDGMENTS

First of all, I would like to express my greatest gratitude to my Ph.D. research advisor, Prof. Jacob Rosen, who patiently educated me the philosophy and methodologies to be a good researcher. I much appreciate his guidance and advice over the past few years, as well as the opportunity working at his Bionics Lab to be exposed to many interesting and challenging research projects.

I would also like to thank the help from my committee, Prof. Tetsuya Iwasaki (MAE), Prof. Tsu-Chin Tsao (MAE), and Prof. Fabien Scalzo (CS), who are always accessible, polite and patient with my research inquiries. My thoughts on projects were much clearer after having discussions with them on dynamics analysis, controller design, and machine learning. I appreciate the comments/suggestions from Prof. Bruce Dobkin (Neurology), Dr. Clarisa Martinez (USC) and Prof. Carolee Winstein (USC). Special thanks to Mr. Fredrick Schwedner, who as a stroke patient, provided so many first-person feedback on the exoskeleton system. My memories are with my past committee member, Prof. Warren S. Grundfest (1952 – 2018), who attended my oral qualification exam and raised many inspiring questions. My best wishes to him, rest in peace.

I will always be grateful to Prof. Myron Hecht (MSOL), Prof. Eric Pei-Yu Chiou (MAE), Prof. Chih-Ming Ho (MAE), Prof. George Abe (Anderson), Prof. Lara Dolecek (EE), Prof. Hamed Mamani (U Washington), Prof. Les M. Lackman (MSOL), and Prof. Jenn-Ming Yang (MSOL), who generously gave me the opportunities to be a TA for their courses. Without financial support along with the teaching experience, I would never be able to finish my Ph.D. study.

I was fortunate to work with Dr. Ji Ma, Brando Dimapasoc, Aaron Feldman, Peter Walker Ferguson, Brandon Po-Yun Hsiao, Seungmin Jung, Jianwei Sun, and Haoran Wang. I learned a lot from them. Special thanks to my mentors: Prof. Qibing Pei, Dr. Eddie Shek and Ms. Ning Ning Yu, who really care about my career development and show me a bigger world.

My family has always been the utmost supportive to me, I appreciate the selfless love and support from my parents and grandparents. I love you.

Lastly, I want to thank my lady, Ms. Jiayi Li, who is always elegant, smart, supportive and inspiring. Without her love, I may struggle to find directions. I love you.

VITA

2013	B.S. in Mechanical Engineering and Automation (Dual-Bachelor with HKU), Outstanding Graduate, Shanghai Jiao Tong University.
2013	B.Eng. (Hons) in Mechanical Engineering (Dual-Bachelor with SJTU), First Class Honor, The University of Hong Kong.
2013 - 2019	Ph.D. Student in Mechanical Engineering, UCLA.
2013 - 2019	Research/Teaching Assistant, Department of Mechanical and Aerospace Engineering & Master of Science Online Program, UCLA.
Summer 2018	Robotics Software Engineering Intern, Seismic Inc. aka SuperFlex @ SRI International, Menlo Park, CA.

PUBLICATIONS

[1] (In Press) **Shen, Y.**, Rosen, J. “*EXO-UL Upper Limb Exoskeleton Series: A Four-Generation Review*” in “*Wearable Robotics: Systems and Applications*” (Rosen, J., ed.), Academic Press, 11/2019

[2] (In Press) **Shen, Y.**, Ferguson, P. W., Rosen, J. “*Upper Limb Exoskeletons: Assistive, Rehabilitation, and Industry*” in “*Wearable Robotics: Systems and Applications*” (Rosen, J., ed.), Academic Press, 11/2019

[3] (Oral Presentation) **Shen, Y.**, Sun, J., Ma, J., Rosen, J. “*Admittance Control Scheme Comparison of EXO-UL8: A Dual-Arm Exoskeleton Robotic System*”, 2019 IEEE-RAS-EMBS International Conference on Rehabilitation Robotics (ICORR), Toronto, Canada, 2019

[4] Ferguson, P. W., Dimaposac, B., **Shen, Y.**, Rosen, J. "*Design of a Hand Exoskeleton for Use with Upper Limb Exoskeletons*", 2018 International Symposium on Wearable Robotics and Rehabilitation (WeRob), Pisa, Italy, 2018

[5] **Shen, Y.**, Ma, J., Dobkin, B., Rosen, J. "*Asymmetric Dual Arm Approach for Post Stroke Recovery of Motor Functions Utilizing the EXO-UL8 Exoskeleton System: A Pilot Study*", 40^{th} Annual International Conference of the IEEE Engineering in Medicine and Biology Society (EMBC), Honolulu, HI, USA, 2018

[6] **Shen, Y.**, Ferguson, P. W., Ma, J., Rosen, J. "*Chapter 4 - Upper Limb Wearable Exoskeleton Systems for Rehabilitation: State of the Art Review and a Case Study of the EXO-UL8 Dual-Arm Exoskeleton System*" in "*Wearable Technology in Medicine and Healthcare*" (Tong, R. K.-Y., ed.), Academic Press, 07/2018

[7] **Shen, Y.**, Hsiao, B. P., Ma, J., Rosen, J. "*Upper Limb Redundancy Resolution Under Gravitational Loading Conditions: Arm Postural Stability Index Based on Dynamic Manipulability Analysis*", 17^{th} IEEE-RAS International Conference on Humanoid Robots (HUMANOIDS), Birmingham, UK, 2017

[8] Feldman, A., **Shen, Y.**, Rosen, J. "*Modeling of Joint Synergy and Spasticity in Stroke Patients to Solve Arm Reach Tasks*", IEEE Signal Processing in Medicine and Biology Symposium (SPMB), Philadelphia, PA, USA, 2017

CHAPTER 1

Introduction

Note: Part of this chapter is adapted from the book chapters:

(In Press) **Shen, Y.**, Ferguson, P. W., Rosen, J. "*Upper Limb Exoskeletons: Assistive, Rehabilitation, and Industry*" in "*Wearable Robotics: Systems and Applications*" (Rosen, J., ed.), Academic Press, 11/2019

Shen, Y., Ferguson, P. W., Ma, J., Rosen, J. "*Chapter 4 - Upper Limb Wearable Exoskeleton Systems for Rehabilitation: State of the Art Review and a Case Study of the EXO-UL8 Dual-Arm Exoskeleton System*" in "*Wearable Technology in Medicine and Healthcare*" (Tong, R. K.-Y., ed.), Academic Press, 07/2018

1.1 Stroke and Neuroplasticity

Stroke is one of the leading causes that leave disabilities on its survivors. Every year there are approximately 800,000 new stroke patients in the US with many of them suffering from various disabilities [BBC17]. As a result of brain lesions, stroke victims often lose part of upper-limb motor capabilities, such as the ability to lift their arms up [LBK11], spasticity, and abnormal synergy. Patients usually have the potential to rehabilitate (to some extent) based on neuroplasticity, and physical therapy intervention helps accelerate the recovery.

1.2 Post-Stroke Training

After a stroke, over 50% of persons have mild to severe weakness of the affected upper extremity that is managed by physical therapies to try to improve skillful arm and hand movements, strength, speed, and coordination [BBC17, Dob05]. Automating rehabilitation training for the affected upper extremity by employing robotic systems has been proposed to increase the number of repetitions of exercise with more normal kinematics [KSA08, BWP08, NGR09, NTU14, ROS15]. For decades, engineers and physical therapists have been developing robots to automate the post-stroke training process, resulting in a shift in research trend from low-dimensional, end-effector style "*manipulanda*" to high-dimensional, fully-covered "*exoskeletons*", which can simultaneously manipulate the multiple degrees-of-freedom (DOFs) of the human arm as well as provide additional features, such as tunnel-like force fields and gravity compensation [LX12]. Figure 1.1 shows the global strategies for rehabilitation training and current implementations on exoskeletons.

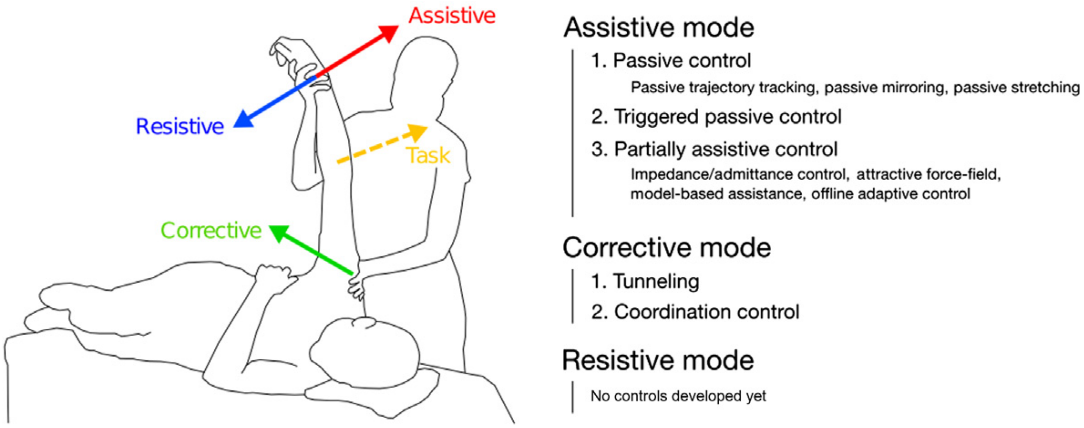

Figure 1.1: Global strategies for robotic-mediated rehabilitation and current implementations on exoskeletons [PCR16].

The devices are often categorized by the number of degrees-of-freedom (DOFs), either active or passive.

1.3 Review: Upper-Limb Robotic Devices for Rehabilitation

During the physical human-robot interaction, exoskeleton systems are at a very special position. Unlike the serial robotic manipulators which interact with human operators at the end-effector, exoskeleton covers the human limb in one or more joints, and synchronically moves with human's joint. This design, on the one hand, enables more application potentials, like strength augmentation, movement correction like an orthosis, or natural teleoperation, on the other hand, brings challenges in mechanism design, manufacturing, and control algorithms development, which require a deep understanding of human anatomy, motor control, biomechanics, etc.

To clarify, there exists a considerable difference between exoskeleton techniques in the upper limb and lower limb applications, based on the motivation as well as the technical difficulties. The authors focus on the upper limb and hand exoskeletons in this chapter, and provide an overview of their applications in assistive, rehabilitation, and industry. This study works as a review of state-of-the-art techniques and development on upper limb exoskeleton-like devices excluding systems worn on the trunk (e.g., spine injury prevention exoskeletons).

Exoskeletons have been developed for a couple of years. Originally as military applications for soldier capabilities augmentation, the exoskeleton focus more on providing assistance; later on more applications on rehabilitation which requires better human-in-the-loop understanding like intention detection and motion control, this branched out as the majority of rehabilitative robotics; since the human labor cost increases in the labor-intensive industries like automobile, manufacturers also would like to reduce the injuries due to moving heavy stuff, application of exoskeleton further expands to industrial application. All in all, the exoskeleton has a trend of need for active systems/inadequacy of purely passive systems. The rest of the chapter would be divided into the following parts: design; control; applications (assistive, rehabilitation, industrial, others); related research. Exoskeletons with design only are excluded, for example: 6-Rexos [GGJ15].

The MIT-MANUS (Hogan et al. [HKC92], 1992; Krebs et al., 2004; [CKV05]; Dipietro et al., 2007), commercialized as the InMotionArm (Interactive Motion Technologies, Inc., Cambridge, MA, United States), is a direct-drive five bar-linkage SCARA robot. The robot is attached to the patient's forearm and produces horizontal planar translations. Additional attachments have been developed to enable active control of forearm pronation/supination, wrist flexion/extension, and wrist abduction/adduction. The system is used with robotic therapy games to motivate and coordinate therapeutic tasks, a strategy adopted by the majority of upper limb robotic rehabilitation systems.

The upper limb motion assist system developed by AIST [HHA98] and NeReBot [RGM05] maneuvers the patient's arm by changing the lengths of three cables suspending orthoses/splints worn by the patient. The upper limb mobile assist system by AIST consists of two such orthoses placed on the forearm near the elbow and the wrist. By changing the positions of both orthoses, two rotations and three translations of the forearm can be controlled. The NeReBot is a cable-driven robot featuring a single splint attached to the entire forearm actuated by three motors.

The GENTLE/s [LAT03] and ACT3D [ESM09] both feature a HapticMaster robot [LL03] connected with a forearm orthosis. The HapticMaster enables each device three active translational degrees of freedom (DOFs) of the forearm. The GENTLE/s system also features a passive elbow orthosis suspended from above by cables for gravity compensation. The ACT3D provides adjustable active gravity compensation.

The iPAM system [CJM10] features two rigid 3D robot arms connected to the patient at the upper arm and wrist. The system can therefore actively control the positions of upper arm and forearm, but both connection points passively permit all orientation DOFs.

Bi-Manu-Track [HSK03], MIME [BLS00], and KINARM [CAD10] are dual-arm robotic systems and are thus capable of bimanual therapy, a desirable feature that is not achievable with a single- arm system. Bi-Manu-Track is a portable reconfigurable device limited to one active and one passive DOF between forearm pronation/supination and wrist flexion/extension. MIME consists of 6-DOF Puma-560 robots and position digitizers attached at each forearm. KINARM is a planar device that mechanically supports the weight of the arm while actuating two-DOF horizontal motions.

An additional notable class of rehabilitation robot that can be used for the upper limbs is the dynamometer. Dynamometers such as: Biodex System 4 Pro [1] and the HUMAC NORM [2] feature a single motor that can be repositioned and connected to various attachments to target specific motions.

End-effector robots have been shown to be effective in rehabilitation, and several have even found commercial success. However, these robots suffer from several critical limitations.

End-effector robots typically have significantly reduced ranges of motion when compared to

---

[1] http://www.biodex.com/physical-medicine/products/dynamometers/system-4-pro

[2] http://www.csmisolutions.com/products/isokinetic-extremity-systems/humac-norm

the human arm. For the workspace of an end-effector robot to encompass the workspace of the human arm, the robot must be very large because the base of the robot must be outside of the reach of the arm to prevent collisions. In addition, the robot would need to reach each part of the workspace of the human arm without physically overlapping with the user.

End effectors move individual points of the human arm. The human arm is a redundant manipulator with seven DOFs, so controlling position and/or orientation of a point on the arm does not control the configuration of the entire arm. Consequently, it is challenging for an end-effector rehabilitation robot to target a specific joint motion for therapy. To the best of the authors' knowledge, there is no end-effector rehabilitation robot that can determine and control all of the DOFs of the human arm.

To circumvent these and other limitations, a large number of upper limb exoskeleton robots have been developed. Upper limb exoskeletons are structured in an anthropometric fashion that supports the partial/full range of motion of the human arm. They are designed to be worn by the user, and are attached at multiple locations. Although this can significantly complicate the design of the robot, it enables much larger ranges of motion and the ability to target specific joint motions for therapy. Exoskeletons can broadly be categorized by application, number of DOFs, and whether the exoskeleton is worn on one or both arms.

The SARCOS Master Arm [MMS05, McM10] and SAM [LAV08, RSD14] are single-arm exoskeletons designed for teleoperation. The Sarcos Master Arm and SAM have the seven main DOFs of the human arm: shoulder flexion/extension, shoulder abduction/adduction, shoulder internal/ external rotation, elbow flexion/extension, forearm pronation/supination, wrist flexion/ extension, and wrist abduction/adduction. SAM is a wearable portable system, weighing just 7 kg.

MULOS [JCP01] uses cable transmissions at the shoulder joints, a bevel gearbox at the elbow, and a timing belt at the forearm. SUEFUL-7 [GKL09] features offset centers of rotation at the wrist to match the slightly offset joint axes of the wrist and a moving center of rotation at the shoulder joint to more accurately match movements of the shoulder. These systems are designed to provide assistance with ADLs.

L-Exos [FRM05, FBB08, MFA05] has a passive forearm DOF, but an attachment makes it active and adds two hand DOFs (thumb and forefinger). L-Exos can apply a 100 N force on the palm in any direction enabling its use as a haptic feedback device for virtual reality (VR). BONES [KSA08, MSC13, WCR08] uses a parallel mechanism for a spherical joint at the shoulder and a serially placed actuator for the elbow DOF. An attachment can add the forearm DOF and wrist flexion/extension. ABLE [GFM08] features screw-and-cable transmission systems that enable the motor to be placed along the limb parallel to the cable. This permits ABLE to have a highly compact design compared to systems with transversal motors or beveled gearboxes.

In order to account for the human shoulder not being a perfect spherical joint, several exoskeletons have been designed with additional or offset shoulder DOFs. ARMin III [NGR09] couples the shoulder elevation angle with a vertical translation of the shoulder, and has an attachable active forearm pronation/supination and wrist flexion/extension module. MGA [CTR09] has an extra vertical translation shoulder DOF. IntelliArm [RPZ09, ZPR07] has not only the added active vertical translation and but also two passive horizontal translation shoulder DOFs. MEDARM [BBS07] replaces the standard three-DOF shoulder mechanism with two rotational DOFs at the sternoclavicular joint and three rotational DOFs at the glenohumeral joint. Exorn [MKB13, MB13] is a portable exoskeleton designed to have all the DOFs of the human arm including two at the shoulder girdle and four at the glenohumeral joint.

SRE [KTC06] is a seven-DOF rehabilitation exoskeleton that has a singularity when the arm is parallel to the ground due to the shoulder joint design. RUPERT IV [WBX08, BWP08] is a five-DOF portable exoskeleton. RehaBot [HLD11] is a commercially developed upper limb exoskeleton that is part of a larger rehabilitation system. ETS-MARSE [ROS15] is a rehabilitation exoskeleton designed for use with electromyography (EMG)-based control.

The earlier single-arm exoskeletons feature a wide range of designs with varying complexities targeting various joints. However, single-arm exoskeletons are inherently incapable of performing tasks requiring coordination between both arms. More importantly, bilateral movement training has been shown to be more effective in specific aspects of stroke rehabilitation than unilateral movement training [KMF13]. To perform bilateral actions, it is therefore necessary to use a dual-arm exoskeleton. Due in part to the complexity of dual- arm systems, they tend to be more recently developed, and there are far fewer, compared to single-arm exoskeletons.

EMY [MVA15] is a dual-arm exoskeleton with active DOFs of shoulder internal/external rotation, shoulder flexion/extension, elbow flexion/extension, and forearm pronation/ supination. It features the same screw-cable-system for actuation that ABLE uses. The forearm DOF is achieved by a parallel structure of three rods on ball-joints connecting a rotating arch to a fixed arch. EMY is designed specifically for the evaluation of Brain Machine Interface.

CAPIO [MWT15] is a dual-arm exoskeleton with 20 active DOFs, including four on the back and an extra translational DOF at each elbow. CAPIO uses serial elastic actuators and is designed for use as a haptic feedback device and teleoperation.

The modular upper limb portion of the full-body Recupera-Reha [KWS16] system is a recent dual-arm exoskeleton designed for stroke rehabilitation. It has six active DOFs, including one for hand grasp, and one passive DOF for wrist flexion/extension for each arm. The shoulder mechanism uses brushless DC motors, while the elbow and forearm DOFs are actuated by two different custom serial elastic actuators.

The following figures provide overviews of robotic rehabilitative devices from different views. Figure 1.2 is a chronological overview of upper-limb exoskeleton systems, categorized in control approaches; similarly, Figure 1.3 also provides an overview of upper-limb exoskeleton systems, categorized in control approaches, but in the number of active DOFs. It is interesting to notice that there are no upper-limb exoskeleton systems developed in nine (9) active DOFs. Figure 1.4 provides an overview of hand exoskeleton systems.

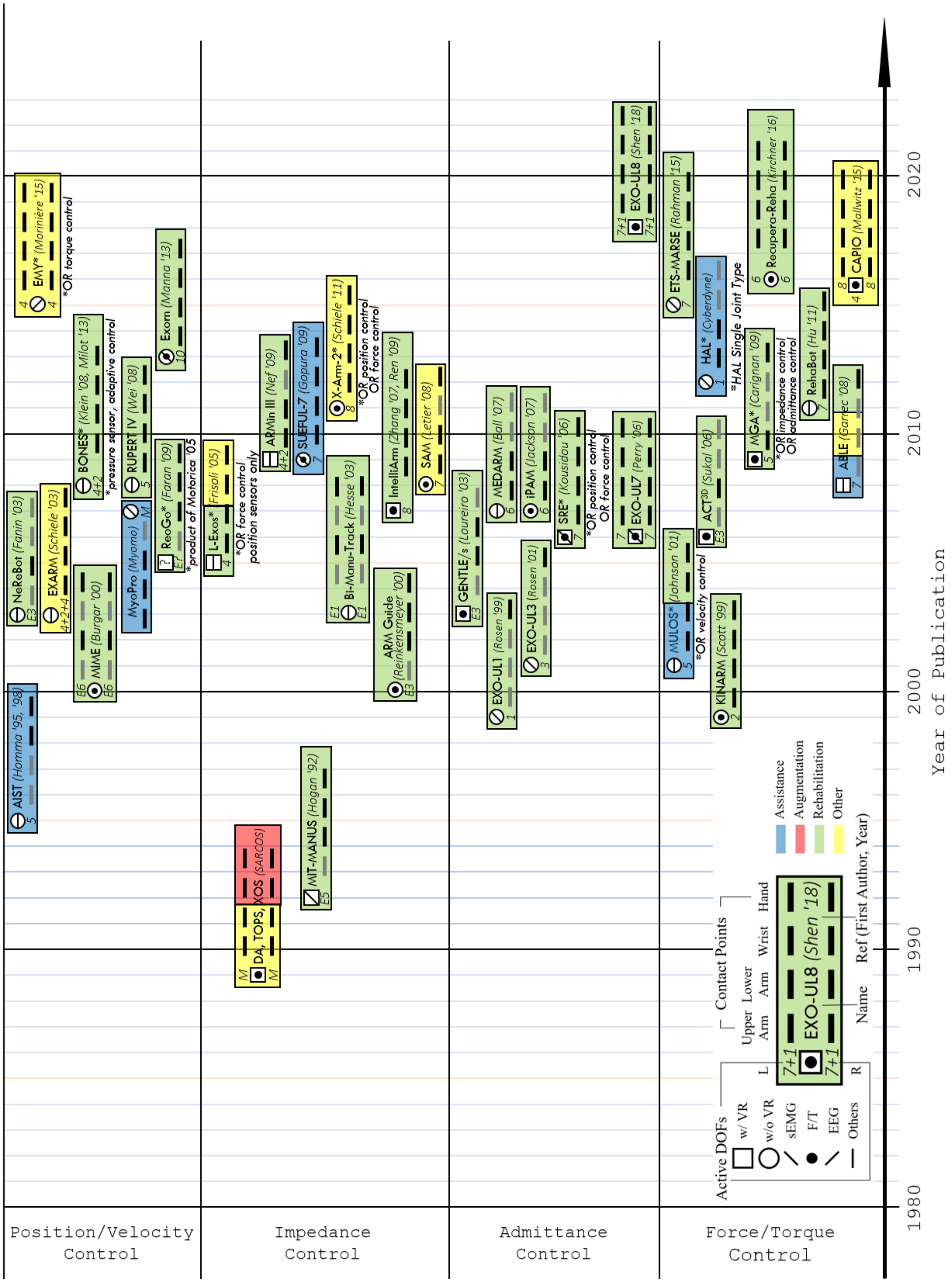

Figure 1.2: A chronological overview of existing upper-limb exoskeleton systems.

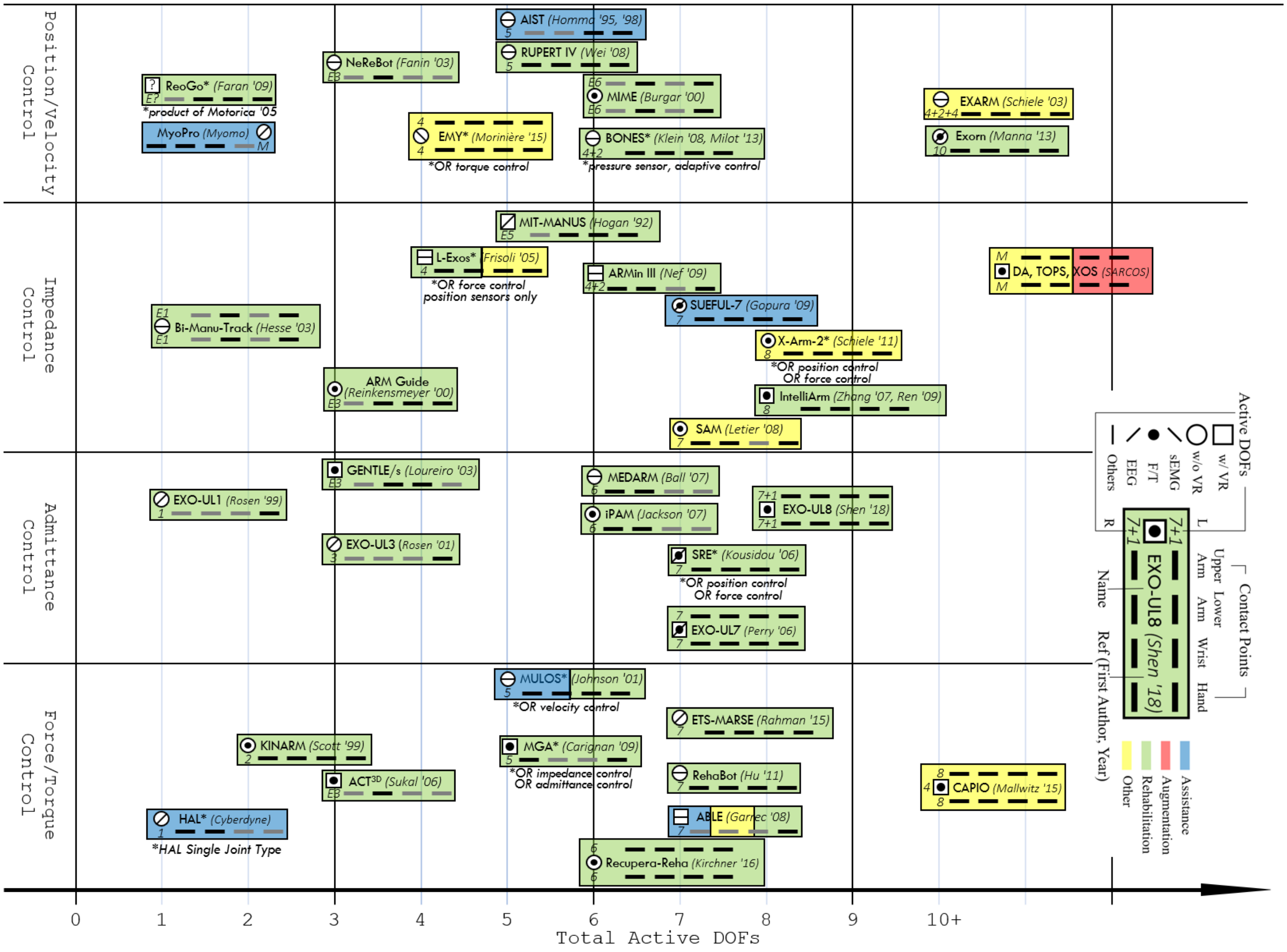

Figure 1.3: An overview of existing upper-limb exoskeleton systems based on the number of active DOFs.

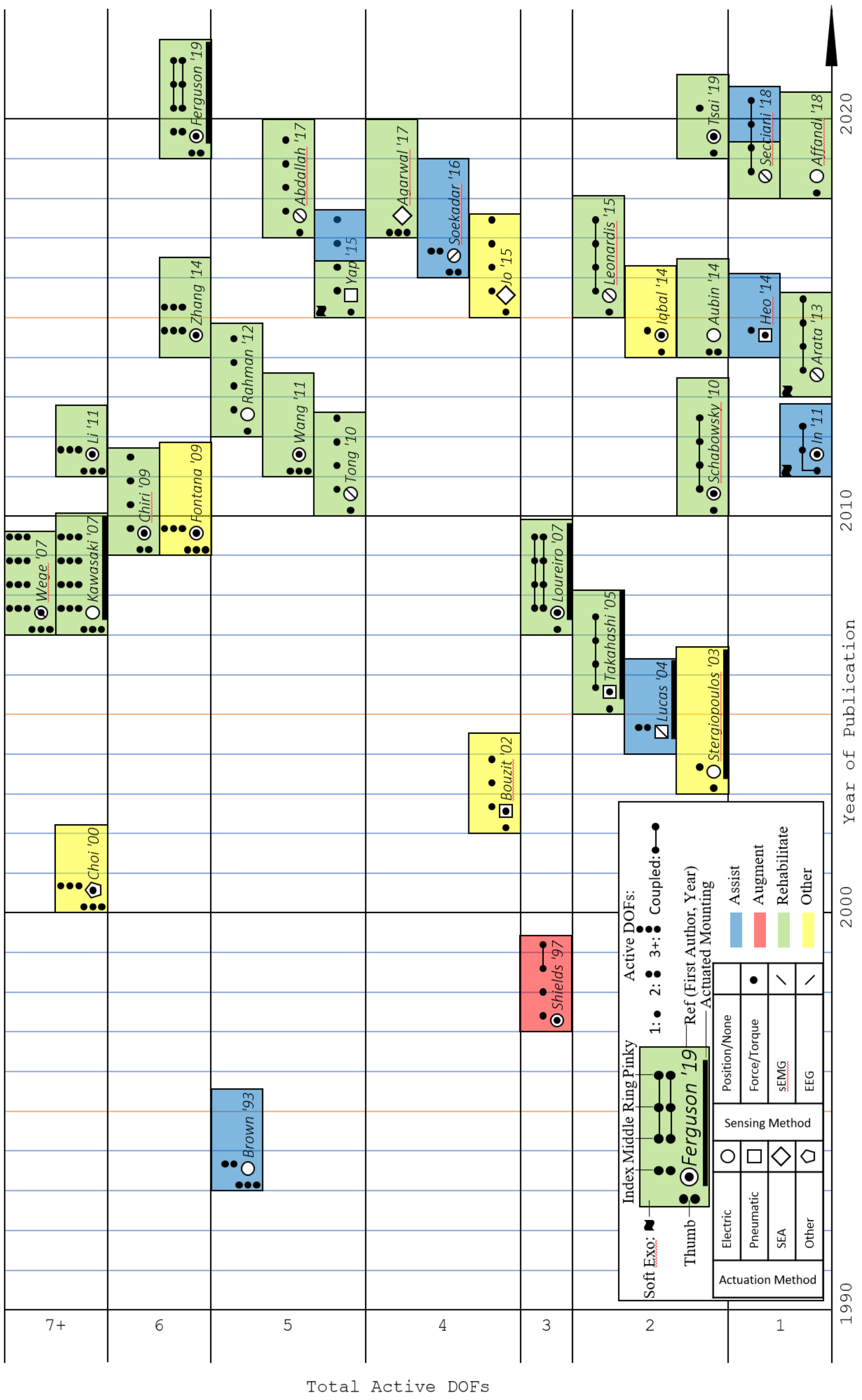

Figure 1.4: A chronological overview of hand exoskeletons.

1.4 Summary

Although many different robotic-assisted rehabilitation devices have been developed, and each platform may have its own advantages and disadvantages, there exist many open questions. I am especially interested in: (1) compliant control, in high-dimensional multi-joint coordination condition; (2) assist-as-needed (AAN) control, in quantitative model-based approach and model-free approach; (3) dual-arm training, in both symmetric and asymmetric modes; (4) system integration, e.g., virtual reality (VR) serious games and graphical user interfaces (GUIs) design and development.

During my Ph.D. research, I developed algorithms and models to (partially) solve the questions above. The rest of my dissertation is divided into the following chapters:

In Chapter 2, the hardware design and implementation of current robotic exoskeleton system, EXO-UL8, would be discussed;

Chapter 3 to 5 focus on the control part. Chapter 3 covers the control architecture of the dual-arm/hand exoskeleton system, EXO-UL8. Control schemes under different training modes would be briefly touched. In Chapter 4, I would focus on the two different admittance control approaches we used to achieve compliant control. In Chapter 5, I would focus on the modified dynamic manipulability model, and the Arm Postural Stability Index (APSI) used to guide assist-as-needed control.

Chapter 6 illustrates the virtual reality part, including environment, GUIs, and serious games design and development.

Chapter 7 provides a pilot study using the exoskeleton to conduct asymmetric bilateral training.

Chapter 8 concludes my dissertation.

CHAPTER 2

Exoskeleton System Hardware

2.1 Overview

Four generations of upper limb exoskeletons for stroke patients' rehabilitation: EXO-UL1, EXO-UL3, EXO-UL7, and EXO-UL8, have been developed in Bionics Lab (PI: Prof. Jacob Rosen). In this chapter, I will generally cover the first three generations of the exoskeleton systems, and then focus on the description of the current generation, EXO-UL8, on which my Ph.D. research and development are based.

Part of this chapter is adapted from the book chapter: (In Press) **Shen, Y.**, Rosen, J. "*EXO-UL Upper Limb Exoskeleton Series: A Four-Generation Review*" in "*Wearable Robotics: Systems and Applications*" (Rosen, J., ed.), Academic Press, 11/2019.

2.2 Previous Generations

2.2.1 First Generation - EXO-UL1

As the beginning of this serial research on the rehabilitative robotic exoskeleton, the first exoskeleton mechanism consisted of a two-link, two-joint device corresponding to the upper and the lower arm and to the shoulder and elbow joints of the human body [Ros97, RFA99, RBF01].

Shown in Figure 2.1(a), the system included a weight plate (external load) that can be attached to the tip of the exoskeleton forearm link. The mechanism was fixed to the wall and positioned parallel to the sagittal plane of the operator. The human/exoskeleton mechanical interface included the upper arm bracelet, located at the upper arm link, and a handle grasped by the operator. This two-

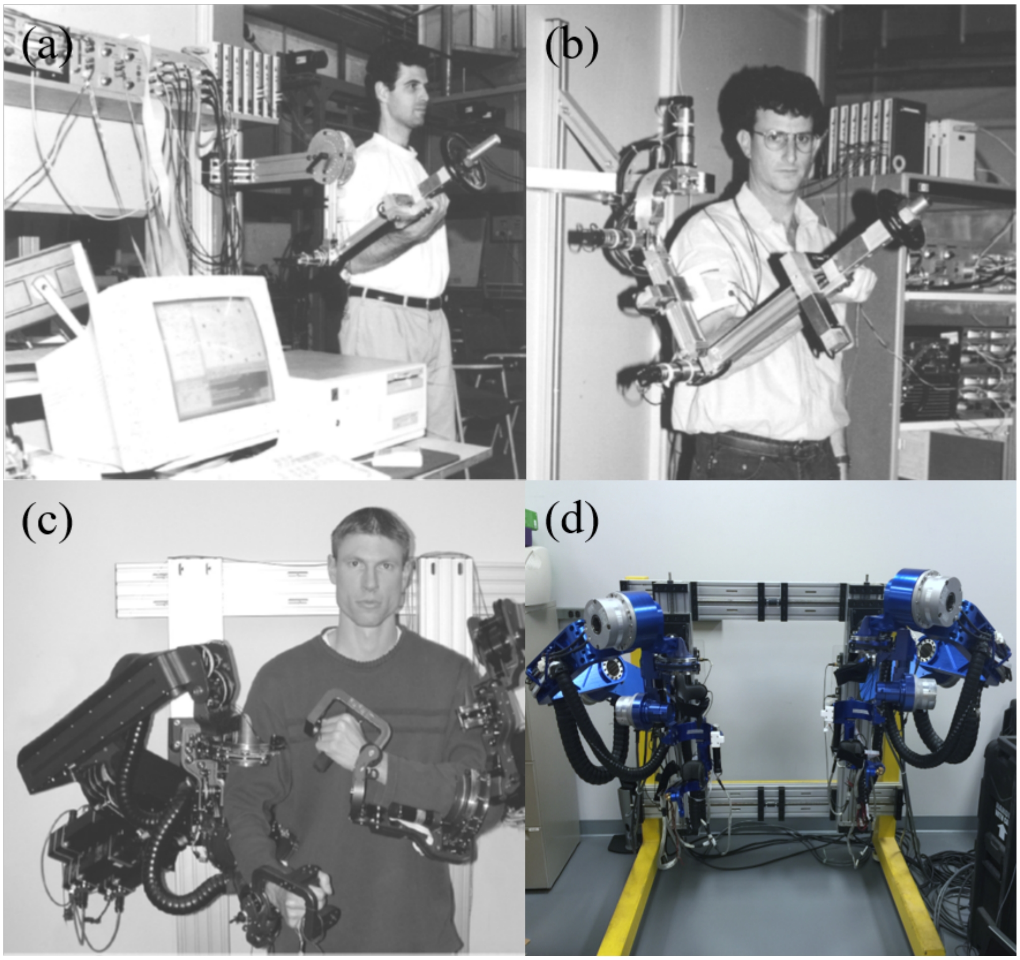

Figure 2.1: The EXO-UL exoskeleton series: (a) 1-DOF EXO-UL1; (b) 3-DOF EXO-UL3; (c) 7-DOF dual-arm EXO-UL7 (aka CADEN-7); (d) 8-DOF dual-arm EXO-UL8.

joint mechanism was used as a one-degree of freedom system by fixing the system shoulder joint at specific angles in the range of 0-180 degrees. The elbow joint was free to move in an angle range of 0-145 degrees, and included built-in mechanical constraints which kept the exoskeleton joint angle within the average human anthropometric boundaries. Since the human arm and the exoskeleton were mechanically linked the movements of the forearms of both the human and the exoskeleton were identical. The basic purpose of the exoskeleton system as an assistance device is to amplify the moment generated by the human muscles relative to the elbow joint, while manipulating loads. The exoskeleton's elbow joint was powered by a DC servo motor (ESCAP-35NT2R82) with a stall torque of 360 mNm equipped with a planetary gearbox (ESCAP-R40) with a gear ratio of 1:193 and a maximal output torque of 40 Nm. An optical incremental shaft encoder (HP HEDS

5500) with 500 lines was attached to the motor shaft. Due to the encoder location and the high gear ratio, the practical encoder's resolution for measuring the joint angle was 0.0036 degree. This setup incorporated a DC motor with the highest torque-to-weight ratio that was available on the commercial market at that time with power consumption that could be provided by a battery. A high energy density of the power supply and an actuator with a high torque-to-weight ratio are two key features of the exoskeleton system as a self-contained mobile medical assistance device for the disabled community. Limits imposed by the technologies at that time on these two key components along with design requirements for developing a compact system with a potential of serving as a medical assistance device for disabled person restricted the payload to be 5 Kg. However, this biomedical oriented design does not restrict the generality of the exoskeleton concept or its operational algorithms. Using other actuation systems, like a hydraulic system, increases the load capacity substantially. The exoskeleton forearm was extended by a rod with a special connector for attaching disk-type weights (external load). Two force sensors (TEDEA 1040) were mounted at the interfaces between the exoskeleton and the tip carrying the external load and between the exoskeleton and the human hand. The first load cell, inserted between the rod holding the external load and the exoskeleton forearm link, measured the actual shear force, normal to the forearm axis, applied by the external load. The second load cell was installed between the handle grasped by the human hand and the forearm link of the exoskeleton. This load cell measured the shear force applied by the operator to the handle. Multiplying the sensors' measurements by the corresponding moment arms indicated the moments applied by the weights and by the human hand relative to the elbow joint. One of the primary innovative ideas of the research was to set the Human Machine Interface (HMI) at the neuromuscular level of the human physiological hierarchy using the body's own neural command signals as one of the primary command signals of the exoskeleton. These signals will be in the form of processed sEMG signals, detected by surface electrodes placed on the operator's skin. The originally proposed HMI takes advantage of the electro-chemical-mechanical delay, which inherently exists in the musculoskeletal system, between the time when the neural system activates the muscular system and the time when the muscles generate moments around the joints. The myoprocessor is a model of the human muscle running in real-time and in parallel to the physiological muscle. During the electro-chemical-mechanical time delay, the system will gather information regarding the physiological muscle's neural activation level based on processed sEMG signals, the joint position, and angular velocity, and will predict using the myoprocessor the force that will be generated by the muscle before physiological contraction occurs. By the time the human muscles contract, the exoskeleton will move with the human in a synergistic fashion, allowing natural control of the exoskeleton as an extension of the operator's body. Surface EMG electrodes (8 mm Ag-AgCl BIOPAC - EL208S) were attached to the subject's skin by adhesive disks for measuring the EMG signal of the Biceps Brachii and Triceps Brachii medial-head muscles. The signals were gained by EMG amplifiers (BIOPAC - EMG100A) using a gain factor in the range of 2000-5000 (depending on the subject). The EMG signals and the load cell signal were acquired by an A/D convector (Scientific Solution Lab Master 12-bit internal PC card) with a 1 kHz sampling rate, whereas the encoder signals were counted by custom-made hardware. The entire data set was recorded simultaneously and stored, for later off-line analysis and simulation. A special real-time software, for operating the system, was written in C and run on a PC-based platform. The software was composed of three main modules. The first module dealt with the hardware/software interface. It controlled the interaction between the PC and the external motor driver and the sensors, through a D/A and an A/D card. The second module included the automatic code generated by the MATLAB - Simulink Real-Time toolbox. The third module was the user interface module which allowed to set various run time operational parameters. All the modules were compiled and linked for generating efficient real-time software.

2.2.2 Second Generation - EXO-UL3

The second exoskeleton mechanism, shown in Figure 2.1(b) [PR08], consisted of a three-link, two-joint device corresponding to the upper and the lower arm and the shoulder and elbow joints of the human body. The hardware is similar to the first mechanism except for that it was used as a two-degree of freedom system: the elbow and the shoulder joints were free to move in their anatomical range of motion.

Four force sensors (TEDEA 1040) were mounted at the interfaces between the exoskeleton and the operator, one at the tip carrying the external load, two between the exoskeleton and the human hand and one at the interface between the upper arm and the exoskeleton. Like the first generation, the first load cell, inserted between the rod holding the external load and the exoskeleton forearm link, measured the actual shear force, normal to the forearm axis, applied by the external load. The other load cells were installed between the handle grasped by the human hand and the forearm link of the exoskeleton and between the upper arm bracelet and the exoskeleton upper link. These load cells measured the shear forces applied by the operator to the mechanism. Multiplying the sensors' measurements by the corresponding moment arms indicated the moments applied by the weights and by the human arm relative to the elbow and the shoulder joints. Expanding the DOFs the mechanism could facilitate from three to seven, and eventually eight, took the research team several years – a leap to EXO-UL7.

2.2.3 Third Generation - EXO-UL7

Shown in Figure 2.1(c), this generation of anthropometric 7-DOF powered exoskeleton system was once termed as "Cable-Actuated Dexterous Exoskeleton for Neuro-rehabilitation" (CADEN-7) [PRB07], but soon later the authors decided to uniform its name under the "EXO-UL" series [PPR09].

Based on the human arm kinematics and dynamics during activities of daily living [RPM05], for the first time in this exoskeleton system series, the EXO-UL7 covers all seven major DOFs of the human upper limb including: shoulder extension/flexion, shoulder adduction/abduction, shoulder internal/external rotation, elbow extension/flexion, forearm pronation/supination, wrist extension/flexion, and wrist radial/ulnar deviation [PR08, PR06, Per06, RP07]. It also contains two arms and enables more training protocols that are further discussed on the EXO-UL8 prototype.

At first the controller was based on the sEMG [CRP05, CRP06], due to the cumbersomeness of setting up sEMG measuring system in practical rehabilitation applications, the research shifted to using force/torque sensors only. For details in gravity compensation implementation please refer to [Mil06], PID control [YR10, YRL11], neural PID control [YR13].

For more details on the design of this generation of exoskeleton system, readers are encouraged to read the Ph.D. dissertation from Joel C. Perry [Per06]; for the general control part, readers are encouraged to read the Ph.D. dissertations from Levi Miller [Mil12] and Hyunchul Kim [Kim12].

2.3 Fourth and Current Generation - EXO-UL8

Clinical trials in stroke rehabilitation training bring inspiration to the features of new rehabilitation robots. One promising training protocol is the so-called "mirror-image" bilateral training [CS05, CCL09], during which the patient moves his/her healthy arm and unhealthy arm simultaneously. This training method may accelerate the recovery of poststroke motor capability as bilateral mirror movements are thought to stimulate the crosstalk between two brain hemispheres. While it is difficult for traditional physical therapists to simultaneously control both arms of a patient in the same movement pattern, multi-DOF powered exoskeletons are intrinsically capable of doing the task. According to the possible efficiency of bilateral rehabilitation training, since the third generation, the system has two arms facilitating unilateral and bilateral training modes. The strength and maximum power output of EXO-UL7 were limited by the cable-driven mechanism. Therefore our team modified the design to the current motor-gear actuated version. Some of the recent progress in the EXO-UL8 (Figure 2.1(d) and 2.2) was covered in [SFM18, SMD18, SSM19].

2.3.1 System Architecture

The dual-arm/hand exoskeleton system includes two major components: (1) Hardware - robotic mechanism, actuation, sensing and electronics; (2) Software - control architecture, and virtual reality environment. The human is physically attached to the exoskeleton system. Contact forces are measured by force sensors placed between the braces (upper arm, forearm, palm, and fingers) and the exoskeleton structure. Joint angles are measured by encoders located on the shafts of the joints. These two types of signals are converted via the A/D and a counter respectively by the real-time PC. Using an array of algorithms, encoded into the real-time PC, joint torque commands are generated and converted via the D/C by the real-time PC as inputs to the servo amplifiers. The servo amplifiers operated in a current mode control the actuation system which in turn result in its movement along with the application of the force fields. Feedback control signals are generated based on modes of operation: unilateral or bilateral. Joint angles are also sent via UDP protocol

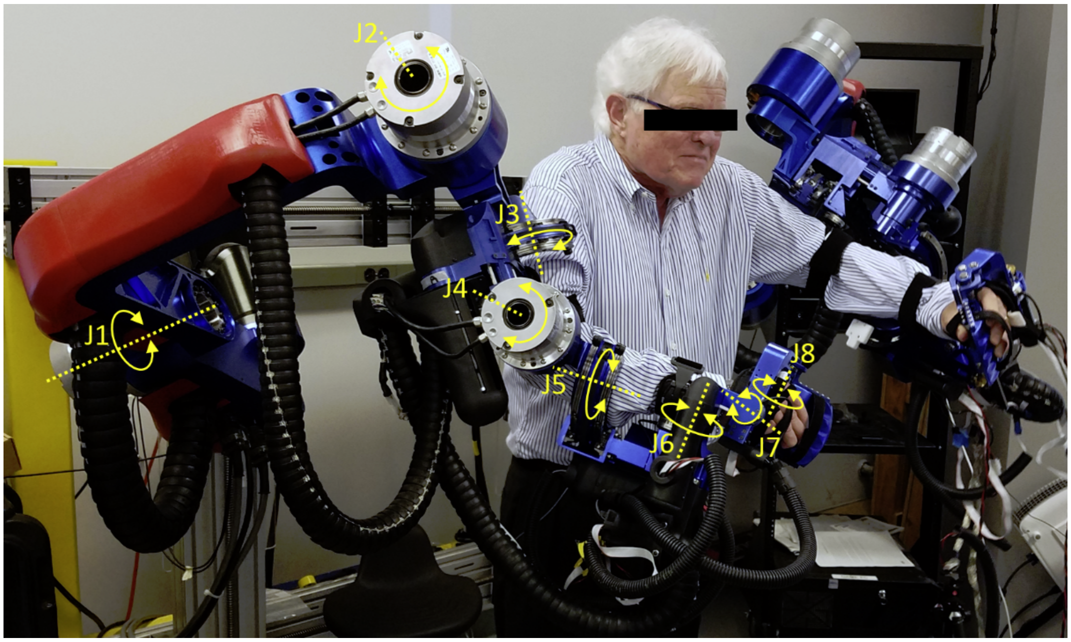

[redacted]

Figure 2.2: One stroke patient is operating the EXO-UL8 upper limb exoskeleton system in dual arm mode (rotation axes of eight active DOFs on the right exoskeleton arm are marked in yellow).

to the virtual reality PC. The virtual reality scene including a representation of the operator's arm along with all the virtual objects is rendered and displayed to the operator on a screen. The physics engine renders the haptic force fields information that is applied to the operator's arms by the exoskeleton system.

The fourth generation (EXO-UL8) of a dual anthropometric arm exoskeleton system was designed and fabricated based on lessons learned for the extensive use of the system in the past in both a lab and clinical settings with stroke patients.

2.3.2 Mechanism

The EXO-UL8, like its predecessor, was kinetically designed to overlap with 95% of a healthy human arm workspace (Figure 2.3). The mechanism includes a total of eight DOFs (3 DOFs for the shoulder joint, 2 DOFs for the elbow joint and 2 DOFs for the wrist joint along with a 1 DOF of hand). The shoulder joint was designed to eliminate singular configurations within the workspace and was repositioned at the edge of the arm workspace. Single-DOF hand grippers were added to increase the total number of DOFs to 8 for each arm and to enable reach-and-grasp motions that are critical to the recovery of the motor control system following stroke. Furthermore, each link is adjustable in length in a telescopic fashion to accommodate a wide range of anthropometric arm dimensions (5 % - 95 %). Each joint includes mechanical limits to prevent motion beyond anatomical limits.

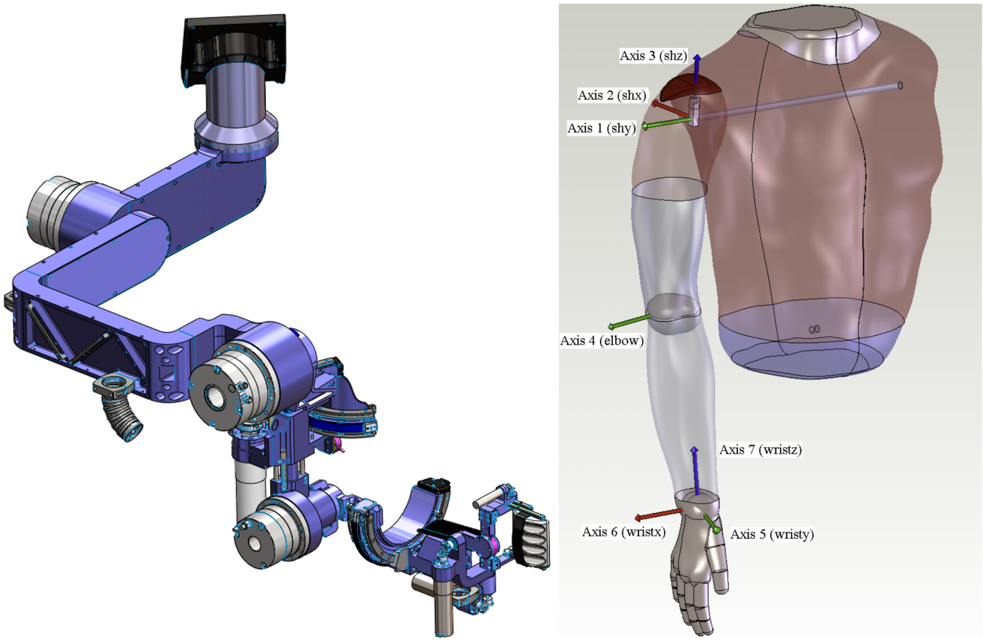

Figure 2.3: The EXO-UL8 design and the corresponding DOFs marked on the human arm.

The entire two exoskeleton arms are attached to a portable frame and a chair allowing to change the high and distance (shoulder span) of the two arms. The rotation axes of the exoskeleton system intersect at the centers of the anatomical joints in a way that eliminates any potential joint dislocation. The mechanical joint includes hard joint limits that match the range of motion of the anatomical joint. Furthermore, a single passive DOF was added to the wrist in addition to the existing two actuated DOF in order to avoid any internal joint torque. The anthropometric design of the exoskeleton allows the user to reach 95% of the workspace accessible by the healthy operator. The human operator is physically attached to the exoskeleton arm and interact with the system through five physical interfaces. Three braces are attached to the upper arm, the forearm, and the palm. Additional two contact surfaces form the claw type hand interface.

2.3.3 Actuation

This generation of the system uses actuators that are directly connected to each of the eight DOFs of the system. Pancake coil brushless DC actuators with harmonic drive are used for the large joints (shoulder and elbow), and small form factor Maxon DC brushed motors with multistage gearboxes are used for the smaller joints (wrist and hand). The selected actuators have the largest torque-to-weight ratio available as off-the-shelf actuation system at the time it was developed.

2.3.4 Sensing

There are two types of sensors embedded into the exoskeleton: (1) position sensors; (2) force torque sensors. Absolute encoders are mounted to the back shaft of all the actuators for measuring the absolute joint angle of every DOF. The human operator is physically attached to the exoskeleton arm and interacts with the system through three physical interfaces of the arm and two to three interfaces at the hand depending on the hand configuration. Three braces are attached to the upper arm, the forearm, and the palm. Additional two contact surfaces of the claw type hand interface and three contact interfaces for the three fingers hand transmits forces between the exoskeleton hand and the operator's fingers. Force sensors embedded into the braces and the supporting surfaces of the fingers enabling the operator to control the arm and the hand using an admittance controller. Details of F/T sensors are illustrated in Figure 2.4.

2.4 Exoskeleton Hand - Preliminary Results

The new generation of the system includes two types of hands: (1) claw-type single DOF hand; and (2) three-finger multi-DOF hand (under development [FDS19]). The exoskeleton arm includes a universal interface at the proximal end of the arm allowing to mount and interchange the two hands. The claw type single DOF hand separates the fingers into two groups including the thumb and the rest of the fingers. The hand with its two supporting surfaces rotated with a single actuated axis allows claw type grasp. The three fingers multi DOF exoskeleton type hand lumps the fingers into three groups: (a) the thumb (b) The index and (c) the middle, the ring, and the pinky fingers.

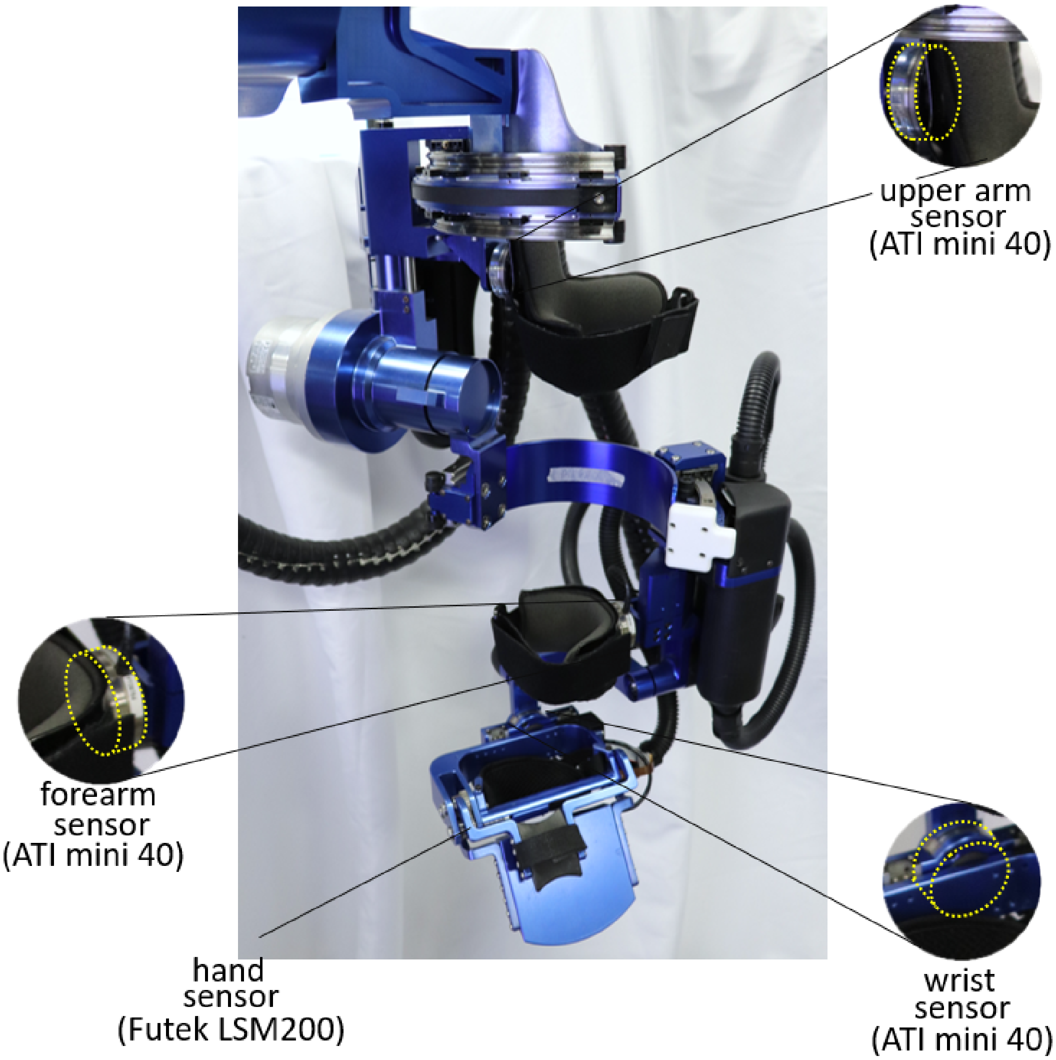

Figure 2.4: Details of EXO-UL8 F/T sensors: ATI mini 40 F/T sensors are used in the upper arm, forearm, and wrist; Futek LSM200 sensor is used in the hand gripper.

Lumping the five fingers of the hand into three groups and a special alignment of the joints of the hand interface allow for comfortable manipulations of the fingers throughout the entire common workspace of each group of fingers.

Originally a single-DOF hand gripper was added to the EXO-UL8 exoskeleton arm on each side, we realized that fine movement training in hand is important and very few research groups have incorporated multi-finger exoskeleton hand to multi-DOF exoskeleton arm, therefore part of the team started working on the exoskeleton hand.

Note: this part is an adapted version of the publication: Ferguson, P. W., Dimaposac, B., **Shen, Y.**, Rosen, J. "*Design of a Hand Exoskeleton for Use with Upper Limb Exoskeletons*", 2018 International Symposium on Wearable Robotics and Rehabilitation (WeRob), Pisa, Italy, 2018.

2.4.1 Design Requirements

The following requirements were formulated for a rehabilitation hand exoskeleton that attaches to an arm exoskeleton: (1) Low Mass: Mass at the hand must be minimized to reduce required torque of the upper limb exoskeleton; (2) Torque: The torque capabilities of the exoskeleton must be sufficiently large to actuate the hand; (3) Workspace: The workspace of the exoskeleton must contain the workspace of the human hand; (4) Grasp: It must be able to actuate a variety of grasps; (5) Open Palm: It must leave the palm and fingers unoccupied to permit inter- action with physical objects; (6) Unisize: It must fit 95% of the general population.

2.4.2 Actuation Method

For the low mass and torque requirements, a Bowden cable transmission system with brushed DC motors was chosen. The cable transmission enabled the remote location of the motor pack, reducing mass at the hand. It also allowed the use of over-sized actuators with sufficient torque for hand rehabilitation.

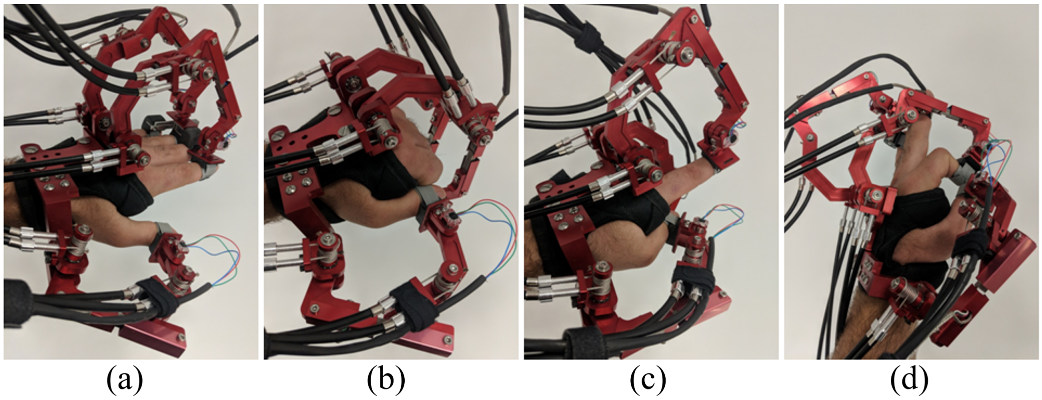
(a) (b) (c) (d)

Figure 2.5: 1-1-3 Configuration shown with (a) Open Hand; (b) Closed Fist; (c) Pointing; (d) Pincer Grasp.

2.4.3 Basic Topology

Workspace, grasp, open palm, and unisize requirements are satisfied by a recon- figurable design topology of three 3R planar serial linkages that attach on the dorsal side of the hand to the distal phalanges. Three linkages are used as 95% of human grasps are achievable with a thumb and two fingers. The topology allows a one-size-fits-all design that neither requires adjustment for different fin- ger lengths nor impedes grasping physical objects. The third joint is made passive to decrease complexity and inertia compared to an active joint. Due to the link lengths, this joint mainly relates to orientation. A passive rotational joint added at the end-effector of each finger linkage permits slight adduction/abduction to improve comfort and allow more natural movement. Bending beam load cells are used as the structure of the first link (L_1) of the thumb linkage and second link (L_2) of the finger linkages, enabling admittance control.

The linkages are reconfigurable to enable a variety of grasps. The first linkage attaches from above the CPC joint to the distal phalanx of the thumb. The plane of the workspace of this linkage is adjustable via rotation around the CPC. The second and third linkages connect from above the MCP joints to the distal phalanges of the fingers. The origin of these linkages is adjustable for different hand widths or to place them in plane with different fingers. The distal end of the second and third linkage feature interchangeable customizable 3D-printed finger attachments that enable different sets of fingers to be actuated by each linkage. Notable configurations include 1-

1-3 (thumb, index, middle+ring+little) and 1-2-2 (thumb, index+middle, ring+little). The 1-1-3 configuration is shown for a set of representative hand positions in Figure 2.5. To account for the motion of little finger relative to the ring finger, a passive slider mechanism connects the finger attachment for the little finger to the third linkage.

2.4.4 Link Length Optimization

To satisfy the unisize requirement, the link lengths were chosen via a brute force optimization algorithm considering fingers in the 95^{th} percentile for length. The lengths of L_1 of the thumb linkage and L_2 of the finger linkages were set to 8.9 cm due to the length of the bending beam load cells. For each linkage, the remaining link lengths were varied across a reasonable range. Each combi- nation, L, of potential link lengths L_1, L_2, and L_3, was checked for kinematic feasibility. Forward and inverse kinematics were used to verify that the linkage could correctly attach to the tip of the distal phalanx of the appropriate finger at all combinations of joint angles $(\theta_1, \theta_2, \theta_3)$ within the workspace with 3 resolution. To correctly attach, L3 must be capable of connecting perpendicularly to the dorsal side of the distal phalanx, and the joints of the linkage must not physically touch or cross through the finger. A design score, J, was calculated for each L based on mechanism isotropy and link length. Mechanism isotropy (ISO), a function of the joint angles is a measure of kinematic performance. It is defined in (2.1) as the ratio of the min (λ_{min}) and max (λ_{max}) eigenvalue of the Jacobian matrix.

$$ISO(\theta_1, \theta_2, \theta_3) = \frac{\lambda_{min}}{\lambda_{max}} \in (0, 1) \tag{2.1}$$

A value of 0 indicates singularity while a value of 1 means the end effector can move equally well in all directions. Mechanism isotropy is calculated for each set of joint angles previously mentioned. To account for varying densities of the end effector location in these sets, the finger workspace area is discretized into a grid of cells, K, and the isotropy is averaged for each cell. Summing the average isotropy of the cells provides an indication of the kinematic capabilities of the mechanism across the entire workspace. It is desirable for the mechanism to avoid singular or near-singular configuration within the workspace of the finger. Therefore, J of each L is proportional to both overall performance (sum of ISO) and to worst-case performance (minimum ISO value calculated).

As mechanical isotropy tends to reward longer link lengths, but it is desirable to keep size and mass of the mechanism low, an additional term is included in J score to reward shorter designs. This was accomplished by making J inversely proportional to the sum of the link lengths raised to a hyperparameter A, as shown in (2.2). A prototype with adjustable link lengths was used to experimentally verify the design produced by a variety of A. Based on this verification, link lengths were chosen for each linkage.

$$J = \frac{\Sigma_K ISO(\theta_1, \theta_2, \theta_3) * \min_K(ISO(\theta_1, \theta_2, \theta_3))}{(L_1 + L_2 + L_3)^A} \tag{2.2}$$

The results of the optimization are illustrated for the linkage that connects to the index finger in Figure 2.6. The hand exoskeleton presented is multi-fingered, multi-DOF, reconfigurable, and designed to attach to a full-arm exoskeleton. The link lengths were determined by optimization to maximize mechanism isotropy and minimize footprint.

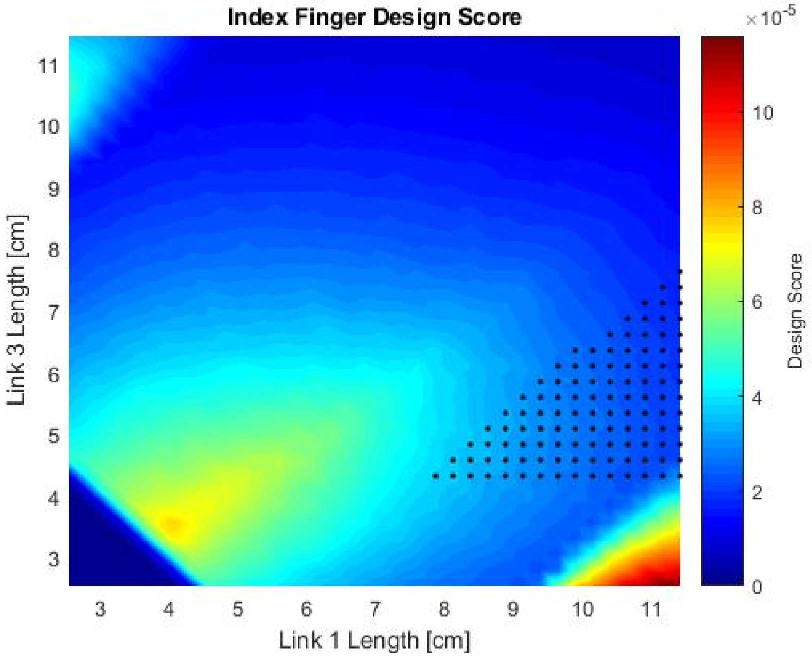

Figure 2.6: Optimization results for the linkage connecting to the index finger for $A = 5$. Dots represent kinematically valid combinations of L_1 and L_3 for L_2 = 8.9cm. Set $L_1 \geq$ 4.4cm due to minimum axes size.

CHAPTER 3

Exoskeleton System Control - Architecture Overview

3.1 Overview

To realize the seamless integration of human arms and the exoskeleton, a comprehensive controller (Figure 3.1) was developed including: (1) admittance control, as the foundation of the control approach translating forces applied by the operator arm and hand on the various F/T sensors into joint angle changes; (2) gravity and friction compensation, as a component of the control algorithm that compensates gravity and friction through feedforward-model-based prediction that is fed into the joint torques; (3) swivel prediction (human arm redundancy resolution) that aims to position the elbow joint at an appropriate swivel angle; and (4) other force fields used to provide patients additional assistance during training. To keep the system simple and easy-to-use, no contextual information like EEG or EMG is used and thus the controller is more complex.

The exoskeleton is capable in other control modes:

(1) when the stroke patient is provided with some predefined trajectory - exoskeleton tracks the trajectory using position control only and does not follow what inputs from the F/T sensors;

(2) in bilateral mirror-image teleoperation mode, the affected-side exoskeleton arm was unilaterally teleoperated by the healthy-side exoskeleton arm (which is under compliant control), via position control;

(3) in assistive control mode (discussed more in Chapter 7), virtual spring could be built between the target object and the affected-side exoskeleton arm on the palm, thus adding additional assistive force into the admittance control loop.

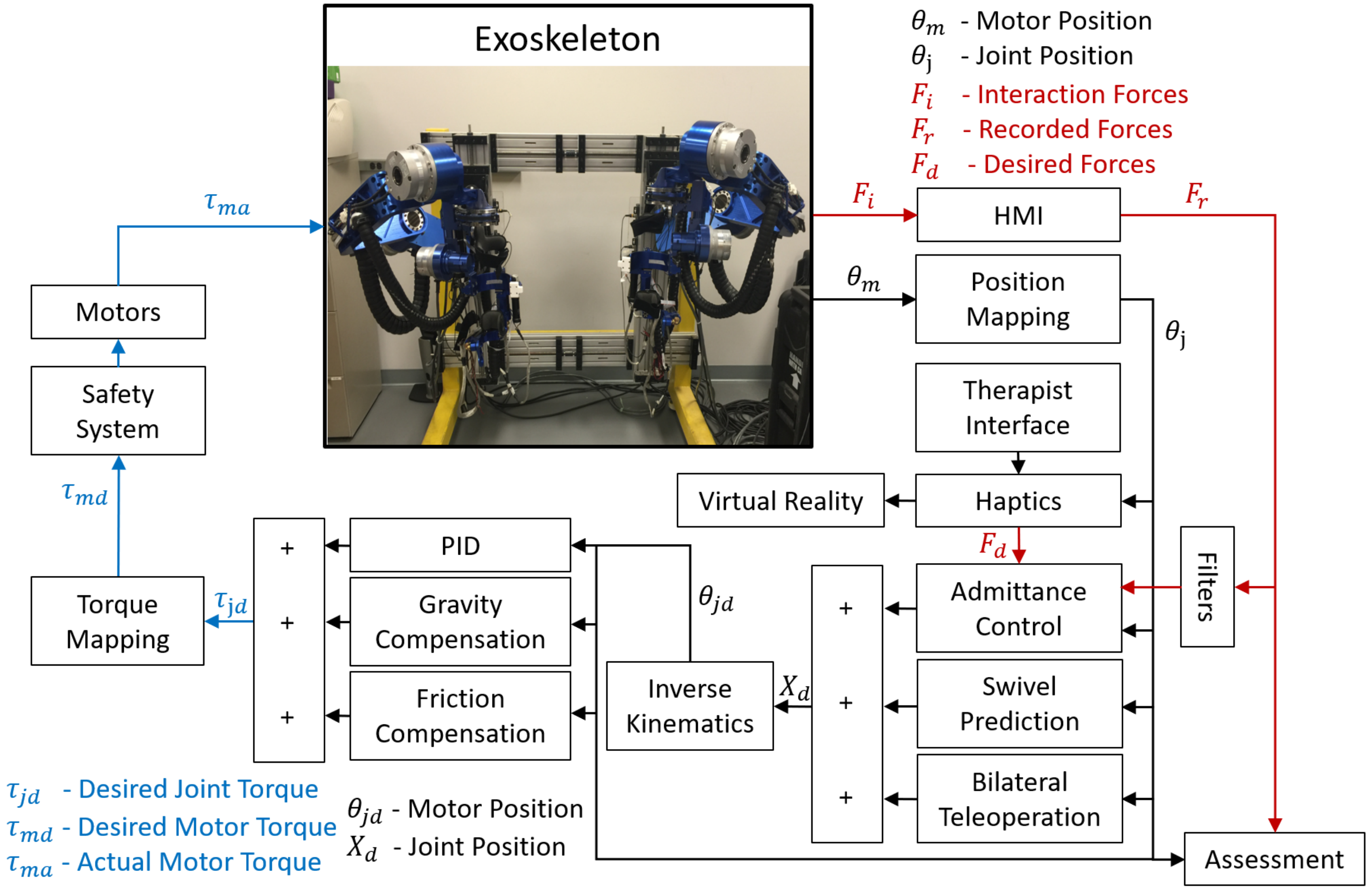

Figure 3.1: Block diagram of the EXO-UL8 controller.

3.2 Gravity and Friction Compensation

The majority of gravity compensation is done based on Levi Miller's work [Mil06]. However, since an additional hand gripper was added, extra gravity compensation is needed and implemented.

Similar to Levi Miller's work, this part we assume the friction is negligible, which is not ideal. This may introduce uncertainty in the feedback admittance control so we later use two different approaches to better control the system.

3.3 Inter-Arm Teleoperation

The current stage of this mode is to enable the mirror image bilateral training. To be specific, the joint space of two exoskeleton arms are coupled with high stiffness and low delay. Unilateral teleoperation may introduce problem like overstretching the patient's arm; on the other hand, bilateral teleoperation may bring more burden to the healthy side, so the work is shifting from the joint space coupling to end-effector space coupling. More details on this work could be found in Chapter 7.

3.4 Record & Replay

The mode is quite useful and promising in helping physical therapists to understand the patients' performance, in joint space, instead of observing in task space. The current stage of EXO-UL8 is one could use the virtual reality game ”record and replay” to record the trajectory and replay the trajectory to another user. However, one of the limitation of this approach is it might overstretch the subject's arm, so additional elasticity/force fields are needed to enhance the safety.

CHAPTER 4

Exoskeleton System Control - Compliant Control

4.1 Overview

Research in upper limb rehabilitation and assistive robotics is shifting its interest from purely assistive to assist-as-needed (AAN) mode. However, approaches of achieving a high physical human-robot interaction (pHRI) transparency still remains an open question for multiple degrees-of-freedom (DOFs) exoskeletons (especially redundant ones). This paper compares two multi-joint admittance control schemes (hyper parameter-based, and Kalman Filter-based) with comfort optimization to improve the human-exoskeleton transparency for a dual-arm upper limb exoskeleton system, the EXO-UL8. Three healthy subjects participated in the study, and accomplished reaching tasks under the two control schemes. Kinematic information in joint space and task space, as well as force- and torque-based power exchanges between the human arm and exoskeleton links are collected and analyzed. Furthermore, power exchange is discussed in comparing the efficiencies of the two approaches. Behavioral adaptation and user profiling could thus be further personalized.

Note: this chapter is adapted from the publication: **Shen, Y.**, Sun, J., Ma, J., Rosen, J. "*Admittance Control Scheme Comparison of EXO-UL8: A Dual-Arm Exoskeleton Robotic System*", 2019 IEEE-RAS-EMBS International Conference on Rehabilitation Robotics (ICORR), Toronto, Canada, 2019. The paper was accepted as an Oral (Podium) Presentation.

4.1.1 Background and Motivation

As the upper limb multi-joint coordination strategies and response mechanism to external resistance are not well understood, designing an intelligent exoskeleton controller is not easy [JPC14]. On the other hand, the role of exoskeletons is evolving from "*purely assistive*" to "*training*", since providing excessive assistance to patients during rehabilitation limits the training effectiveness [RBC16]. To increase patients' engagement, better *assist-as-needed* (ANN) algorithms are needed [BFP14]. However, to achieve good performance for ANN algorithms, one first needs to ensure a high human-exoskeleton transparency, i.e., when a patient no longer needs assistance, the exoskeleton should perfectly detect the patient's intention and follow the movement, rather than apply unwanted resistance, which may alter the natural moving patterns. Previous work in intention detection [LKS14], multi-joint coordination [HHS95], adaptive systems and human adaptation [PNP16] has aimed to improve human-exoskeleton transparency. Exoskeleton modeling and simulation have also improved (e.g., MuJoCo [TET12]), but benefits are more prominent in lower limb applications due to the cyclic movement patterns of walking and constraints imposed by the ground.

4.1.2 Objective and Contribution

In the process of improving compliance while maintaining system stability, there are nonlinearities, unpredicted variations, and uncertainties, which are difficult to model/estimate:

- The physical human-robot interaction interface (soft hand-cuffs attached to force/torque sensors) brings users "wearable" comfort but introduces nonlinearities
- Tissues (i.e., skin and muscles) surrounding the bones, deform when a human moves his/her arm, and add uncertainties to the interface attached to the arm [JM12]
- Human motion pattern varies from subject to subject, direction to direction (Figure 4.1)

In previous studies, researchers have used Kalman Filter-related techniques to deal with sEMG or EEG signals, and with lower limb or low-DOF non-redundant upper limb exoskeletons [LWS14, HHX15, KPG13]. To the best of my knowledge, it is the first time the Kalman Filter techniques are used in the high-DOF, redundant, upper limb exoskeleton control, with force/torque as the only sensor input. The exoskeleton's performance with the Kalman Filter-based admittance control scheme is compared with the existing hyper parameter-based admittance control.

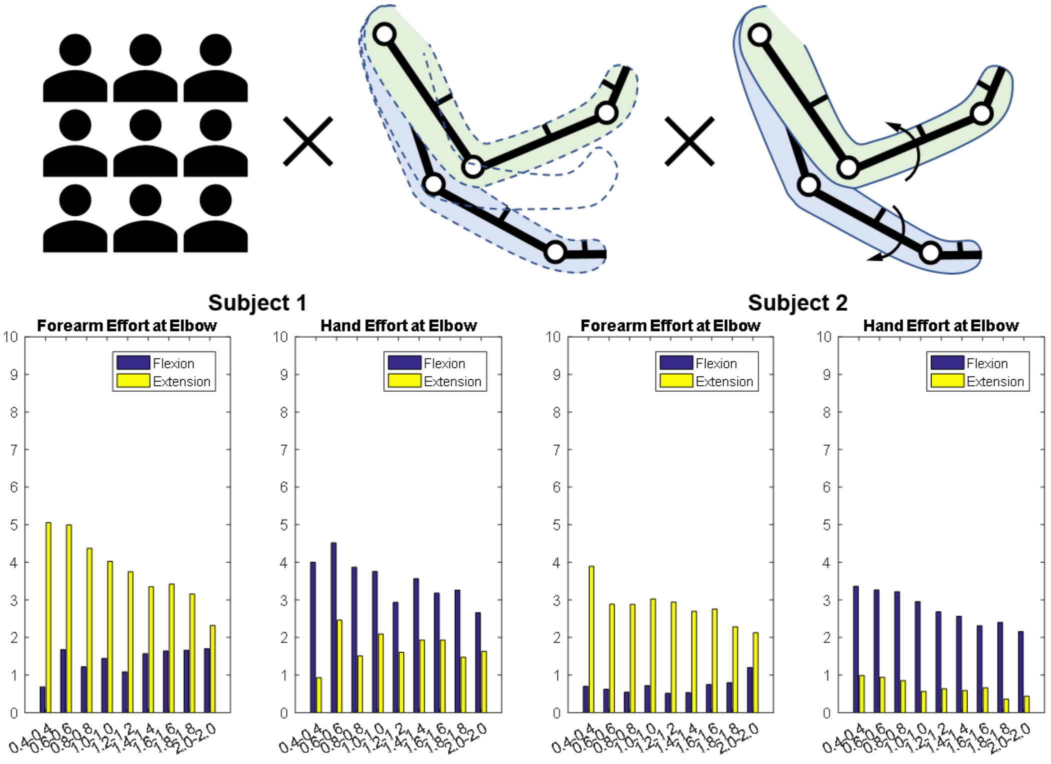

Figure 4.1: Effort needed to actuate an exoskeleton is different among subjects, as well as moving directions (e.g., elbow flexion and extension). Data is from two healthy subjects in the experiment.

The rest of the chapter is organized as follows: Section 4.2 compares the two admittance control schemes; Section 4.3 shows the experiment design; Section 4.4 provides quantitative results and analytical discussion including interaction visualization; and Section 4.5 concludes the chapter.

4.2 Admittance Control Schemes

Before the dual-arm system, training modes were limited to pre-defined trajectories or pure-following. Although many have worked on assist-as-needed modes (Figure 4.2) for years, generalized findings that can be reused in different systems are limited.

The development of the dual-arm system enabled symmetric mirror image movement training based on between-arm teleoperation. The authors have also developed asymmetric bilateral training using an interactive virtual reality environment [SMD18]. In either training mode and regardless of the health of the human, the exoskeleton arm needs to have high "transparency",

Figure 4.2: To the authors' understanding, assist-as-needed mode lives somewhere between "pure–follower" and "pure-assistance", which is difficult to locate.

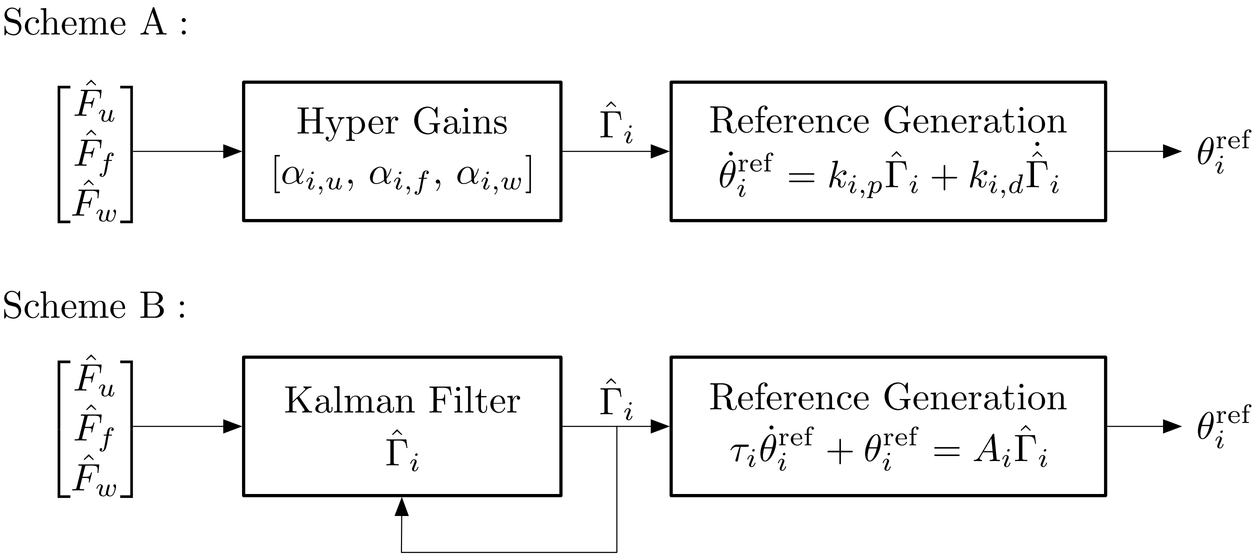

Figure 4.3: Comparison of admittance control schemes. Scheme A combines the contributions of the force sensors using a weighted sum (hyper gains), while Scheme B estimates the human-applied joint torques with a Kalman Filter.

which means that it is sensitive enough, in a heuristic way, to not exert unwanted resistance on the human arm (otherwise the human's movement, e.g., redundancy resolution, would be affected [SHM17]), as well as be robust enough to prevent instability in all configurations. A trade-off between sensitivity and stability exists, and thus a dynamic equilibrium is needed.

An admittance controller allows a system to have an arbitrary apparent mechanical admittance by regulating the system's output to a reference trajectory that a virtual system with the desired mechanical admittance would take [AD13]. The result is that to a human, the system behaves with the desired apparent admittance. In the case of the EXO-UL8 exoskeleton, admittance control allows the exoskeleton's arms to appear much lighter so that the user can easily move them around.

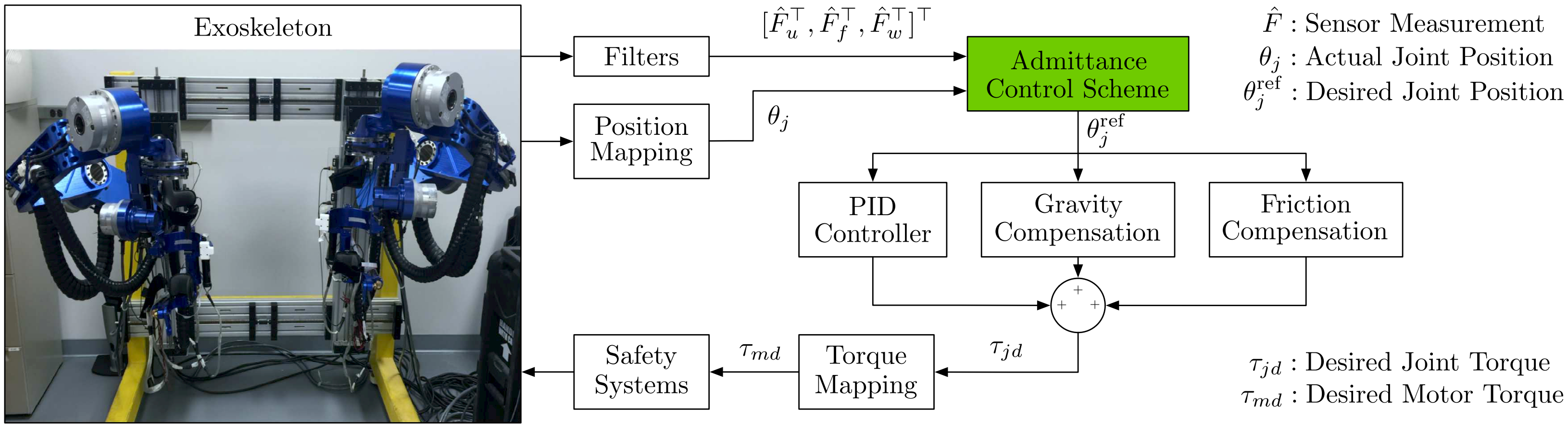

Figure 4.4: The exoskeleton controller implements a cascaded control strategy in which low-level motor controllers track references generated by the admittance control scheme. In this comparison study, the green box implements either Scheme A or Scheme B, as discussed in Section 4.2.

The admittance control scheme implemented consists of two aspects: estimating the torques applied by the human to the exoskeleton's joints, and generating reference trajectories for the exoskeleton's joints in response to the human-applied forces. In this study, two admittance control schemes, as shown in Figure 4.3, are compared. In Scheme A (the existing control scheme [SMD18]), the human-applied joint torques are calculated from a weighted combination of each sensor's contribution, while in Scheme B, a Kalman Filter is used. In both schemes, the estimated torques are then used to generate an appropriate reference trajectory in joint space so that the exoskeleton appears to have the desired mechanical admittance.

4.2.1 Calculating Human-Applied Torques from Sensor Data

Human-applied forces are measured by the force sensors located in the upper arm, lower arm, and wrist handle of the exoskeleton, and are used to calculate the resulting human-applied torques on each of the seven joints. Determining the particular hyper gains for the sensor contributions is a difficult iterative process, which motivated the Kalman Filter as an alternative approach. In either approach, let $\Gamma \in \mathbb{R}^7$ be the actual joint torques resulting from human-applied forces, and $\hat{\Gamma} \in \mathbb{R}^7$ be the estimated joint torques using data from the sensors. Each of the six degrees-of-freedom (DOF) force sensors provides force and torque measurements in the three axes of the sensor's reference frame: $\hat{F} \in \mathbb{R}^6$, $\hat{F} := \mathrm{col}(\hat{f}_x, \hat{f}_y, \hat{f}_z, \hat{\tau}_x, \hat{\tau}_y, \hat{\tau}_z)$. The actual force and torque at each sensor's location, $F \in \mathbb{R}^6$, $F := \mathrm{col}(f_x, f_y, f_z, \tau_x, \tau_y, \tau_z)$, relate to the joint torques through the appropriate Jacobian matrix: $J_u \in \mathbb{R}^{6\times 7}$ for the upper arm sensor, $J_f \in \mathbb{R}^{6\times 7}$ for the forearm sensor, and $J_w \in \mathbb{R}^{6\times 7}$ for the wrist sensor. The generalized force at each sensor is unaffected by joint torques corresponding to joints located past the sensor's position along the exoskeleton arm. As a result, the Jacobians corresponding to the upper and forearm sensors have certain columns that only contain zeros: $(J_u)_{*,4:7} = \mathbb{0}_{6\times 4}$ and $(J_f)_{*,6:7} = \mathbb{0}_{6\times 2}$. These Jacobian matrices result in the following relationship between the joint torques and actual generalized forces at each sensor location:

$$\Gamma_{1:3} = (J_u^\top F_u)_{1:3}, \tag{4.1}$$

$$\Gamma_{1:5} = (J_f^\top F_f)_{1:5}, \tag{4.2}$$

$$\Gamma_{1:7} = (J_w^\top F_w)_{1:7}. \tag{4.3}$$

4.2.1.1 Scheme A: Hyper Gains

To address the uncertainties and nonlinearities in multi-joint coordination, hyper gains $\alpha_{j,s}, j \in \{1,\ldots,7\}, s \in \{u,f,w\}$ are introduced:

$$\hat{\Gamma}_j = \alpha_{j,u}\hat{\Gamma}_{j,u} + \alpha_{j,f}\hat{\Gamma}_{j,f} + \alpha_{j,w}\hat{\Gamma}_{j,w}, \tag{4.4}$$

where $\hat{\Gamma}_{j,s} = (J_s^\top \hat{F}_s)_j$. In a complete form, equation (4.4) (with the gripper DOF considered separately) is:

$$\begin{bmatrix} \hat{\Gamma}_1 \\ \hat{\Gamma}_2 \\ \hat{\Gamma}_3 \\ \hat{\Gamma}_4 \\ \hat{\Gamma}_5 \\ \hat{\Gamma}_6 \\ \hat{\Gamma}_7 \end{bmatrix} = \begin{bmatrix} \alpha_{1,u}\hat{\Gamma}_{1,u} + \alpha_{1,f}\hat{\Gamma}_{1,f} + \alpha_{1,w}\hat{\Gamma}_{1,w} \\ \alpha_{2,u}\hat{\Gamma}_{2,u} + \alpha_{2,f}\hat{\Gamma}_{2,f} + \alpha_{2,w}\hat{\Gamma}_{2,w} \\ \alpha_{3,u}\hat{\Gamma}_{3,u} + \alpha_{3,f}\hat{\Gamma}_{3,f} + \alpha_{3,w}\hat{\Gamma}_{3,w} \\ \alpha_{4,f}\hat{\Gamma}_{4,f} + \alpha_{4,w}\hat{\Gamma}_{4,w} \\ \alpha_{5,f}\hat{\Gamma}_{5,f} + \alpha_{5,w}\hat{\Gamma}_{5,w} \\ \alpha_{6,w}\hat{\Gamma}_{6,w} \\ \alpha_{7,w}\hat{\Gamma}_{7,w} \end{bmatrix}. \tag{4.5}$$

Contributions to specific joints could be compromised due to uncertain nonlinearities, which may lead to the coactivation of other exoskeleton DOFs (unwanted movements) during movement. To overcome this unindended effect, the user may be forced to exert additional effort in order to achieve the desired motion.

To quantify the comfort level (denoted as *cl*), we normalize the effort at each joint based on [LWZ90]:

$$cl_j = 1 - \tau_j / \tau_{j,max},\ j \in \{1,\ldots,7\}. \tag{4.6}$$

Note that cl_j is direction-dependent due to the difference in concentric and eccentric contractions. As shown in Table 4.1, the second and third columns list positive and negative rotations on exoskeleton, respectively. The hyper gains are manually tuned so that the comfort level is approximately optimized. The exoskeleton's gravity and friction are separately compensated.

Table 4.1: Different joint torque limits

Body Part	Max Strength (N-m)	Max Strength (N-m)
Shoulder	Flexion: 13.13 Adduction: 14.49 Internal Rotation: 11.59	Extension: 8.90 Abduction: 15.62 External Rotation: 11.63
Elbow	Flexion: 10.75	Extension: 8.76
Wrist	Pronation: 3.39 Extension: 2.11 Radial Deviation: 2.67	Supination: 1.42 Flexion: 1.55 Ulnar Deviation: 1.98

4.2.1.2 Scheme B: Kalman Filtering

The Kalman Filter approach is based off the work of [AD13], in which the joint torques to estimate are modeled as entirely driven by Gaussian noise:

$$\dot{\Gamma} = w_{\Gamma}, \tag{4.7}$$

where $w_{\Gamma} \sim \mathcal{N}(\mathbb{0}_{7\times 1}, Q_{\Gamma})$, with Q_{Γ} being a covariance matrix. Tuning Q_{Γ} allows tuning how responsive a particular joint is to the human-applied torques. For use in the Kalman Filter, equation (4.7) is descretized to:

$$\Gamma[k+1] = \Gamma[k] + (\Delta t) w_{\Gamma}[k], \tag{4.8}$$

where Δt is the time-step.

Since Γ is the state that the Kalman Filter tries to estimate, equations (4.1), (4.2), and (4.3) provide a measurement model for Γ. At each sampling time-step $k \in \mathbb{Z}$, assume the sensor's measurement data is corrupted with additive Gaussian noise, and let

$$\bar{z}[k] := \begin{bmatrix} [1.3](J_u^{\top} \hat{F}_u)[k] \\ (J_f^{\top} \hat{F}_f)[k] \\ (J_w^{\top} \hat{F}_w)[k] \end{bmatrix}. \tag{4.9}$$

Then,

$$\bar{z}[k] = \begin{bmatrix} \mathbb{I}_{3\times 3} & \mathbb{0}_{3\times 4} \\ \mathbb{I}_{5\times 5} & \mathbb{0}_{5\times 2} \\ \multicolumn{2}{c}{\mathbb{I}_{7\times 7}} \end{bmatrix} \Gamma[k] + \begin{bmatrix} [1.2]v_u[k] \\ v_f[k] \\ v_w[k] \end{bmatrix}, \tag{4.10}$$

$$:= H[k]\Gamma[k] + \mathrm{col}(v_u[k], v_f[k], v_w[k]), \tag{4.11}$$

where $v_u[k] \in \mathbb{R}^3$, $v_u[k] \sim \mathcal{N}(\mathbb{0}_{3\times 1}, R_u)$; $v_f[k] \in \mathbb{R}^5$, $v_f[k] \sim \mathcal{N}(\mathbb{0}_{5\times 1}, R_f)$; and $v_w[k] \in \mathbb{R}^7$, $v_w[k] \sim \mathcal{N}(\mathbb{0}_{7\times 1}, R_w)$.

Equations (4.8) and (4.10) are the Kalman Filter's process and measurement models, respectively. At each time-step, the prior and a posteriori updates are performed to yield $\hat{\Gamma}[k]$, which is the minimum mean square error (MMSE) estimate of $\Gamma[k]$. Let P_p be the prior's variance, P_m be the a posteriori's variance, and $R := \mathrm{diag}(R_u, R_f, R_w)$. Then, the update equations of the Kalman Filter for this system in particular are as follows.

Initialization:

$$\hat{\Gamma}[0] = \mathbb{0}_{7\times 1}, \tag{4.12}$$

$$P_m[0] = (\Delta t)^2 Q_\Gamma. \tag{4.13}$$

Prior Update:

$$P_p[k] = P_m[k-1] + (\Delta t)^2 Q_\Gamma. \tag{4.14}$$

A Posteriori Update:

$$K[k] = P_p[k] H^\top[k] (H[k] P_p[k] H^\top[k] + R)^{-1}, \tag{4.15}$$

$$\hat{\Gamma}[k] = (\mathbb{I} - K[k]H[k])\hat{\Gamma}[k-1] + K[k]\bar{z}[k], \tag{4.16}$$

$$\begin{aligned} P_m[k] = {} & (\mathbb{I} - K[k]H[k]) P_p[k] (\mathbb{I} - K[k]H[k])^\top \\ & + K[k] R K^\top[k]. \end{aligned} \tag{4.17}$$

The process and measurement noise covariance matrices are manually tuned in an iterative approach until the exoskeleton's movements are heuristically determined to be smooth, yet responsive. Smaller process noise covariance results in smoother estimated torques, while smaller measurement noise covariance terms for a particular sensor measurement increases its contribution to the estimated torque. Note that the Joseph form is used for the covariance's a posteriori update in equation (4.17) for numerical stability.

The estimated $\hat{\Gamma}[k]$ is subsequently used to generate the appropriate reference signal in joint space.

4.2.2 Joint Space Reference Generation

While second-order models have been used by other works [AD13, Eq. 3][HYL17, Eq. 4], a first-order model was chosen over a second-order model to allow the exoskeleton to feel more responsive to the user.

4.2.2.1 Scheme A

The calculated torque signals are filtered and input into a PD admittance controller:

$$\dot{\theta}_j^{\text{ref}} = k_{j,p}\hat{\Gamma}_j + k_{j,d}\dot{\hat{\Gamma}}_j,\ j \in \{1,\dots,7\}, \tag{4.18}$$

where $k_{j,p}$ and $k_{j,d}$ are manually tuned gains, and each θ_j^{ref} is tracked by the corresponding low-level motor controller.

4.2.2.2 Scheme B

The estimated human-applied joint torques $\hat{\Gamma}$ are used to each drive a first-order reference generation model for the corresponding joint:

$$\tau_j\dot{\theta}_j^{\text{ref}} + \theta_j^{\text{ref}} = A_j\hat{\Gamma}_j,\ j \in \{1,\dots,7\}, \tag{4.19}$$

where τ_j and A_j are the desired time constant and DC gain for the joint, respectively. These parameters are manually tuned to achieve the desired responsiveness of the particular joint. For implementation, equation (4.19) is discretized using exact discretization to yield:

$$\theta_j^{\text{ref}}[k+1] = e^{-\frac{\Delta t}{\tau_j}}\theta_j^{\text{ref}}[k] + A_j(1-e^{-\frac{\Delta t}{\tau_j}})\hat{\Gamma}_j[k], \tag{4.20}$$

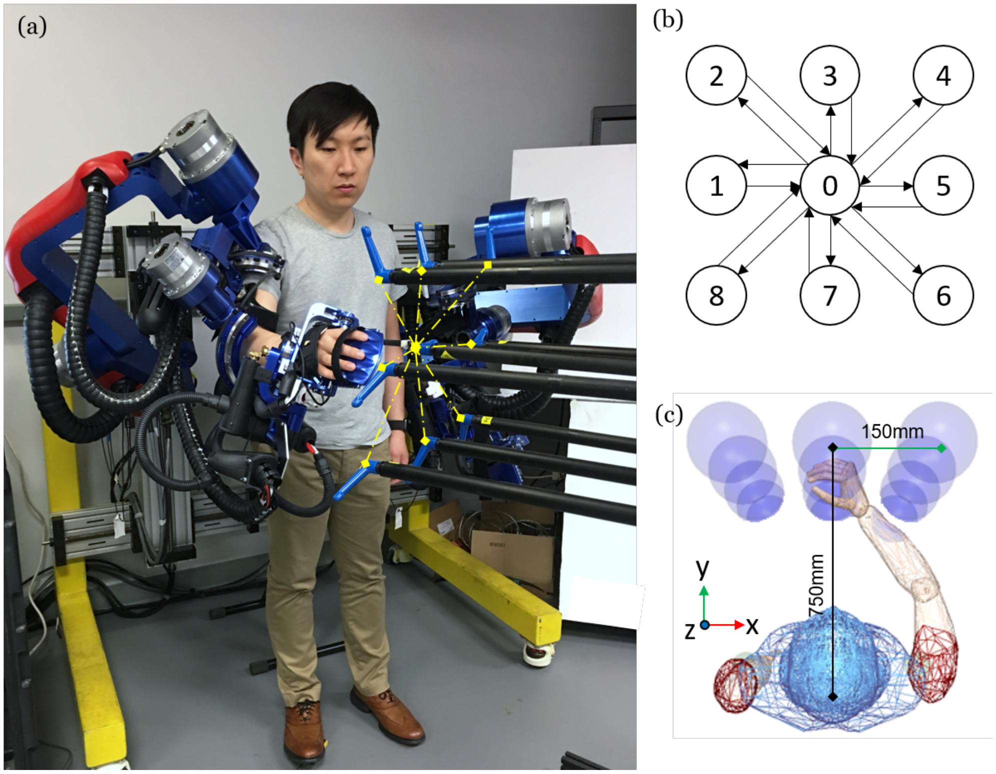

Figure 4.5: Experiment setup: (a) A subject is wearing the exoskeleton to accomplish trajectory tracking tasks; (b) Planned trajectory (detailed in Algorithm 1); (c) Top view of the experiment setup.

for $j \in \{1, \dots, 7\}$. The generated reference signal, θ^{ref}, is then tracked by the individual motor controllers, as shown in Figure 4.4.

4.3 Experiment

This experiment explored the performance of each control scheme through interaction with three healthy subjects, recruited according to an approved IRB protocol (IRB #17-001646). Only the right arm of the exoskeleton was utilized (all subjects are right-handed).

4.3.1 Setup

Shown in Figure 4.5(a), Assistance was provided to help subjects into the exoskeleton and attach the cuffs. Subjects were instructed to wear short-sleeve t-shirts to reduce any nonlinearity effects resulting from deformation of clothing. To eliminate possible interference from the VR environment feature of the exoskeleton system, the experiment limited interaction to be with real objects only.

4.3.2 Tasks

The subjects were asked to move their right arm, while wearing the exoskeleton, to touch a sequence of targets as shown in Figure 4.5(b). The #0 target is located at the center of a 3×3 target matrix. The complete experiment task description is illustrated in Algorithm 1.

Algorithm 1: Experiment Protocol on Each Subject

```
Subject wear the exoskeleton on the dominant arm begin
    for $Scheme = A, B$ do
        Become familiar with the system for 5min, and rest for 1min
        for $i = 1, 2, ..., 8$ do
            Move the tip from Target #0 to Target #$i$ (in 3sec, as instructed by a
              metronome)
            if not touched then
                Keep moving
            else
                Move the tip back to Target #0 (in 3sec, instructed by a metronome)
        Take off the exoskeleton, and rest for 5min
```

4.3.3 Data Collection

Both kinematic and force data were collected: joint position was recorded from the optical encoders at the seven motors on the exoskeleton arm at 100Hz; force/torque information, $\hat{F}$, was measured by the three sensors on the exoskeleton arm at 100Hz as well. The data was post-processed using MATLAB R2018b (MathWorks, USA).

4.4 Results & Discussion

Several aspects of the subject's physical interaction with EXO-UL8 are quantitatively analyzed and discussed below to compare the controllers' performance.

4.4.1 High-Level Trajectory Tracking - Joint Space

4.4.1.1 Joint space position trajectory

The joint space position trajectory of all seven DOFs of Subject #1 is plotted in Figure 4.6. The summary of joint position distribution is shown in Figure 4.7(a).

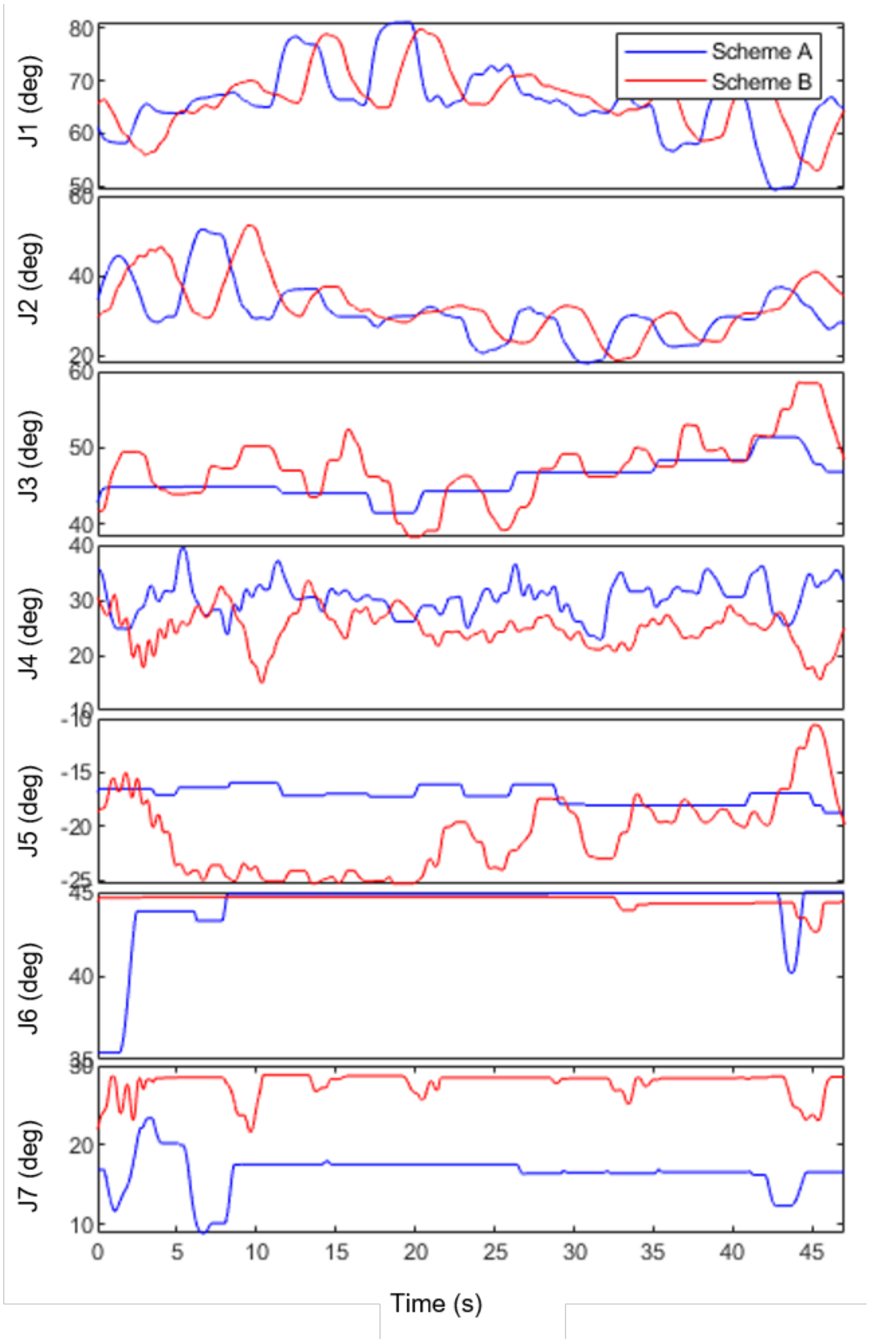

Figure 4.6: Joint space position trajectory of Subject 1, under Scheme A and B. Although completion time and task space error (Table 4.2) are close in two different control schemes, joint usage preference is different. Joints 3 and 5 are less used in Scheme A compared with Scheme B: Kalman filter seems to better estimate supination/pronation (joint 5) and shoulder internal/external rotation (joint 3).

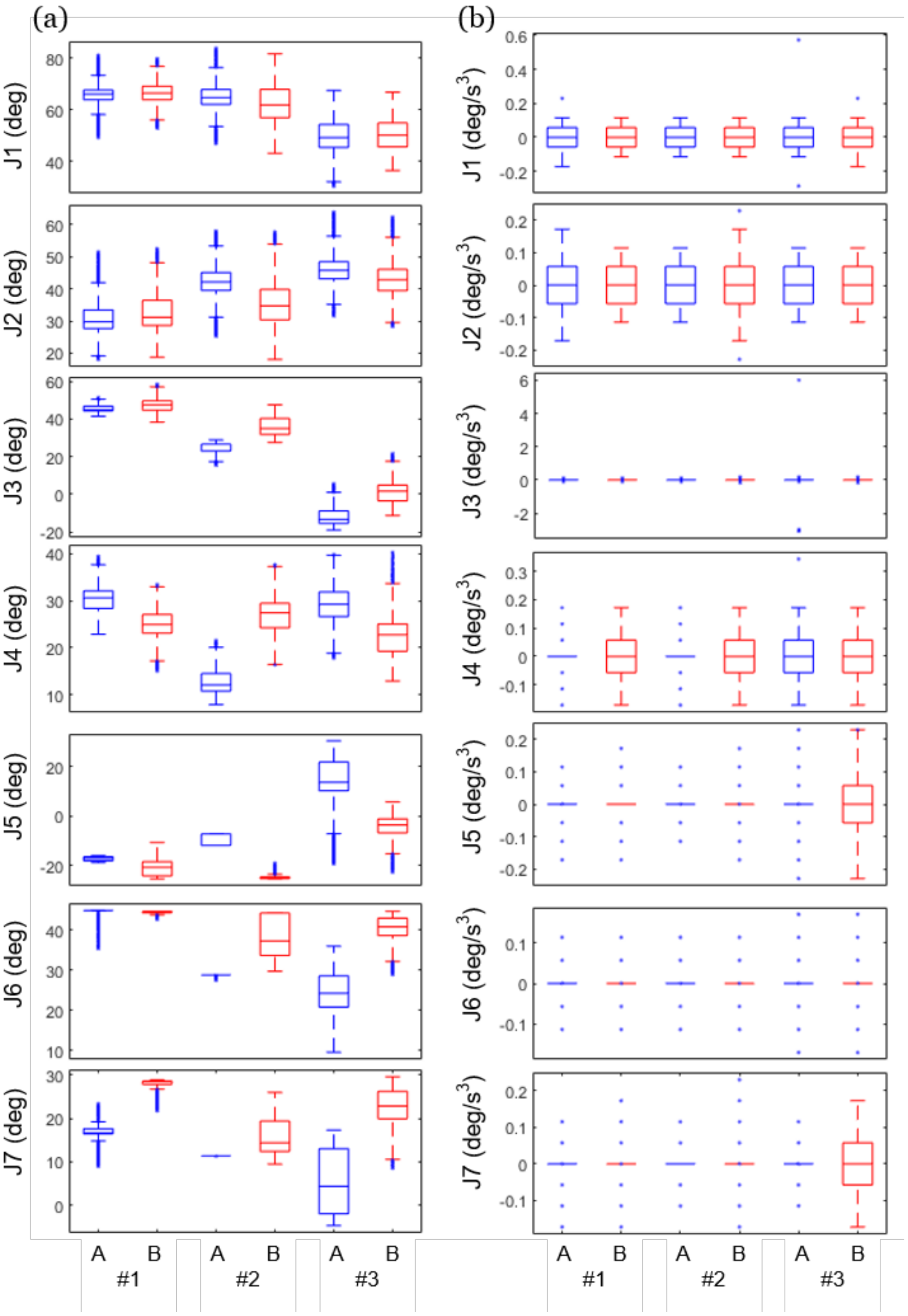

Figure 4.7: Joint space position (a) and joint space jerkiness (b) distributions of all subjects under Scheme A and Scheme B.

4.4.1.2 Joint space jerkiness

As observed in the distribution in Figure 4.7(b), the joint space jerkiness (third-order time derivative of joint position) in both Scheme A and Scheme B are comparable.

4.4.2 High-Level Trajectory Tracking - Task Space

4.4.2.1 Task space position trajectory

The position over time of the end-effector in task space for both admittance control schemes is shown in Figure 4.8. By qualitative observation, both admittance control schemes are adequate in responding to the estimated human-applied torques by moving the exoskeleton to the desired positions.

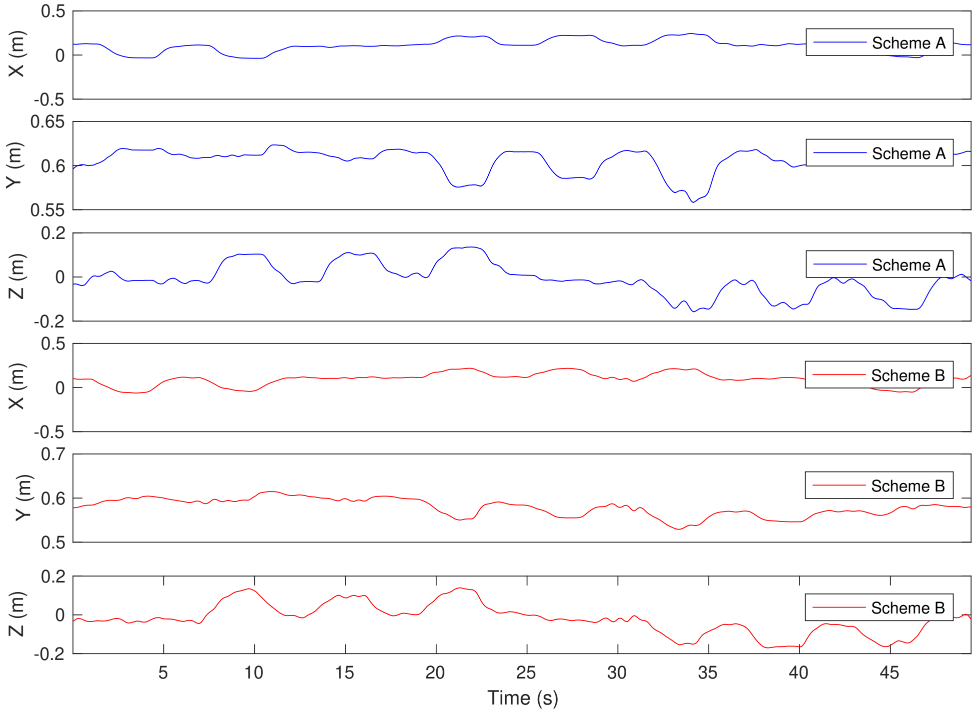

Figure 4.8: Task Space Position Trajectory of Subject 1, under Scheme A and B. Both control schemes show satisfactory functionality for the duration of the test time. Similar observations were made for all three test subjects.

4.4.2.2 Task space error

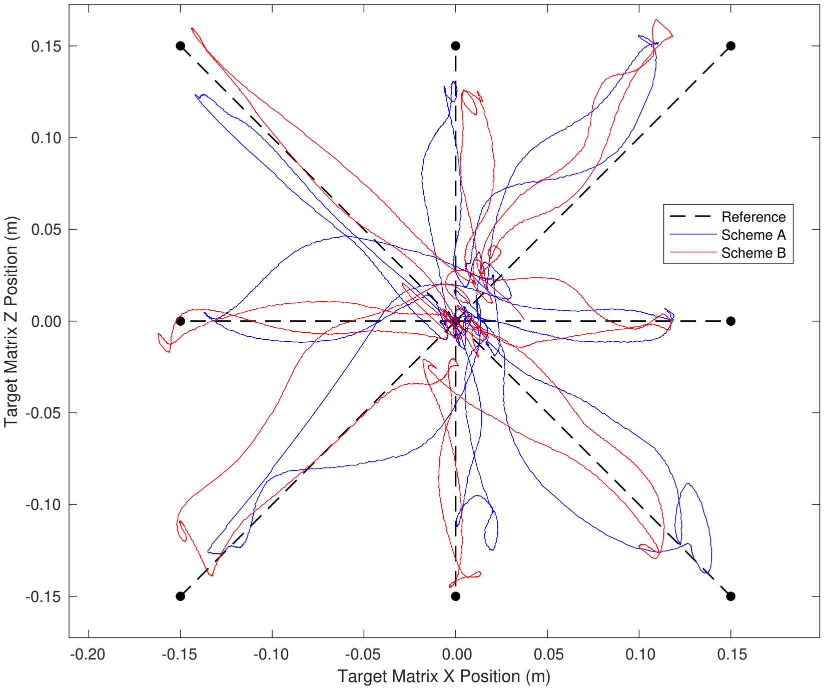

Figure 4.9: Task Space Reference Following of Subject 1, under Scheme A and B. Both control schemes show similar magnitudes of error in guiding the exoskeleton's end-effector along the reference trajectories.

The task space error for each subject under each admittance control scheme is the total deviation of the actual human controlled trajectory from the reference trajectory of Figure 4.5 (b). A sample plot of Subject 1's trajectory in the plane of the target matrix is shown in Figure 4.9. To quantify the error, let it be defined as the root-mean-square (RMS) of the minimum distance of the actual trajectory to the reference trajectory summed over all segments of the reference trajectory, similar to the approach presented in [SHM17]: $\sum_{\gamma \in \text{segments}} \sqrt{(d_{\gamma,1}^2 + \cdots + d_{\gamma,n}^2)/n}$, where $d_{\gamma,i}$ is the minimum distance to segment γ of the reference trajectory.

4.4.3 Power Exchange

The power exchange is the amount of mechanical power the user inputs into the exoskeleton device through the three sensors. In an ideal situation, the power exchange is minimal, which is indicative

Table 4.2: Task space errors under both schemes for each subject

Subject	Scheme A (unit: m)	Scheme B (unit: m)
1	0.0610	0.0634
2	0.0777	0.0778
3	0.1219	0.1091

Table 4.3: Mean power exchange under both schemes for each subject

	Scheme A (unit: mW)			Scheme B (unit: mW)		
Subject	Upper	Lower	Handle	Upper	Lower	Handle
1	89	176	345	155	544	507
2	74	185	248	89	208	200
3	123	210	91	69	203	182

of high human-exoskeleton transparency. The mean power exchange of each test subject for each admittance control scheme is shown in Table 4.3.

4.5 Conclusions

This study compares two different admittance control schemes (existing hyper parameter-based, and Kalman Filter-based) on the EXO-UL8, a dual-arm, high-DOF redundant exoskeleton system for upper-limb post-stroke rehabilitation. The device's functionality in facilitating single movements based on three healthy subjects' pHRI was experimentally validated and quantitative data, such as joint space/task space trajectories and human-exoskeleton power exchange, was analyzed. Initial results show promising performance in terms of functionality, human-exoskeleton transparency, reference-following error, and mechanical power exchange. The proposed control schemes will continue to be further investigated and modified for additional features (e.g., a multi-finger hand exoskeleton under development [FDS19]).

CHAPTER 5

Exoskeleton System Control - Assist-as-Needed

5.1 Overview

Note: The majority of this chapter is adapted from the publication:
Shen, Y., Hsiao, B. P., Ma, J., Rosen, J. "*Upper Limb Redundancy Resolution Under Gravitational Loading Conditions: Arm Postural Stability Index Based on Dynamic Manipulability Analysis*", 17th IEEE-RAS International Conference on Humanoid Robots (HUMANOIDS), Birmingham, UK, 2017.

This work, for the first time, provides a quantitative model for robotic exoskeleton system to understand when and where to provide assistance. In other words, this is a model-based approach to realize "assist-as-needed".

Resistance training may be considered as one promising approach for improving the motor capabilities of post-stroke patients. A successful introduction of this depends on the proper resolution of human arm redundancy under gravitational loading. The spatially heterogeneous changes of the human arm swivel angle (which represents the upper limb redundancy) are studied under different loading conditions, the effects of which are incorporated into a modified dynamic manipulability ellipsoid model. A new scalar index describing the arm postural stability (APSI) is then proposed. As part of the experimental protocol, ten (10) healthy subjects performed multiple reaching tasks with different weights mounted on the forearm. Kinematic data was collected via a ten-camera motion capture system and the corresponding APSI was calculated for each task. APSI is found to have a strong linear correlation with the swivel angle under loading conditions. Furthermore, the data suggest that the swivel angle may serve as an indicator of arm postural stability and task difficulty. The results of additional experiments conducted with three (3) subjects indicate that the external loads could deteriorate the arm's control performance in tasks like line tracing (root mean square deviation from straight lines). These findings may be applicable to robot-based (exoskeleton) resistance therapy, assist-as-needed gravity compensation, and human-like motion control of humanoid robotic systems.

5.2 Introduction

5.2.1 Background

Among different post-stroke rehabilitation strategies, resistance training like coupled bilateral load exercises have shown positive evidence in improving motor capabilities of the impaired upper limb and additional investigations are needed [PLB04, CCL09]. On the other hand, rehabilitation robots like EXO-UL8 have been developed to automate the training process by providing controllable and repetitive motion [NMK07, BAP13]. Surprisingly, although resistance controllers have been reported in manipulanda-like training devices, no robotic exoskeleton has this feature available [PCR16]. To the authors' knowledge, this is because:

- Unlike manipulanda devices which are manipulated using hands, multi-link exoskeletons usually have multiple contact points with the human arm. The redundancy and temporal/spatial synergies existing in human arm movement bring more uncertainty and complexity.
- Many rehabilitation exoskeletons are originally developed to provide assistance rather than resistance (e.g., pre-defined trajectories). To achieve good human-robot interaction transparency, joint torque output capabilities are often compromised by system backdrivabilities.

Given that both the human arm and exoskeleton have a redundant degree-of-freedom (DOF), one question that needs to be answered for achieving high human-robot transparency in resistance training is whether external resistance changes the natural redundancy resolution strategy of the human arm and thus provides referential information to the exoskeleton controller. Although applications of virtual reality could visualize different force directions, this study, as a starting point, considers external loadings as the only resistance since additional weights deteriorate performance in activities of daily living (ADLs): intuitively, swiping cards, rotating a doorknob, and waving hand become more difficult when a heavy bag is hanging on the arm.

To quantitatively characterize the effect of additional loading, a modified dynamic manipulability ellipsoid is used. Traditionally studied in robotics research, the manipulability models have been applied back to human motion analysis and proven effective. Table 5.1 provides examples of past research ranging from rehabilitation robotics to ergonomics. However, no study on upper limb considered the effect of gravity when using a manipulability model.

Anatomical Interests	Example Studies	Manipulability Models	Resistance	Applications
Upper Limb	Sasaki *et al.*, 2010 [SIM10]	MFE, FP	N	Wheelchair Operations
	Jacquier-Bret *et al.*, 2012 [JGR12]	DME, FP	N	Upper Limb Movement Capabilities
	Tanaka *et al.*, 2015 [TNY15]	HFM	N	Operational Comfort
Lower Limb	Walsh *et al.*, 2006 [WPH06]	N/A	Y(Loads)	Load-Carrying Augmented Exo
	Gordon *et al.*, 2009 [GWK09]	N/A	Y(Loads)	Hip Kinetics & EMG
	Yu *et al.*, 2012 [YL12]	MM, ME	N	Assistive Mechanism Design
Hand/Fingers	Gupta *et al.*, 2008 [GOP08]	MM	N	Wrist Rehabilitation
	Valero-Cuevas, 2009 [Val09]	MFE, FP	N	Neuromuscular Control
	Endo, 2015 [End15]	MM, ME	N	Smartphone Touch Operations

Table 5.1: Examples of Research Using Manipulability Models

5.2.2 Main Contributions

- For the first time, this paper quantitatively discusses the spatial heterogeneity of human arm redundancy resolution (swivel angle) due to gravitational resistance;
- A new scalar arm postural stability index (APSI), is proposed. Its high correlation with swivel angles is observed when additional loads are present. We conjecture that the swivel angle under loading conditions may work as an indicator of arm postural stability/task difficulty.

The rest of the chapter is arranged as: Part II gives detailed mathematical modeling of a 2-link 4-DOF human arm; Part III describes the experiments including two tasks; Part IV provides results and discussion; Part V concludes the paper.

5.3 Modeling

5.3.1 Modified Dynamic Manipulability Ellipsoid

First proposed by Yoshikawa [Yos84], the manipulability measure (MM) and its visualization - the manipulability ellipsoid (ME) have been modified and extended to versions like the "dynamic manipulability ellipsoid (DME)" [CCS92], the "manipulability force ellipsoid (MFE)" [Yos85] and the "manipulability velocity ellipsoid (MVE)" [Chi88]. Considering the effect of loading as well as the relatively low arm moving speed during post-stroke upper limb rehabilitation training, the authors adopted and extended a modified DME model [Chi00], the derivation of which is provided as follows.

First, a serial (with actuators at each joint) manipulator's dynamics could be described as:

$$M(\mathbf{q})_{n\times n}\ddot{\mathbf{q}}_{n\times 1}+\mathbf{c}(\mathbf{q},\dot{\mathbf{q}})_{n\times 1}+\mathbf{g}(\mathbf{q})_{n\times 1}+J^{T}(\mathbf{q})_{n\times m}\mathbf{f}_{m\times 1}=\boldsymbol{\tau}_{n\times 1} \tag{5.1}$$

where the torque vectors $M(\mathbf{q})_{n\times n}\ddot{\mathbf{q}}_{n\times 1}$, $\mathbf{c}(\mathbf{q},\dot{\mathbf{q}})_{n\times 1}$ and $\mathbf{g}(\mathbf{q})_{n\times 1}$ are inertia, Coriolis/centrifugal, and gravity-related terms, respectively. $J^{T}(\mathbf{q})_{n\times m}$ is the transpose of Jacobian matrix linking end-effector force vector $\mathbf{f}_{m\times 1}$ and joint torque vector $\boldsymbol{\tau}_{n\times 1}$. $J(\mathbf{q})_{m\times n}$ also links joint space (n-DOF) velocity with task space (m-DOF) velocity:

$$\dot{\mathbf{x}}_{m\times 1} = J(\mathbf{q})_{m\times n}\dot{\mathbf{q}}_{n\times 1} \tag{5.2}$$

A non-redundant, unconstrained stationary assumption ($m = n, \dot{\mathbf{q}} = \mathbf{0}, \mathbf{f} = \mathbf{0}$) simplifies (1) to (3), and the time derivative of (2) to (4).

$$M\ddot{\mathbf{q}} + \mathbf{g} = \boldsymbol{\tau} \tag{5.3}$$

$$\ddot{\mathbf{x}} = J\ddot{\mathbf{q}} = JM^{-1}\boldsymbol{\tau} + \ddot{\mathbf{x}}_g \tag{5.4}$$

where:

$$\ddot{\mathbf{x}}_g = -JM^{-1}\mathbf{g} \tag{5.5}$$

represents the translation of ellipsoid center away from original end-effector position. To the authors' best knowledge, this translation has never been quantitatively analyzed or applied in previous related research, although it could help determine if the arm wrist is already out of the dynamic manipulability ellipsoid and if making gravity compensation necessary. Details are discussed later in this section. Historically, for simplicity researchers assume that the manipulator's torque capability could be normalized using $\tilde{\boldsymbol{\tau}} = T^{-1}\boldsymbol{\tau}$, $T = diag(\tau_{1,max}, ..., \tau_{n,max})$ as the scaling matrix and represented by a unit sphere (Euclidean norm) in joint space (6) and then a distorted/rotated ellipsoid could be calculated and visualized in task space (7), indicating the feasible acceleration directions and magnitudes.

$$\tilde{\boldsymbol{\tau}}^T\tilde{\boldsymbol{\tau}} \leq 1 \tag{5.6}$$

$$(\ddot{\mathbf{x}} + JM^{-1}\mathbf{g})^T J^{-T} Q J^{-1} (\ddot{\mathbf{x}} + JM^{-1}\mathbf{g}) \leq 1 \tag{5.7}$$

where:

$$Q = MT^{-2}M \tag{5.8}$$

In this study, the 2-link 2-DOF non-redundant robotic manipulator model example in [CCS92] is extended to a 2-link 4-DOF redundant human arm model, and an index indicating the arm postural stability is later proposed in II. B.

Illustrated in Figure 5.1, following the Y-X-Z rotation order at the center of the (right) shoulder, the elbow and wrist joint positions $P = [\mathbf{P_e}, \mathbf{P_w}]$ are calculated in the base frame (9), with

q_1 to q_4 representing shoulder extension(+)/flexion(-), shoulder adduction(+)/abduction(-), shoulder internal(+)/external(-) rotation, and elbow extension(+)/flexion(-), respectively. L_1 and L_2 represent the lengths of upper arm and forearm respectively. For simplicity, $c\cdot := cos(q\cdot)$ and $s\cdot := sin(q\cdot)$:

$$P = \begin{bmatrix} -s1c2L_1 & -(s1s2s3+c1c3)s4L_2 - s1c2(L_1+c4L_2) \\ s2L_1 & -c2s3s4L_2 + s2(L_1+L_2c4) \\ -c1c2L_1 & -(c1s2s3-s1c3)s4L_2 - c1c2(L_1+c4L_2) \end{bmatrix} \tag{5.9}$$

Due to the redundancy, the dynamic manipulability ellipsoid (10) uses a weighted pseudoinverse of Jacobian $J_Q^\dagger = Q^{-1}J^T(JQ^{-1}J^T)^{-1}$ (with $J_{3\times 4}$ detailed in Appendix):

$$(\ddot{\mathbf{x}} + JM^{-1}\mathbf{g})^T J_Q^{\dagger^T} Q J_Q^\dagger (\ddot{\mathbf{x}} + JM^{-1}\mathbf{g}) \leq 1 \tag{5.10}$$

This represents the modified dynamic manipulability ellipsoid for a redundant 2-link 4-DOF human arm in its 3-DOF task space. Any vector starting from the wrist and ending within the ellipsoid visualizes an acceleration (with magnitude and orientation) that the arm could achieve. As the ellipsoid center moves under loading conditions (5.5), once large enough loads are applied to the arm the ellipsoid no longer encompasses the wrist. In this case, the wrist loses the ability to move in at least half of the directions, and the arm configuration is theoretically no longer stable. To quantify the change from stable (no loads, ellipsoid centers at the wrist) to unstable (large loads, ellipsoid no longer encompasses the wrist), we propose a scalar index below.

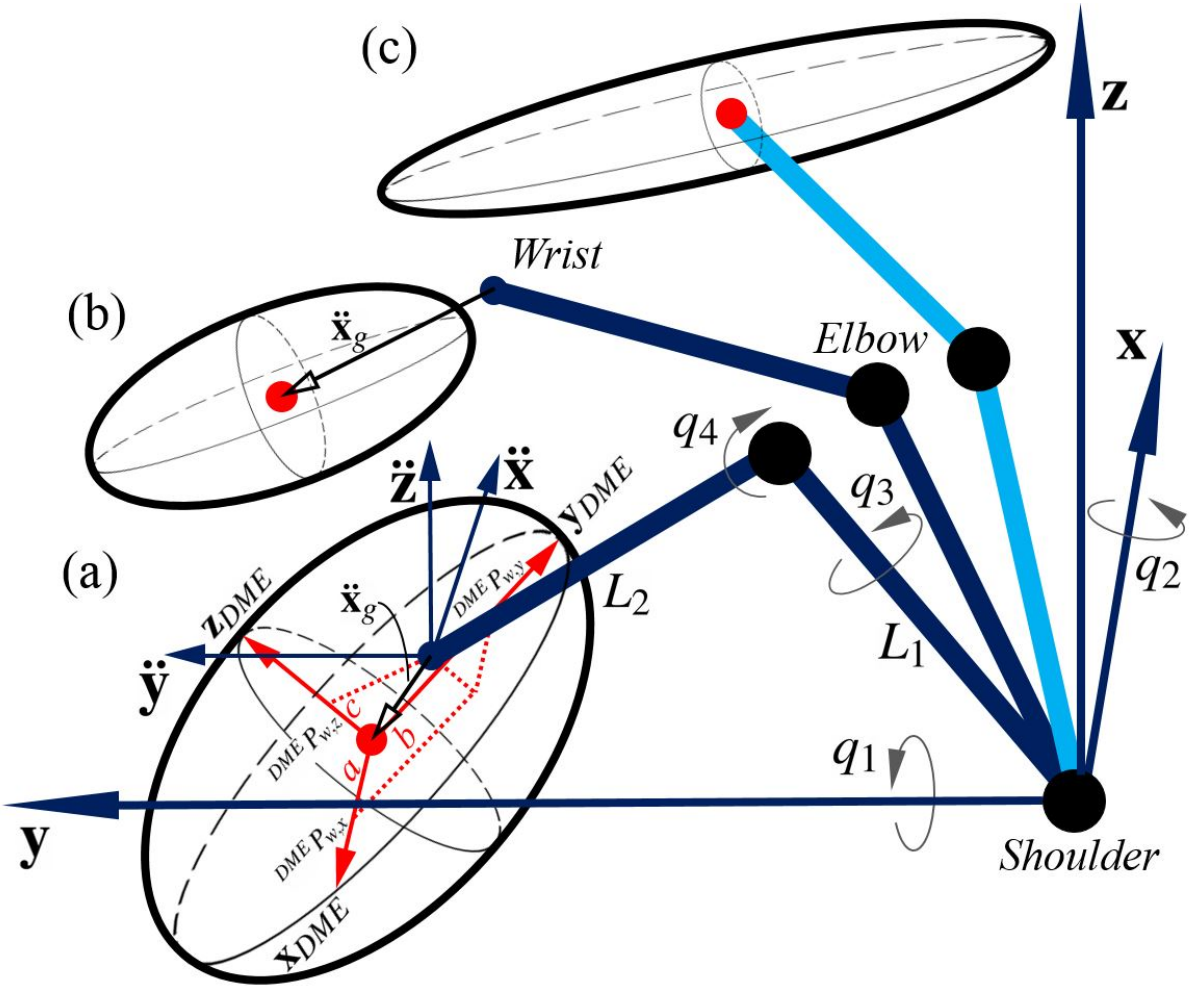

Figure 5.1: The DMEs of a 2-link 4-DOF arm: (a) with loading, $0 < APSI < 1$; (b) with loading, $APSI \leq 0$; (c) no loading, $APSI = 1$. A local coordinate system for DME is built on $\mathbf{x}_{DME}$, $\mathbf{y}_{DME}$ and $\mathbf{z}_{DME}$, along major, intermediate, and minor axes respectively. The DME's size/orientation/position change with arm configurations and loading.

5.3.2 Arm Postural Stability Index (APSI)

A singular value decomposition (SVD) on the core of (5.10), $N = J_Q^{\dagger^T} Q J_Q^{\dagger}$ provides three eigenvalues ($\sigma_{1,2,3}$, which determine the ellipsoid size and volume used as traditional manipulability measure) and the corresponding eigenvectors which determine the ellipsoid orientation. Using the translation equation (5.5), any arm configuration is labeled with a scalar index $\in (-\infty, 1]$ shown below (5.11). The index is proposed to quantify arm postural stability (i.e., APSI) when loads are present:

$$APSI = 1 - \sqrt{({}^{DME}P_{w,x}/a)^2 + ({}^{DME}P_{w,y}/b)^2 + ({}^{DME}P_{w,z}/c)^2} \tag{5.11}$$

where $a = 1/\sqrt{\sigma_1}$, $b = 1/\sqrt{\sigma_2}$ and $c = 1/\sqrt{\sigma_3}$ are the semi-axis lengths of the DME. The wrist position in the DME coordinate frame, ${}^{DME}\mathbf{P_w}$ is calculated by (5.12):

$${}^{DME}\mathbf{P_w} = R^{-1}(-\ddot{\mathbf{x}}_g) = -R^{-1}JM^{-1}\mathbf{g} \tag{5.12}$$

where $R_{3\times3}$ is a rotational matrix based on the eigenvectors of N. Geometrically, the APSI represents the normalized distance to the ellipsoid boundary. If $APSI \leq 0$ (Figure 5.1(b)), the configuration is theoretically unachievable or unstable as the wrist position is out of the ellipsoid and only a small portion of feasible acceleration directions is left. If $0 < APSI < 1$ (Figure 5.1(a)), the wrist is within the ellipsoid and thus the configuration is achievable. As the $APSI$ gets closer to 1, the arm is supposed to have higher postural stability, e.g., $APSI = 1$ in Figure 5.1(c), when loading is not considered. Notice that the units of the DME coordinate system are different from those of the Cartesian one. For visualization purposes, the DME coordinate system is scaled. Therefore, one could tell if the DME encompasses the wrist only by the method given in (5.11), rather than by visual comparison.

5.3.3 Parameter Estimation

To reduce interference in natural arm movement, loads will be applied on the forearm only, with the center of mass (CoM) located L_{c2} from the elbow. The upper arm and forearm masses are m_1 and m_2 respectively. Estimated from [SIM10, PEA83]: $L_{c2} = 0.3m$, $m_1 = 2.44kg$, $m_2 = 1.40kg$, $T = diag(35, 50, 30, 20)Nm$. Based on [PRB07], the anatomical joint angles (in deg) are limited by: $q1 \in [-120, 0]$, $q2 \in [-100, 20]$, $q3 \in [-40, 60]$, and $q4 \in [-130, -10]$.

5.4 Experiment

5.4.1 Subjects

Ten (three females and seven males) healthy, right-handed adults participated (mean ± s.d.; age: 22.50 ± 2.59y, weight: 66.70 ± 8.31kg, height: 174.60 ± 8.30cm). All ten accomplished Task I; three of ten (#1-male, #2-female, #7-female) were randomly selected to accomplish the additional Task II.

5.4.2 Setup

Figure 5.2(a) provides an overview of the experiment setup. Based on the subjects' average range of motion (ROM) in the task space, the targets are evenly positioned in a reachable 3×3 matrix, parallel to the subject's frontal plane, at two different distances (*close* and *far*), marked on the ground (same to all subjects). The subject, wearing reflective markers on hand, elbow and shoulder, is asked to sit against the backrest of an armless chair to constrain the movement of his/her trunk. 3-D kinematics of the right upper limb is recorded at 100Hz by ten cameras of a motion capture system (Vicon, UK).

5.4.3 Task I (Reach-Out Arm Posture)

Redundancy resolution remains an open question, especially when with loads. Illustrated in Figure 5.2(b), if one keeps the shoulder and wrist positions unchanged, s/he could still change the elbow position to some extent, along a circle perpendicular to a line connecting the shoulder and wrist. This redundant DOF, represented by an angle swiped by the elbow and starting counterclockwise from the zero point where the elbow is lowest in Cartesian space, is called "swivel angle". Each subject is loaded with three different weights: 0, 2.72, and 4.54kg (= 0, 6, and 10lb). This is done by wrapping weight adjustable sandbags (CAP Barbell, USA) on the subject's forearm. The subject is asked to rest his/her right arm on his/her lap and once s/he receives a "start" instruction, reach and touch the target with a stylus (gripped between forefinger and middle finger) using elbow and shoulder movements only, hold for 3 seconds and rest the arm back. After a 10-second-break, the subject moves to the next target and repeats the above until all nine targets are touched. A different load is then applied. Once all three loads are tested, the subject moves to the other distance. The swivel angles at the targets are individually calculated, based on the marker positions. After each session, a 10-min-break is provided.

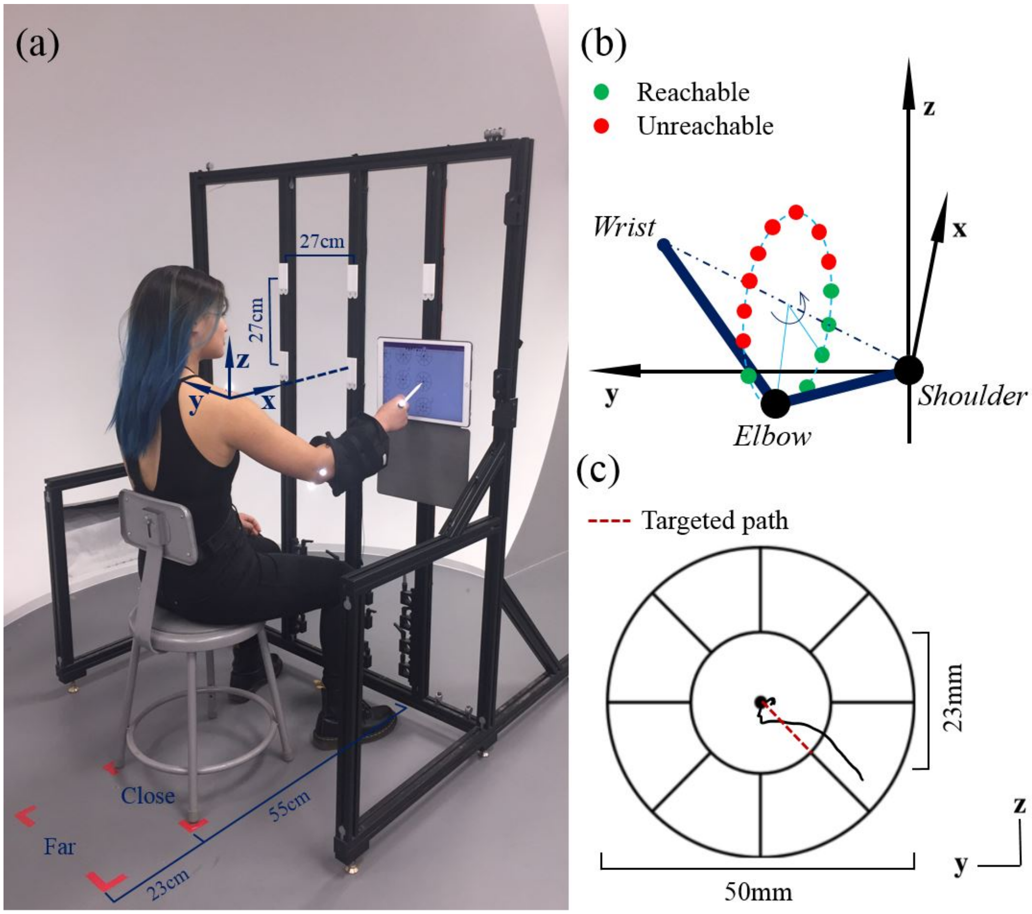

Figure 5.2: (a) Experiment setup: one subject is using a stylus to accomplish Task I & II, the targets (white) are positioned so that the x-axis on right shoulder points to the center of 3×3 target matrix; (b) Swivel angle (Task I): looking from shoulder to wrist, positive swivel angle starts from lowest elbow position counterclockwise (i.e., elbow rotates away from the body); (c) Target (center) and sub-tasks (Task II): the subject has finished the subtask from center to (0,-1,-1) direction. The targeted path is later added for image processing and not shown to subjects. The deviation is calculated from the center to inner circle only.

5.4.4 Task II (Arm's Control Performance in Drawing Task)

Similarly, with two different loads: 0 and 2.72kg (= 0 and 6lb), the subjects are asked to reach and touch the target using the same stylus as described in Task I. The difference is, once the target is reached, the subject is asked to draw a line segment from the target center to any sub-target marked along the inner circle of the target (Figure 5.2(c), 23mm in diameter), every 45 degrees. Then the stylus goes back to the center without drawing anything, and repeats the drawing task to another sub-target until all eight sub-targets are connected to the center. The subtasks are done in the subject's preferred order. The images drawn on the tablet are recorded and synchronized to a PC instantly via OneNote (Microsoft, USA). In this way, each sub-task could be studied individually even if visually overlap together. The post-processing work on the images is done using MATLAB (MathWorks, USA). All the procedures above have been conducted twice to obtain averaged results.

5.5 Results & Discussion

Four aspects of upper limb movement under loading conditions are quantitatively analyzed and discussed: *manipulability*, *redundancy resolution* (i.e., swivel angles), *swivel angles vs. APSI*, and *arm's control performance*.

5.5.1 Manipulability

First, to clearly demonstrate the effects of additional loads, a subject's kinematics data at 3×3 targets, *far* distance, under two different loads of 0 and 2.72kg (= 0 and 6lb) is processed and illustrated in Figure 5.3. Increasing the load shrinks the ellipsoid size (manipulability measure), but also changes axes orientation and center position. The results support the intuition that an arm with additional loads would be more difficult to move, especially in some directions.

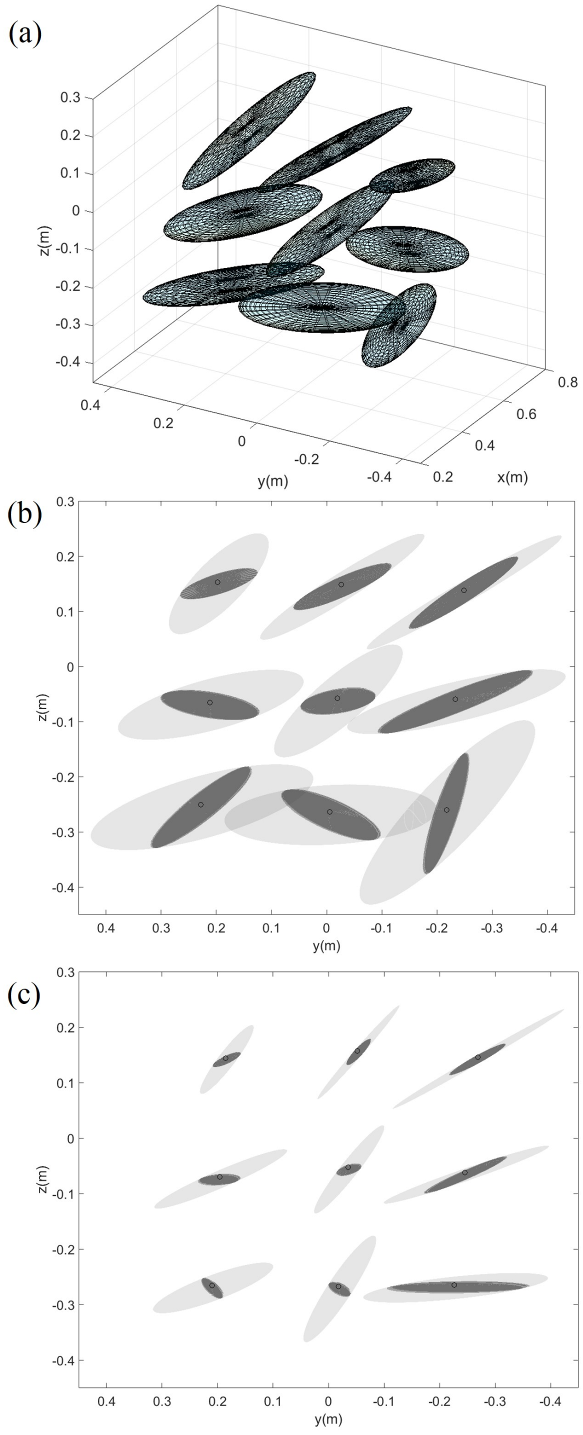

Figure 5.3: A subject's DMEs at 3×3 targets (*far* distance, $x \approx 0.5m$): (a) 0kg, 3D view; (b) 0kg, y-z view; (c) 2.72kg (6lb), y-z view. In (b) and (c), small circles show wrist positions, and DMEs' y-z projections are in light gray while DMEs' cross-sections at $x \approx 0.5m$ are in dark gray.

5.5.2 Swivel Angles

Effects of loading on redundancy resolution could be demonstrated by the change in swivel angles. Figure 5.4 provides the swivel angle data obtained from Task I, for all ten subjects. Two 3×3 plots (a) and (b) illustrate the data at *far* and *close* distances, respectively. Each subplot (a small square) shows all ten subjects' swivel angles at that specific target, under three different loads of 0, 2.72, and 4.54kg (= 0, 6, and 10lb). Note that as shown in Figure 5.2(a), the shoulder position points to the center of 3×3 targets.

A linear regression analysis is performed in Figure 5.4, and it shows a consistent but counter-intuitive trend at all target positions that adding loads will increase swivel angles. It means when adding loads, the elbow position will be elevated. The authors conjecture that as more effort is made during the shoulder flexion, a multi-joint synergy is activated.

Another observation from the data is the spatial heterogeneity of linear regression coefficients (slope and intercept) which is detailed in Figure 5.5. The swivel angles at the top-right targets have the highest increasing rate (slope, deg/kg) when adding loads (*far*: 3.91, *close*: 3.80), while the lowest slope appears at the bottom-left (*far*: 0.84, *close*: 0.93). This distribution in task space may be due to the obstacle (human body) collision avoidance: when the wrist is at top-right target the arm has much more swivel freedom than at bottom-left.

The other coefficient, intercept is actually the swivel angle when no loading is applied. The top-left targets always have the highest intercept (deg) (*far*: 30.37, *close*: 35.45), while the lowest zero-load swivel angle for the *far* posture appears at the top-right (13.06) but shifts to the middle-right for *close* posture (13.63). This, similarly, could also be explained by obstacle collision avoidance.

(a) *far*

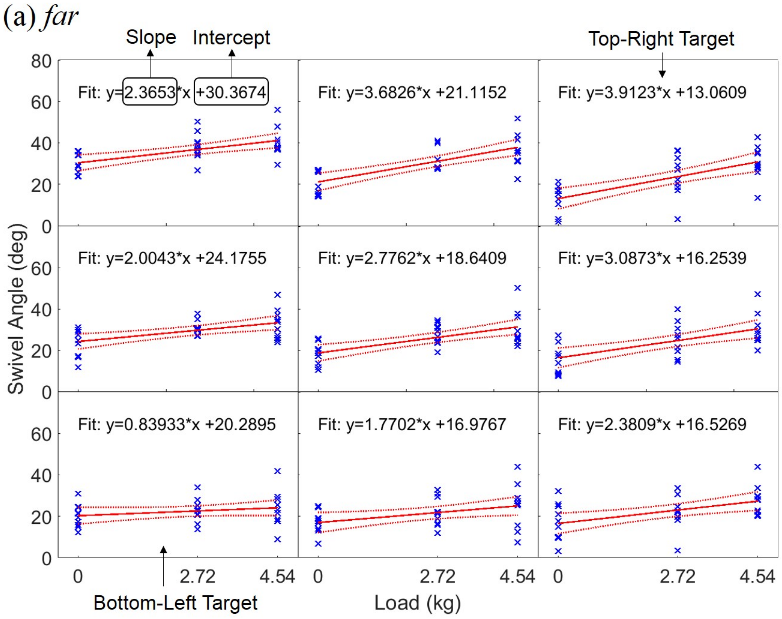

(b) *close*

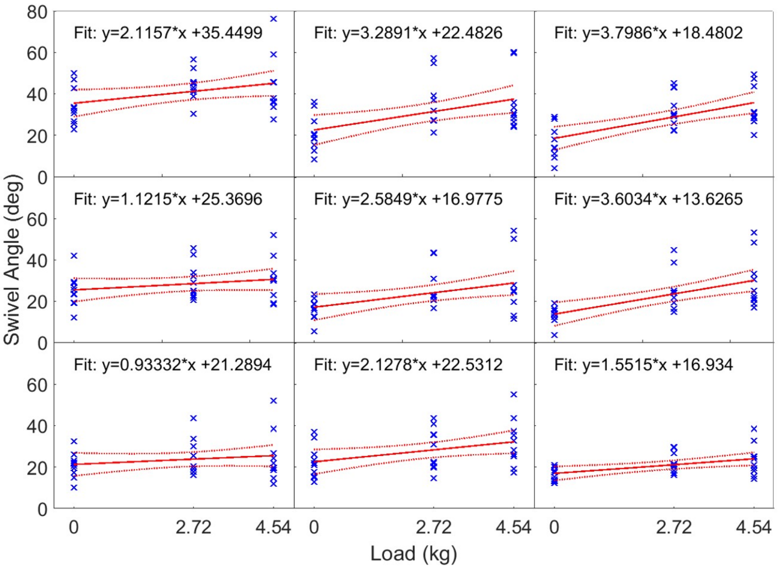

Figure 5.4: Swivel angles of all ten subjects at 3×3 targets loaded with 0, 2.72 and 4.54kg: (a) *far* reach-out postures; (b) *close* reach-out postures. Cross dots with the same x value represent measured data from all ten subjects under each load, and dotted lines show a 95% confidence boundary.

(a) *far*

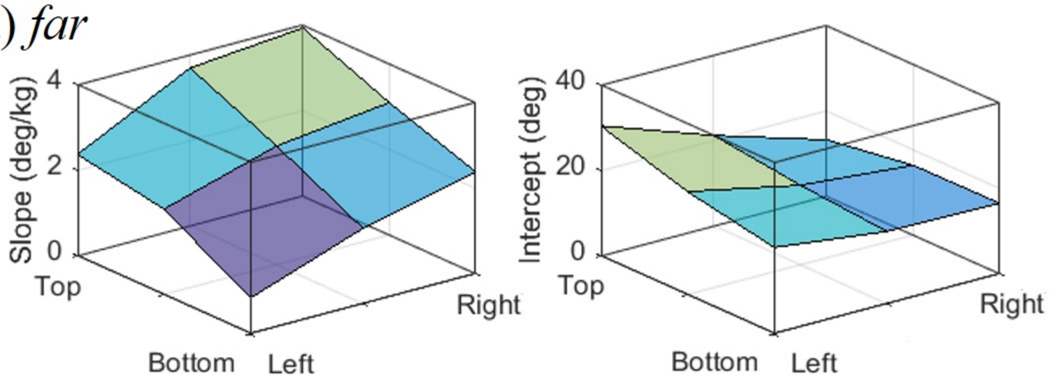

(b) *close*

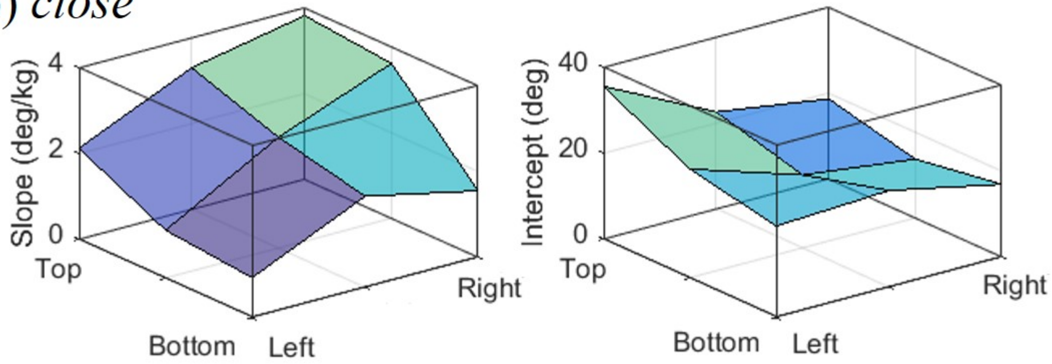

Figure 5.5: Linear regression analysis from Figure 5.4 shows that the swivel angle increasing rate (i.e., slope) is highest at top-right and lowest at bottom-left, for both (a) *far* and (b) *close* reach-out postures; while the swivel angle with no loading (i.e., intercept) is always at top-left.

5.5.3 Swivel Angles vs. APSI

(a) *far*

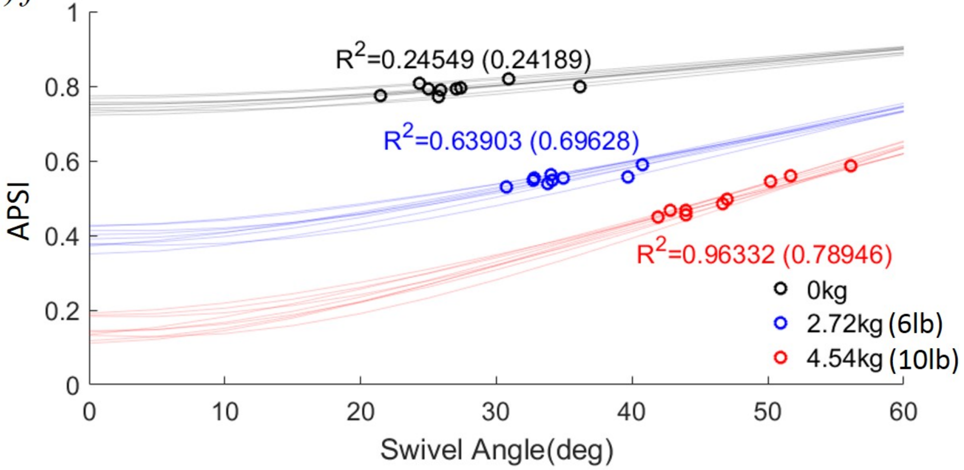

(b) *close*

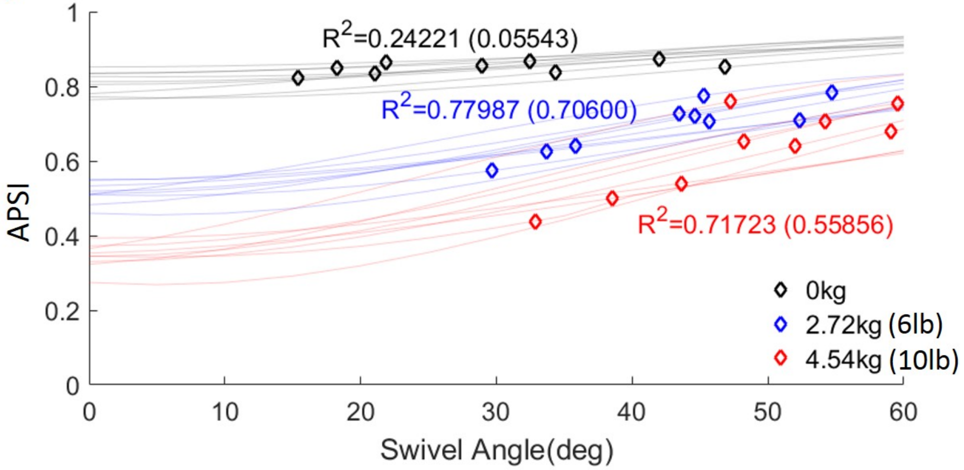

Figure 5.6: Measured swivel angles at (a) *far* and (b) *close* reach-out postures and calculated APSI have a high correlation, with large loads. In other words, with large loads the swivel angle may work as a quantitative tool to differentiate spatial targets in postural stability. As the load increases, the average *APSI* decreases. Distribution of measured data at *far* distance is more concentrated. Circles and diamonds are experimental data, lines are computational data.

As pointed out in 5.5.2, adding loads will increase swivel angles, but one may wonder if this change in the swivel angle necessarily indicates a more instable situation. This could be explained by APSI. Figure 5.6 illustrates the results from one subject to show the relationship between the swivel angle and APSI. For each swivel angle measured, the corresponding APSI is calculated and plotted as a “circle” $\circ$ in (a) *far* or a “diamond” $\diamond$ in (b) *close*. As mentioned above, with one’s wrist and shoulder fixed, the elbow could still move along a circle by changing the swivel angle. The swivel angles in this feasible range (but not actually chosen by the subject) and the corresponding APSI values are plotted and connected as individual lines via each measured data point. Under each loading condition, the R^2 value (the median of ten subjects’ in brackets) from linear regression of measured swivel angle and corresponding APSI value are added to the plots.

Computationally, although both the swivel angle and its corresponding APSI are calculated very nonlinearly, there is a highly linear correlation between them, especially for *far* reach-out postures. Experimentally, higher R^2 values and a more concentrated swivel angle distribution are observed in the *far* reach-out posture than in the *close* one. Thus swivel angles under loading conditions may work as an indicator of the task difficulty.

5.5.4 Arm’s Control Performance

The goal of additional Task II is to find if APSI or swivel angle could explain the arm’s control performance in tasks where movement is involved.

Shown in Figure 5.2(c), the root mean square (RMS) deviation of each drawing stroke from the targeted path is calculated as $d_{RMS} = \sqrt{({d_1}^2 + {d_2}^2 + ... + {d_n}^2)/n}$, where d_i is the distance between a sampled point on the stylus stroke and the targeted path, n is the number of samples from target center to subtask inner circle. The RMS values for eight subtasks are averaged and its relationship with loads and distances are shown in notched boxplots in Figure 5.7, which provides the data from three subjects who participated in Task II. It is found that extra loads at the *far* reach-out posture result in higher average RMS values of drawing deviation, indicating a deterioration of arm’s control performance. However, no significant correlation is observed between arm’s control performance and the proposed APSI, or swivel angles.

To further understand the information embedded in the data, a three-way analysis of variance (ANOVA) is performed and p-values are illustrated in Figure 5.8, where $p < 0.05$ is shown in black. Based on the three-way ANOVA, the p-value distributions in Figure 5.8 show that (a) load

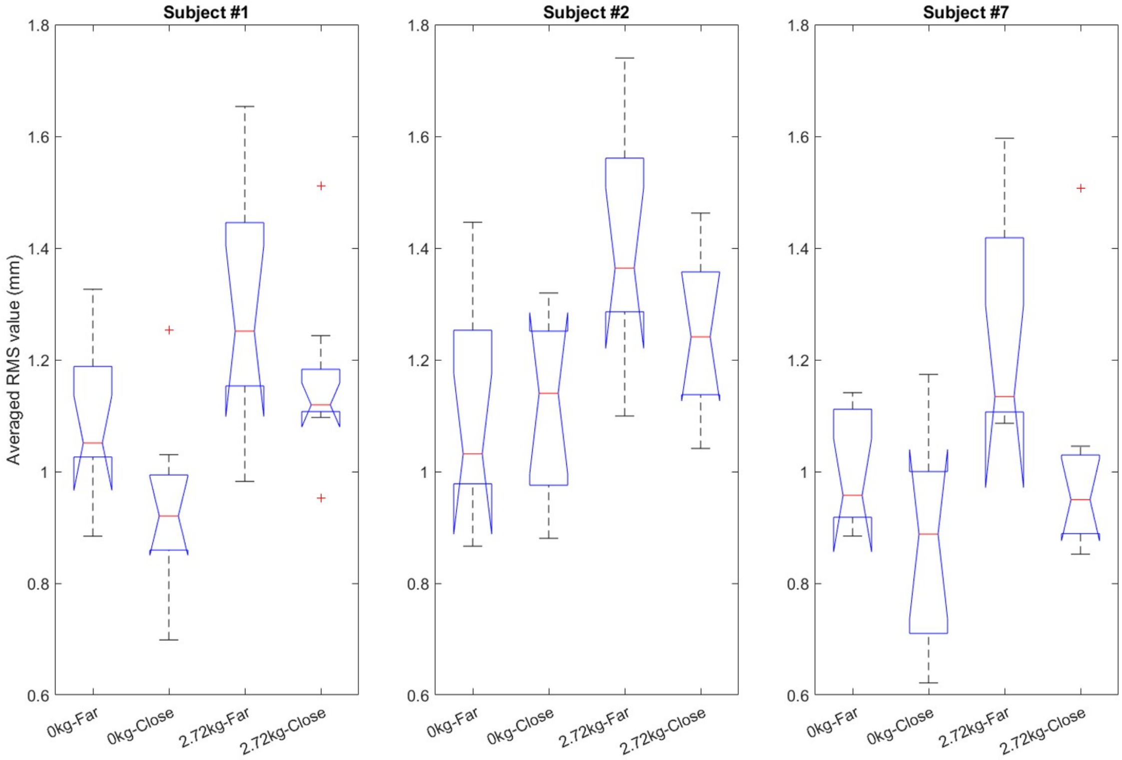

Figure 5.7: Subject #1, #2 and #7: Drawing deviation (in averaged RMS value) versus loading and distance, in notched boxplots. A higher averaged RMS value indicates poorer arm's control performance.

significantly influences the performance in most targets, but (b) the distance between the subject and target plane does not, statistically, play a strong role in more than half of the targets. This might be due to the human arm's inherent tremor, when no additional load is present. No significant difference is observed among subjects, except at the bottom-left targets. The authors consider that the possible arm-body collision avoidance strategy dominates here.

5.5.5 Model Simplifications in the Study

In this study, for computational efficiency a dynamical manipulability ellipsoid (DME) model was chosen although a force polytope (FP) model that uses a hypercube joint torque constraint may better describe the heterogeneity of arm capabilities in space [FGR98]. Also, since joint torque capabilities change with joint angles, a **q**-dependent T matrix might be more accurate [SIM10].

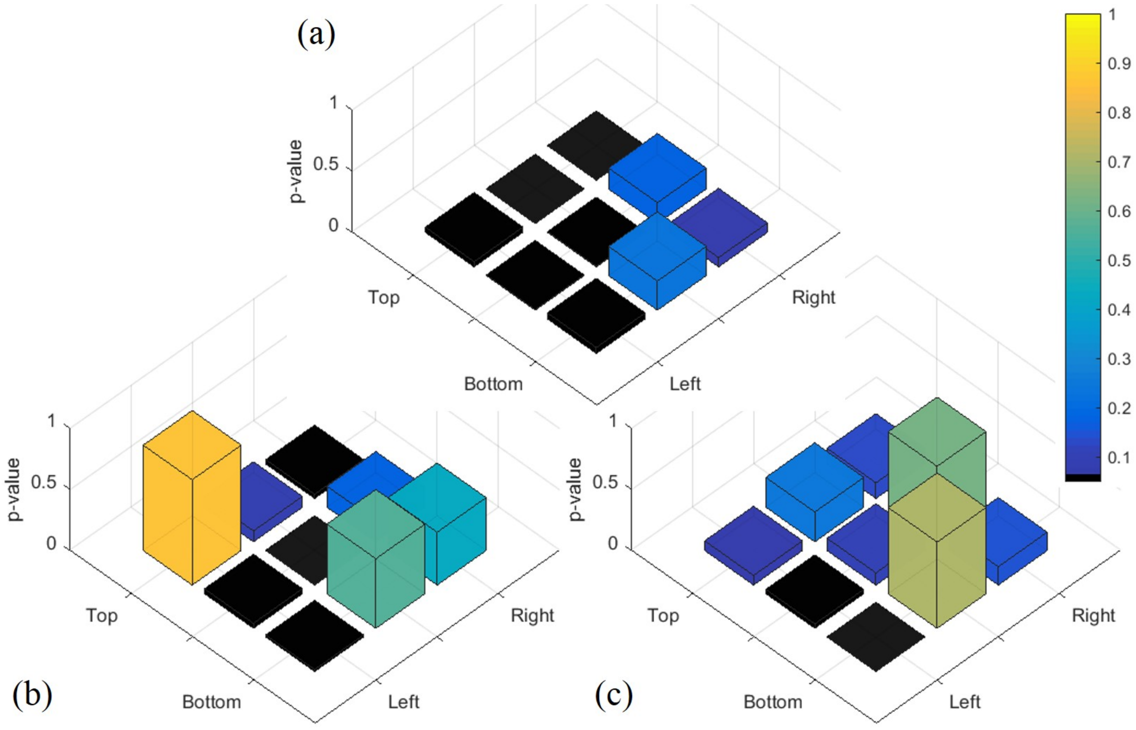

Figure 5.8: P-values vary in 3×3 targets and black squares mean $p < 0.05$: (a) Load statistically influences arm control performance in most targets, concentrated at top-left; (b) Distance statistically influences arm's control performance in four out of nine targets; (c) Difference in subjects changes performance significantly in only two bottom-left targets.

5.6 Conclusion & Future

In this chapter, the human arm redundancy resolution under gravitational loading conditions is quantitatively studied. Additional loading does change the arm's movement in several aspects like manipulability and redundancy resolution strategy. A new scalar index describing the arm postural stability (APSI) is proposed and the authors conjecture that swivel angle may work as an indicator of the arm postural stability and task difficulty. The load-induced effects observed in this study may lend important referential information for designing force and position controllers of redundant robotic exoskeleton systems used for resistance rehabilitation training and assist-as-needed gravity compensation. The model and findings may also be extended to general humanoid research and applications including human-like motion controller design.

5.7 Appendix: Details of the Jacobian Matrix $J_{3\times4}$

Each entry of the non-square Jacobian matrix $J_{3\times4}$ is provided below.

$$j_{11} = s1c3s4L_2 - c1s2s3s4L_2 - c1c2L_1 - c1c2c4L_2 \tag{5.13}$$

$$j_{12} = -s1c2s3s4L_2 + s1s2L_1 + s1s2c4L_2 \tag{5.14}$$

$$j_{13} = c1s3s4L_2 - s1s2c3s4L_2 \tag{5.15}$$

$$j_{14} = -c1c3c4L_2 - s1s2s3c4L_2 + s1c2s4L_2 \tag{5.16}$$

$$j_{21} = 0 \tag{5.17}$$

$$j_{22} = s2s3s4L_2 + c2L_1 + c2c4L_2 \tag{5.18}$$

$$j_{23} = -c2c3s4L_2 \tag{5.19}$$

$$j_{24} = -c2s3c4L_2 - s2s4L_2 \tag{5.20}$$

$$j_{31} = s1s2s3s4L_2 + c1c3s4L_2 + s1c2L_1 + s1c2c4L_2 \tag{5.21}$$

$$j_{32} = -c1c2s3s4L_2 + c1s2L_1 + c1s2c4L_2 \tag{5.22}$$

$$j_{33} = -c1s2c3s4L_2 - s1s3s4L_2 \tag{5.23}$$

$$j_{34} = -c1s2s3c4L_2 + s1c3c4L_2 + c1c2s4L_2 \tag{5.24}$$

CHAPTER 6

Virtual Reality: Environment, GUIs, and Serious Games

6.1 Overview

Virtual reality was used to provide a quantitative environment for collecting data as well as for physical therapists to give instructions in the task space. Instead of using proprietary software developed by others, we developed a set of eighteen (18) serious virtual reality games for post-stroke rehabilitation training. Although there are discussions on the effectiveness of virtual-reality-based rehabilitation training, we believe that to our exoskeleton system, the virtual reality environment is an indispensable interface for giving patients instructions.

To enable the future incorporation of haptics into virtual reality training, we chose the open source haptic/graphics framework/C++ libraries, CHAI3D [CBB03], for prototype development. A similar version is under development on Unity platform.

6.2 Graphical User Interface Design

Microsoft Foundation Class Library (MFC) was used for developing graphical user interfaces (GUIs). Hierarchically, there are three different customized GUIs:

The first GUI is for physical therapists to choose a game and basic setting at a high level (Figure 6.1). In ”GAMES” section, the physical therapist, every time, could select up to one game, which is categorized in “STATIC” or “DYNAMIC” (depends on whether there are moving objects), and “1D”, “2D”, and “3D”. In “ARMS CONFIG”, the physical therapist, could select either of the four modes: left arm only, right arm only, left controls right, or right controls left. Subject information could be added for profiling and personalized training.

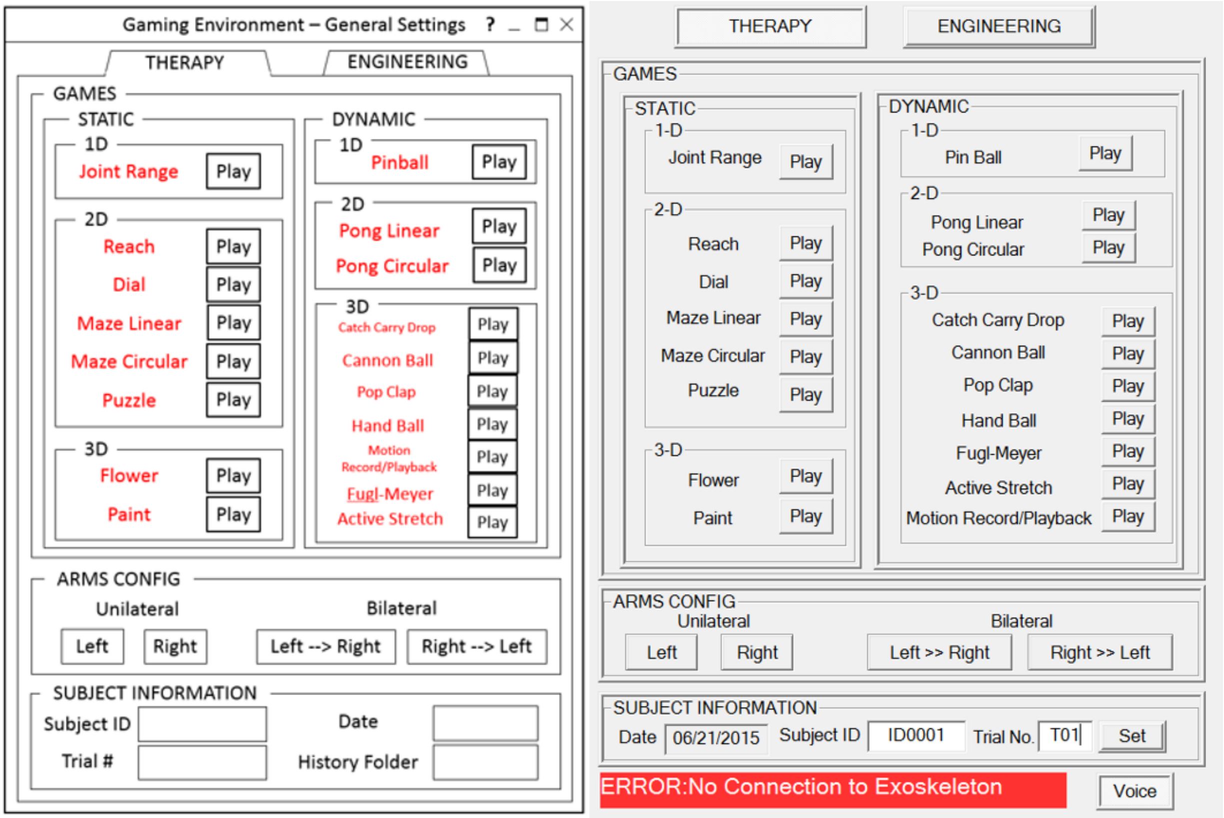

Date 06/21/2015 Subject ID ID0001 Trial No. T01

ERROR:No Connection to Exoskeleton

Figure 6.1: GUI for physical therapists. Left: design; Right: implementation.

The second GUI is for engineers to do reliability and maintenance work (Figure 6.2). In "PC CONFIG", engineers could check the connection status; in "ARM DATA", all position and F/T sensors' readings would be reflected in real-time.

The third (group of) GUI (Figure 6.3) allows the game setting change in various aspects. In "OPERATION", time limit/start/pause/stop/exit/demo could be selected; in "CONFIGURATION", multiple predefined levels with different difficulty levels could be selected; in "CAMERA SETTINGS", first-person or third-person view could be selected; along with a real-time completion status for the player.

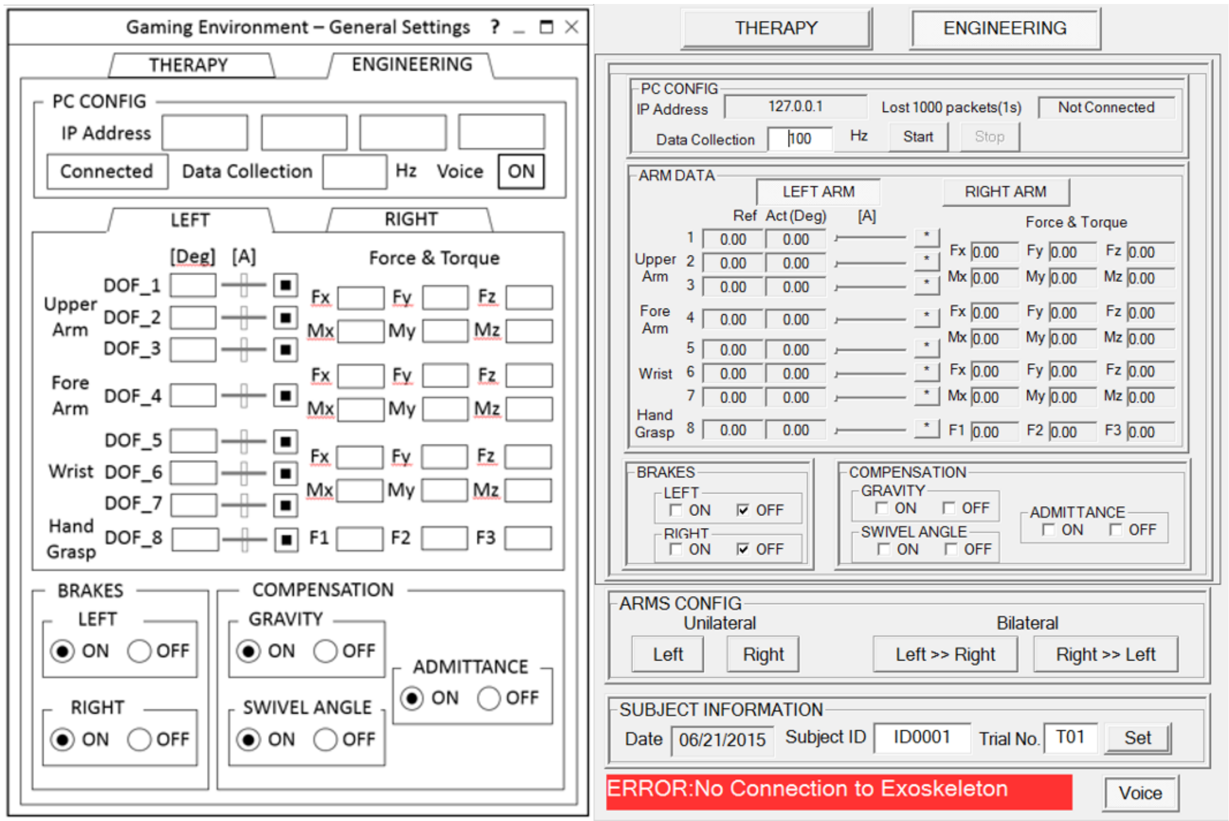

IP Address 127.0.0.1 Lost 1000 packets(1s) Not Connected

Data Collection 100 Hz

BRAKES: LEFT ☐ ON ☑ OFF; RIGHT ☐ ON ☑ OFF

Date 06/21/2015 Subject ID ID0001 Trial No. T01

ERROR:No Connection to Exoskeleton

Figure 6.2: GUI for engineers. Left: design; Right: implementation.

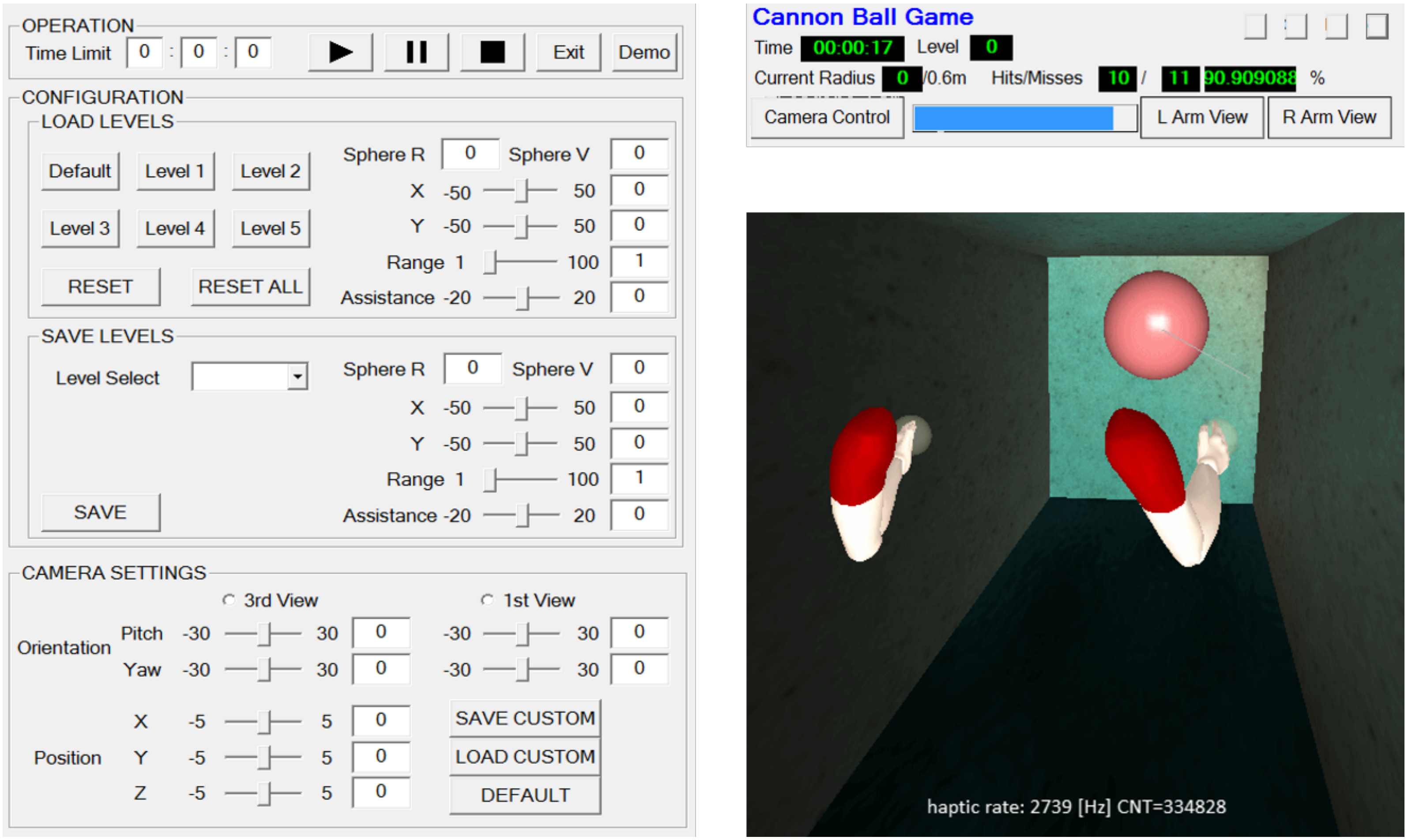

OPERATION
Time Limit 0 : 0 : 0

CONFIGURATION
LOAD LEVELS
Sphere R 0
Sphere V 0
X -50 50 0
Y -50 50 0
Range 1 100 1
Assistance -20 20 0

SAVE LEVELS
Level Select
Sphere R 0
Sphere V 0
X -50 50 0
Y -50 50 0
Range 1 100 1
Assistance -20 20 0

CAMERA SETTINGS
○ 3rd View
Orientation Pitch -30 30 0
Orientation Yaw -30 30 0
Position X -5 5 0
Position Y -5 5 0
Position Z -5 5 0
○ 1st View
Pitch -30 30 0
Yaw -30 30 0

Cannon Ball Game
Time 00:00:17
Level 0
Current Radius 0 /0.6m
Hits/Misses 10 / 11 90.909088 %

haptic rate: 2739 [Hz] CNT=334828

Figure 6.3: Left: GUI for game setting; Top-right: feedback interface during the game; Bottom-right: game view.

6.3 Serious Games Design

Shown in Figure 6.4 provides an overview of most of the serious games we designed. The details of each following game are illustrated in the Appendix of this chapter:

6.3.1 Joint Range

Shown in Figure 6.7. This preliminary step is conducted to measure capable range for each joint, followed by games. The capable workspace of each DOF is visualized in 3D space.

6.3.2 Reach

Shown in Figure 6.8. The goal of this game is to knock all balls off along some predefined trajectories. When the balls are touched by the virtual avatar controlled by the subject, the balls would change color and fall off. Multiple arm DOFs could be trained using this game, in both unilateral and bilateral (mirror-image) modes. It could be played in both "swipe" and "grasp" (needs extra grasping movement while touching the target) modes.

6.3.3 Dial

Shown in Figure 6.9. This game is inspired by phone dialing, one of the activities of daily living. The goal is to dial the required number by touching/grasping number pad in the right order. Similar to the "Reach" game, this game could be played in both unilateral and bilateral, swipe and grasp modes.

6.3.4 Maze Linear

Shown in Figure 6.10. The goal of this game is to touch/grasp all small balls hiding in the maze in the right order. When the subject is moving his/her hand in the virtual maze, s/he is basically doing repetitive arm movements, but in a more engaged way. Similarly, the game could be played in both unilateral and bilateral, swipe and grasp modes. However, in reality it is rather challenging.

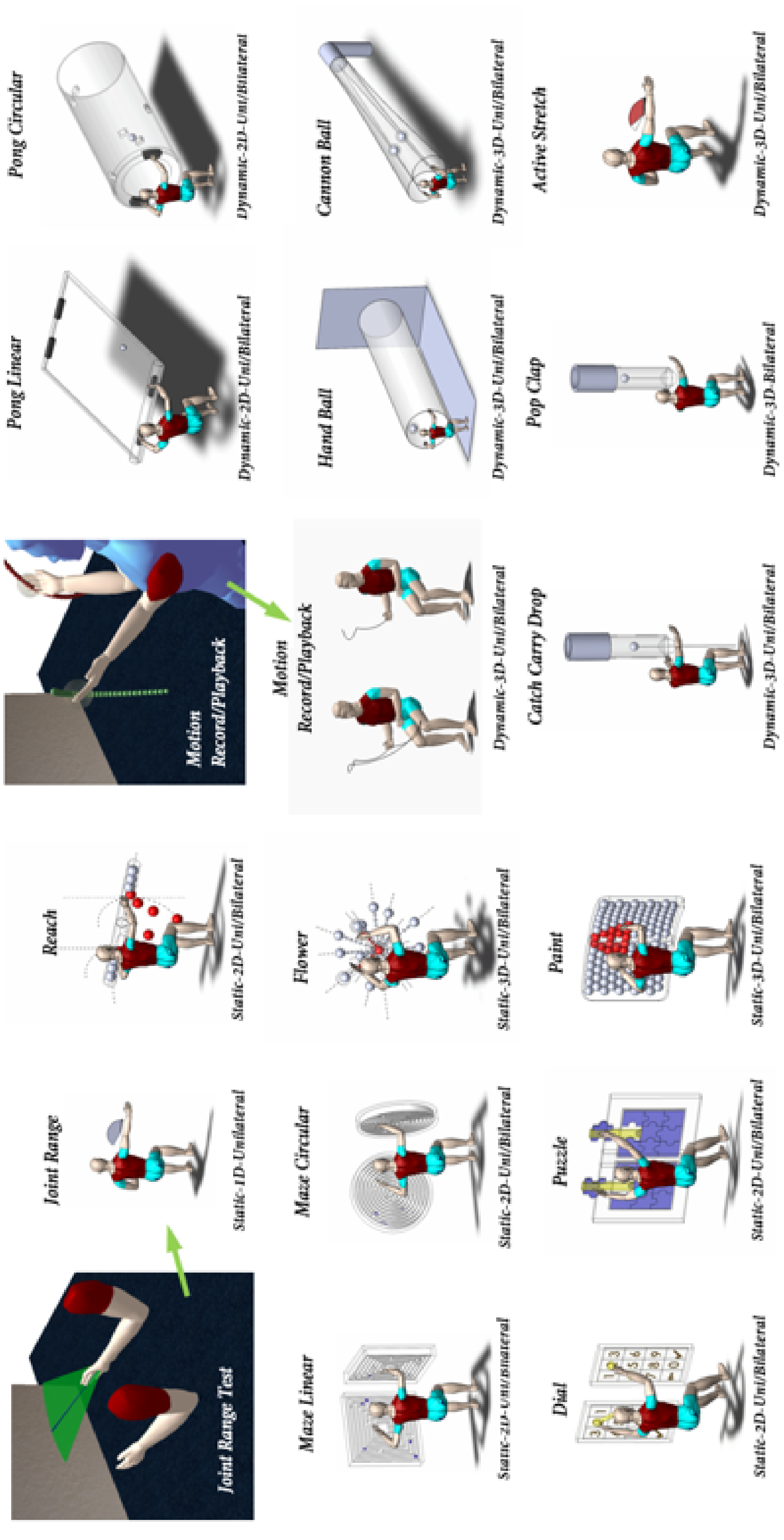

Figure 6.4: A collection of all virtual reality games.

6.3.5 Maze Circular

Shown in Figure 6.11. Similar to "Maze Linear" game, the maze is designed to be circular.

6.3.6 Puzzle

Shown in Figure 6.12.The goal of this game is touch/grasp parts and move them into a complete jigsaw board. It is expected that both cognitive capability and upper-limb mobility could be challenged in this game. Unilateral/bilateral, swipe and grasp modes are all feasible for this game.

6.3.7 Flower

Shown in Figure 6.13. Similar to the "Reach" game, this game requires the player to touch/grasp all the balls along the same flower branch line, then branches will form a 3D flower. Specific subtasks could be skipped if too much time is spent in that direction. Unilateral/bilateral, swipe and grasp modes are all feasible for this game.

6.3.8 Paint

Shown in Figure 6.14. Unlike "Reach" and "Flower" games, this game provides the player some flexibility in determining the target order, while it has a similar goal: touch/grasp all the balls along the painting wall, painted part will turn into red. This game is highly welcome by the users, and we assume the "continuous" visual feedback helps.

6.3.9 Pinball

Shown in Figure 6.15. The goal of this game is to stay alive in the traditional pinball game by moving one of the joints. Therefore, the game could be used to train a specific DOF, e.g., the pedal's angle could be coupled with someone's elbow flexion/extension. The game could be played in either unilateral or (asymmetric) bilateral mode, but only in swipe mode.

6.3.10 Pong Linear

Shown in Figure 6.16. The goal of this game is to stay alive in the traditional ping pong game by moving pedals. Unilateral or (asymmetric) bilateral mode is feasible, but only in swipe mode.

6.3.11 Pong Circular

Shown in Figure 6.17. Similar to “Pong Linear”, the end-effector’s movement is changed from 1-D to 2-D.

6.3.12 Catch Carry Drop

Shown in Figure 6.18. The goal of this game is to touch the falling ball at the right time, grasp it, drop it at the right time. Both unilateral and bilateral, swipe and grasp modes are feasible.

6.3.13 Cannon Ball

Shown in Figure 6.19. The goal is to touch the coming ball from the distant cannon at the right time. Both unilateral and bilateral, swipe and grasp modes are feasible.

6.3.14 Pop Clap

Shown in Figure 6.20. The goal is to touch the falling ball at the right time, clap it with both hands. Only bilateral, swipe mode is feasible.

6.3.15 Hand Ball

Shown in Figure 6.21. Similar to “Cannon Ball”, this game requires the player to touch the coming ball from the wall at the right time. However, the ball will bounce back and forth, which makes the task more challenging. Both unilateral and bilateral, swipe and grasp modes are feasible.

6.3.16 Motion Record/Playback

Shown in Figure 6.22. This is essentially a feature of the exoskeleton system aforementioned: train patient with repetitive motion trajectory introduced by the demonstration of therapist.

6.3.17 Fugl-Meyer

Shown in Figure 6.23 and Figure 6.24. This game requires the subject to finish motion trajectory indicated by the animation, based on Fugl-Meyer assessment. The score would be calculated - the assessment is thus automated.

6.3.18 Active Stretch

Shown in Figure 6.25. With help from the exoskeleton, the game aims to increase motion range to alleviate spasm. The increment of ROM in each DOF is visualized in real-time.

6.4 Working Modalities

Originally developed as a part of our exoskeleton system, the virtual reality environment and the series of serious games could be integrated with multiple working modalities, to be utilized in different scenarios. For example, “virtual reality + exoskeleton” mode best fits the rehabilitation centers or research labs, while “virtual reality + Kinect v2 camera” mode works better for home-based rehabilitation training. Another modality using inertial measurement units (IMUs) is under development.

6.4.1 Exoskeleton

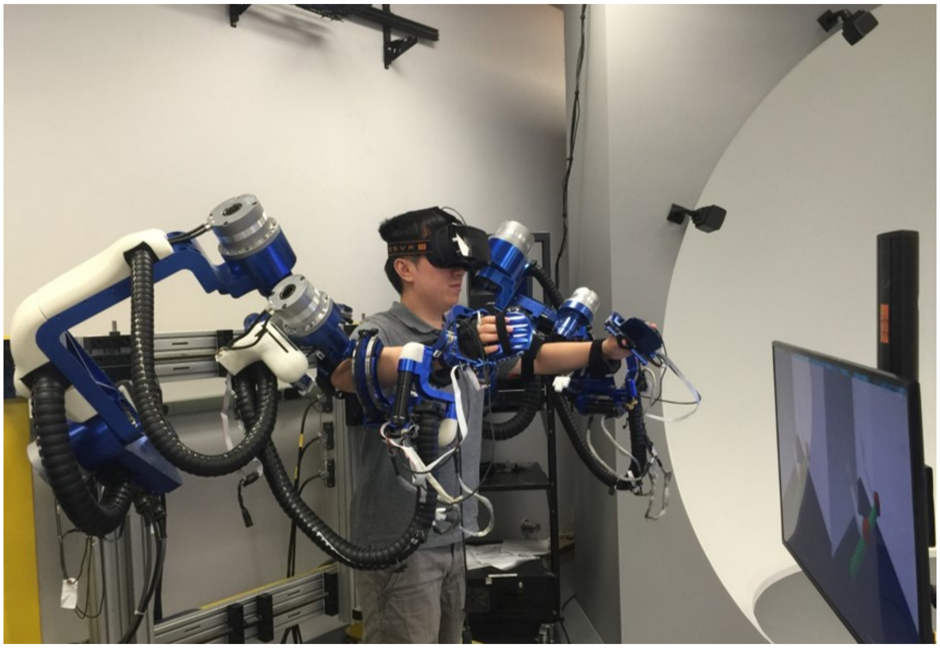

Figure 6.5: A subject is interacting with virtual reality “Reach” game via the wearable exoskeleton.

Figure 6.5 shows a subject using the exoskeleton, while interacting with virtual reality. Whether to put on a head-mounted device (HMD) is always optional. At some stage, we used the OSVR HDK 2 from Razer; later we turned to Oculus.

6.4.2 Kinect v2 Camera

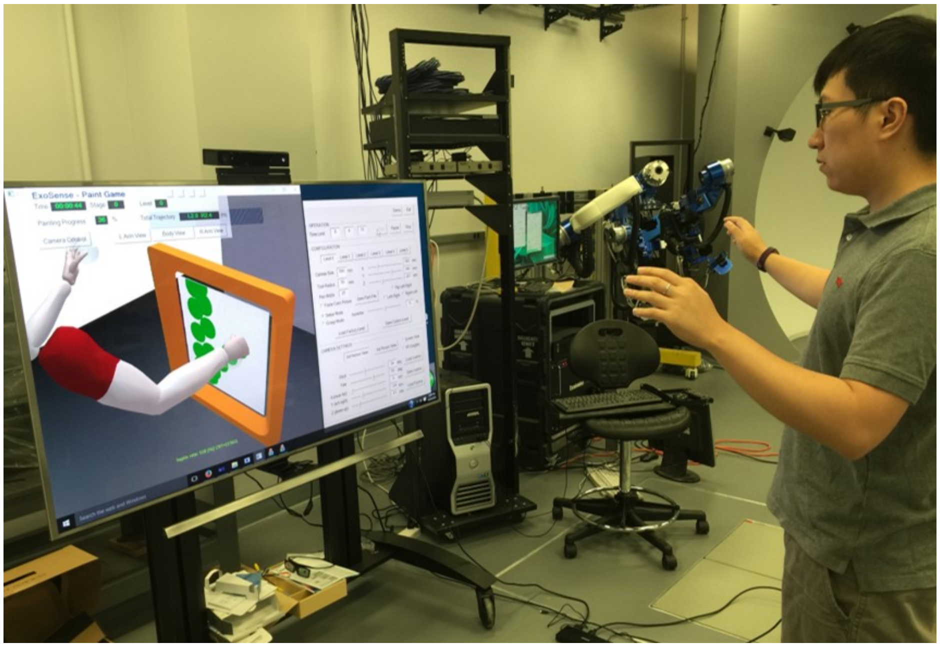

Figure 6.6: A subject is interacting with virtual reality ("Paint" game) via Kinect v2 camera.

Another way to capture the real-time human movement data is to use vision-based devices like Kinect v2 camera from Microsoft. However, since the product is no longer supported by Microsoft, we turned to wearable IMU sensor-based approach, which is in good progress but still under development.

6.5 Discussion and Future Works

Using virtual reality in post-stroke rehabilitation is promising. However, there exist multiple challenges, in hardware as well as the software algorithms. There are several projects going on in Bionics Lab.

6.6 Appendix: All Games

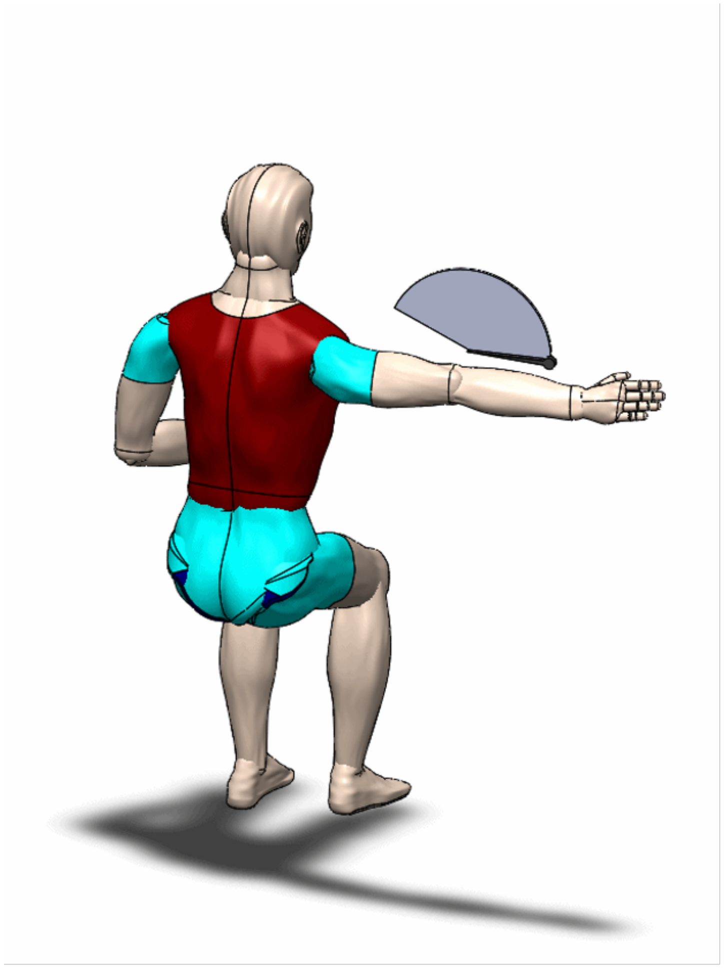

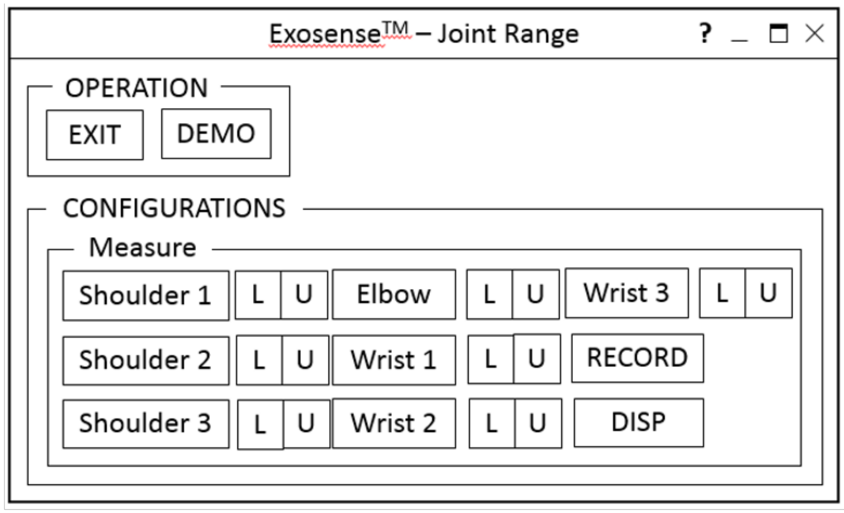

- 1D Static
- Preliminary step: to measure capable range for each joint, followed by games
- Assistive modes: None
- Swipe mode only
- Unilateral mode only

Figure 6.7: Game: "Joint Range".

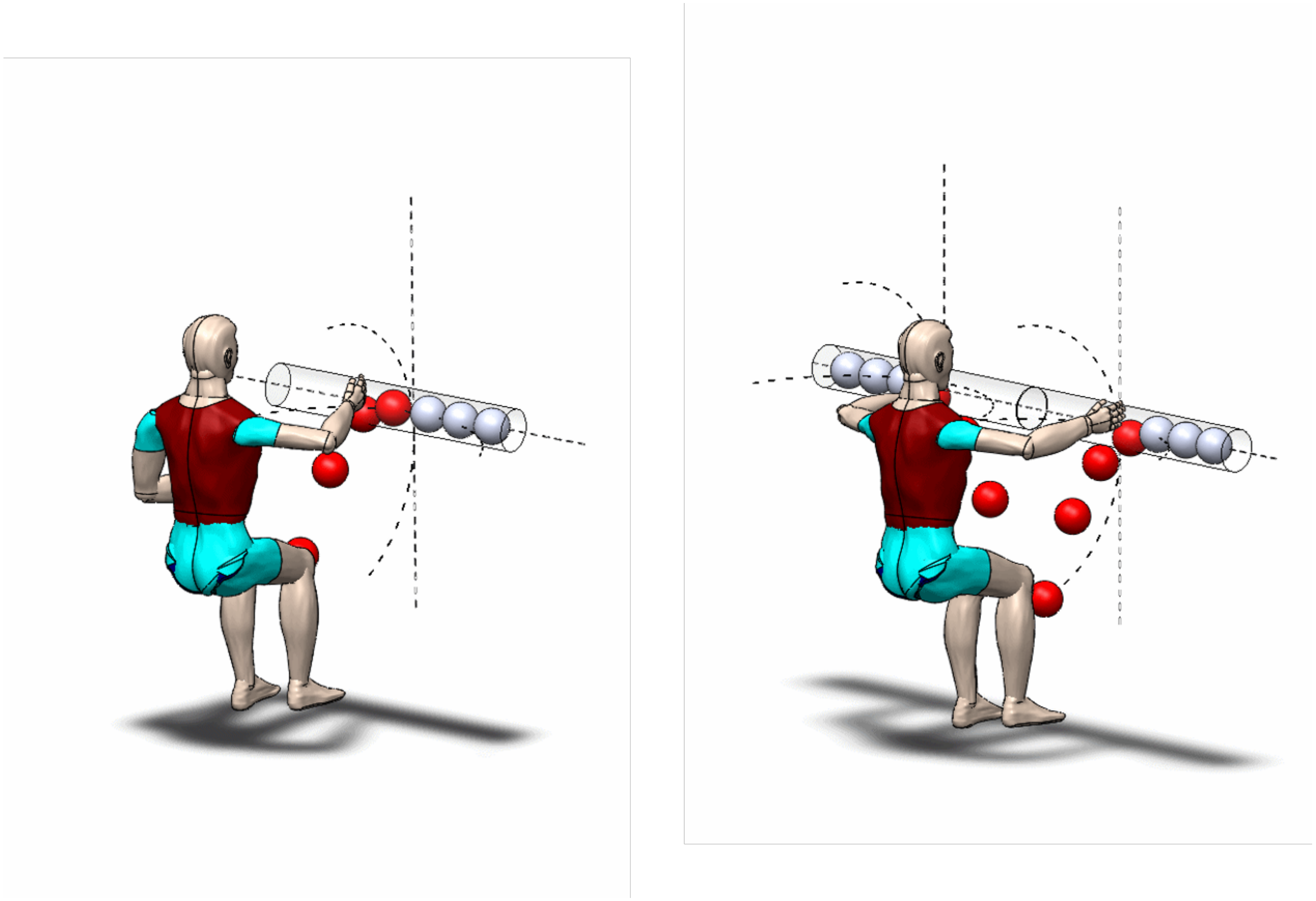

Figure 6.8: Game: “Reach”. Left: unilateral mode; Right: bilateral mode.

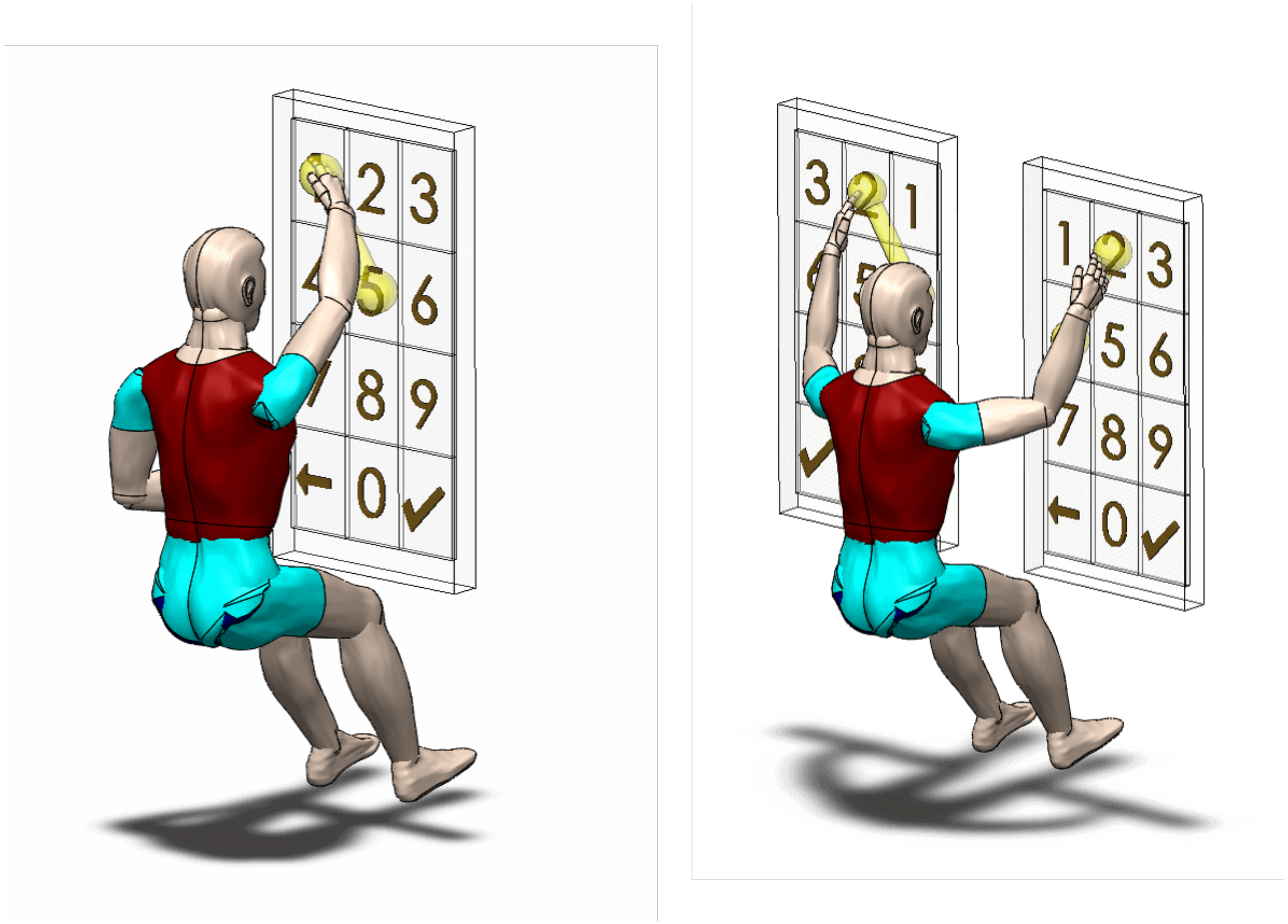

Figure 6.9: Game: “Dial”. Left: unilateral mode; Right: bilateral mode.

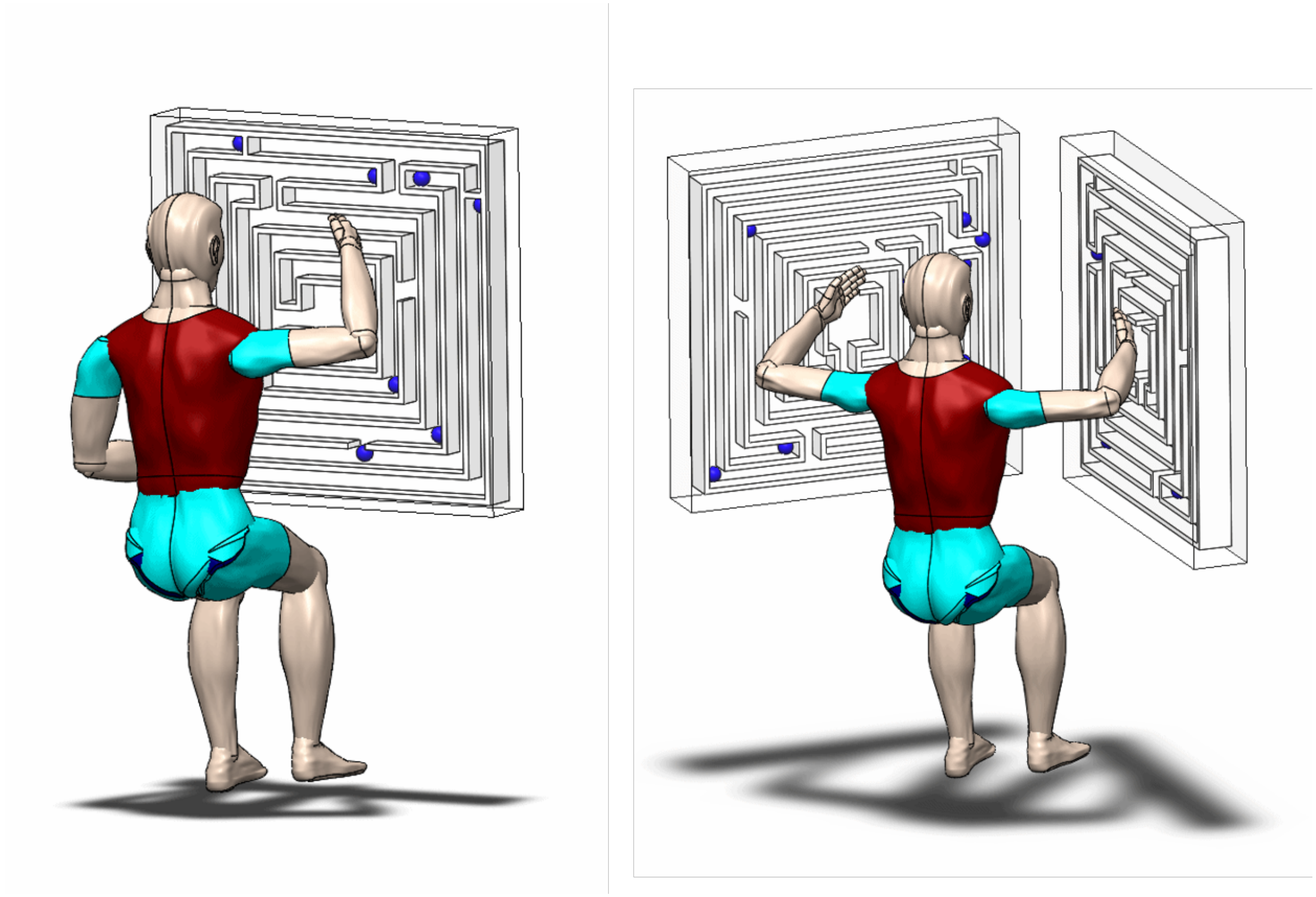

Figure 6.10: Game: “Maze Linear”. Left: unilateral mode; Right: bilateral mode.

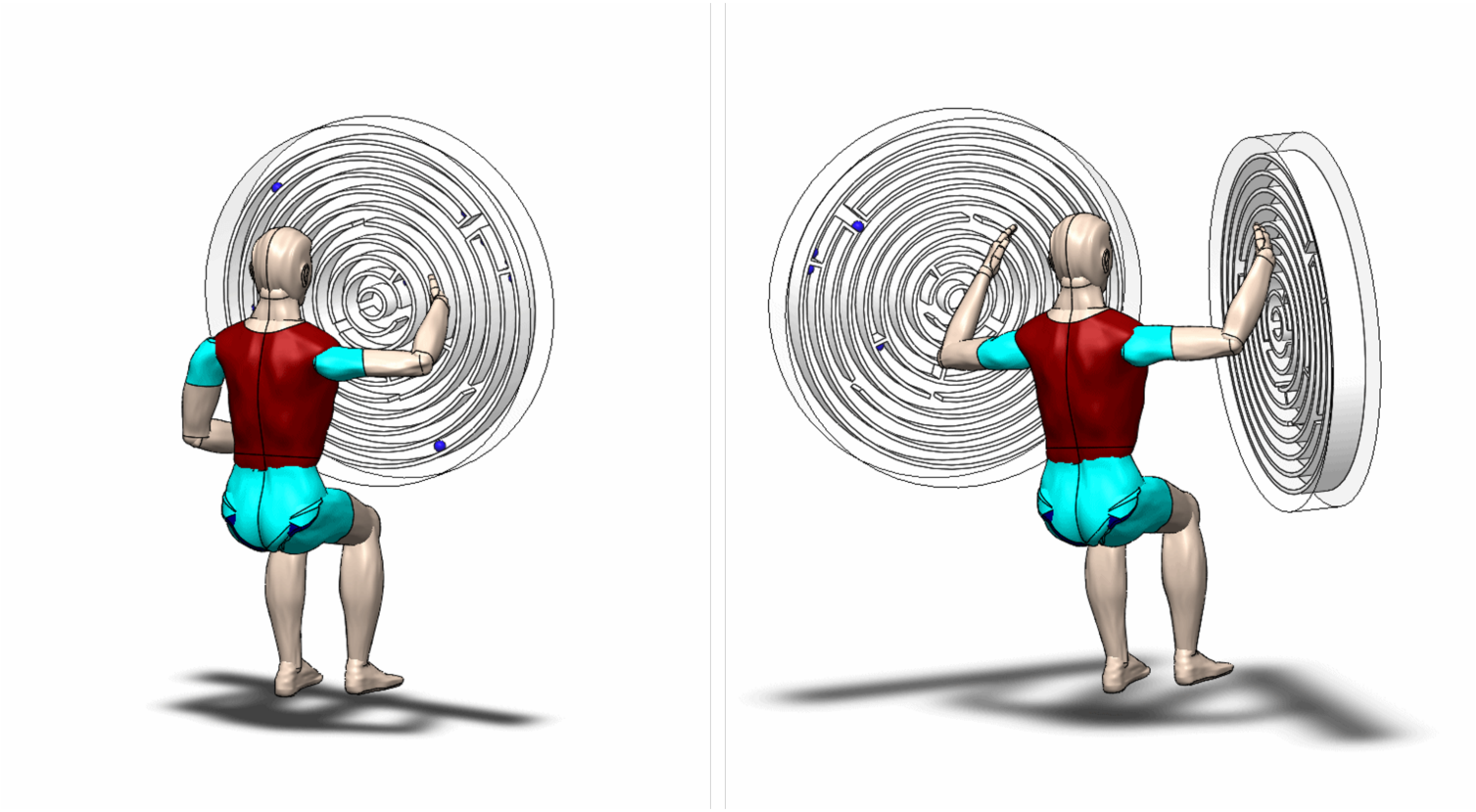

Figure 6.11: Game: “Maze Circular”. Left: unilateral mode; Right: bilateral mode.

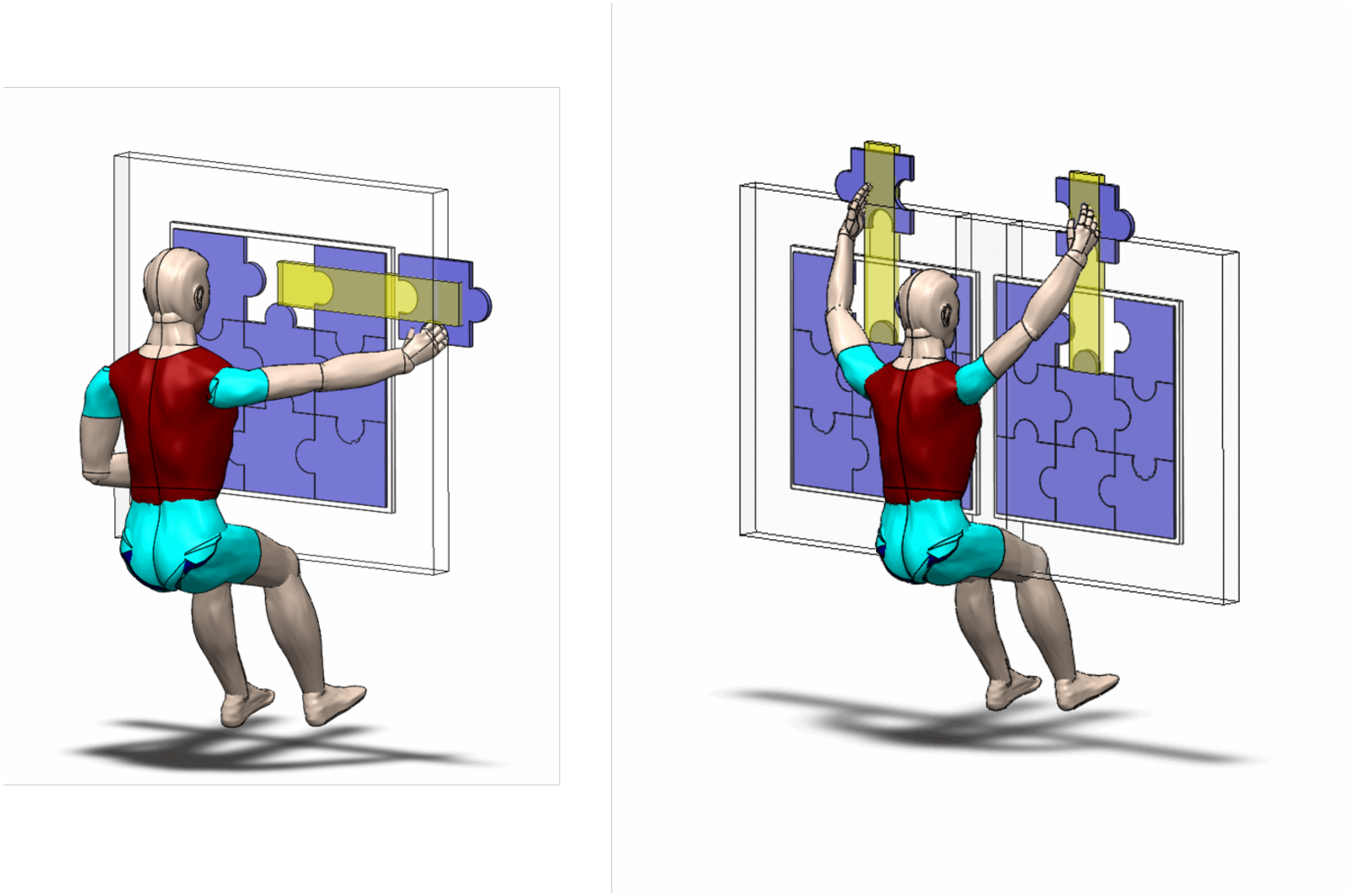

Figure 6.12: Game: “Puzzle”. Left: unilateral mode; Right: bilateral mode.

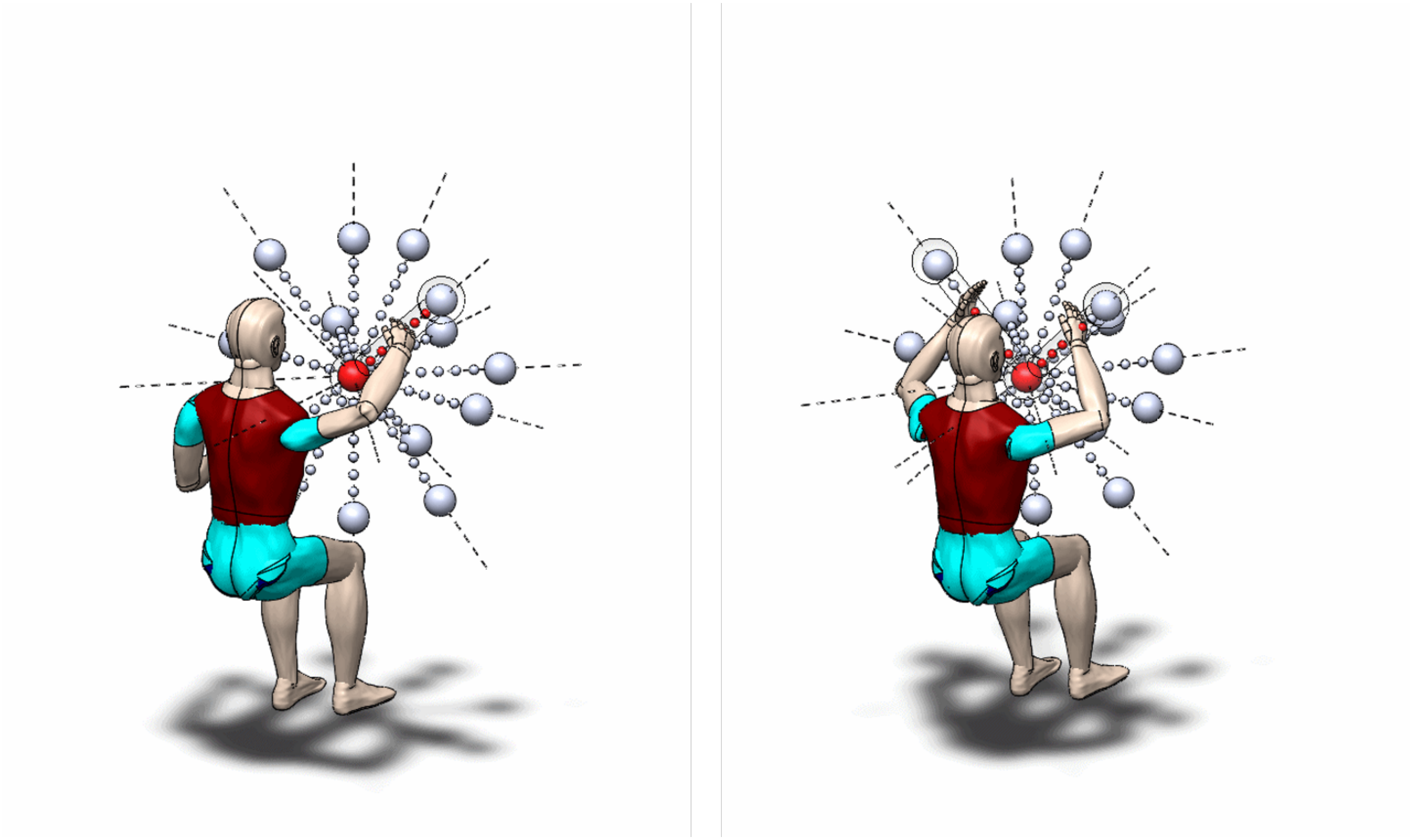

Figure 6.13: Game: “Flower”. Left: unilateral mode; Right: bilateral mode.

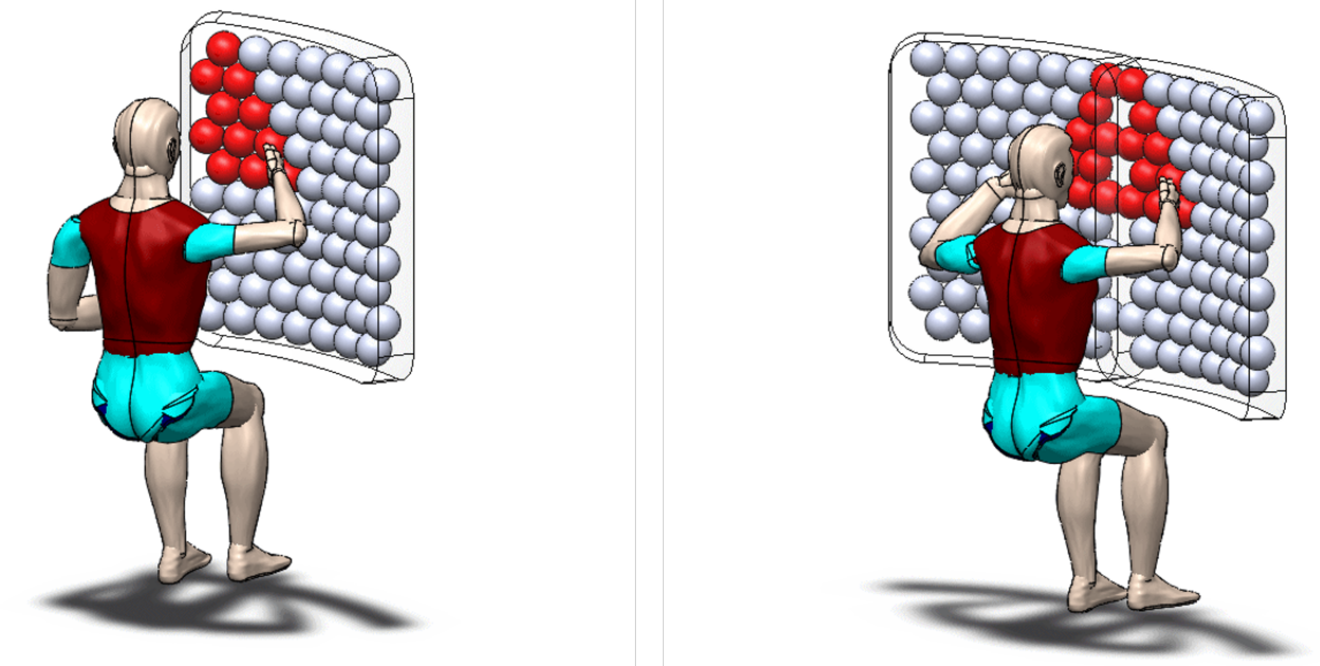

Figure 6.14: Game: “Paint”. Left: unilateral mode; Right: bilateral mode.

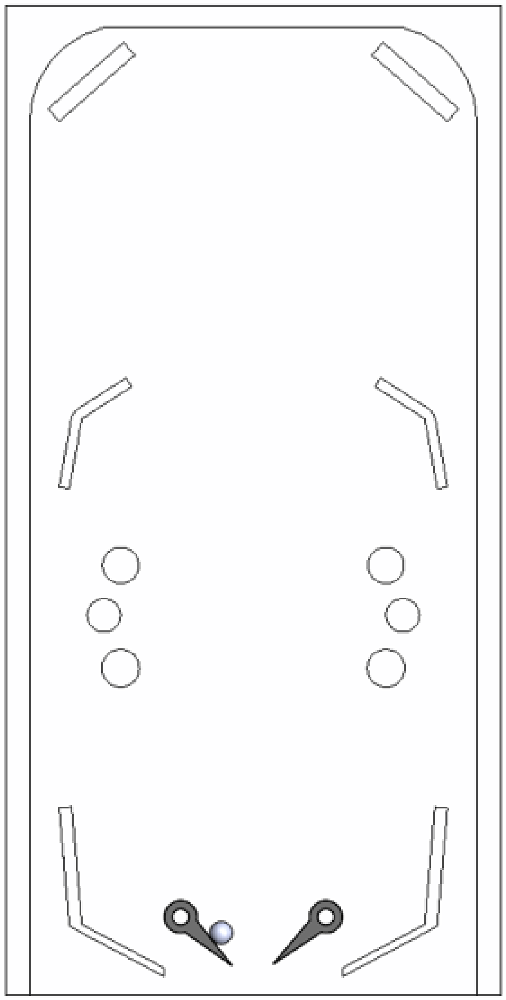

Figure 6.15: Game: “Pinball”. Left: unilateral mode; Right: bilateral mode.

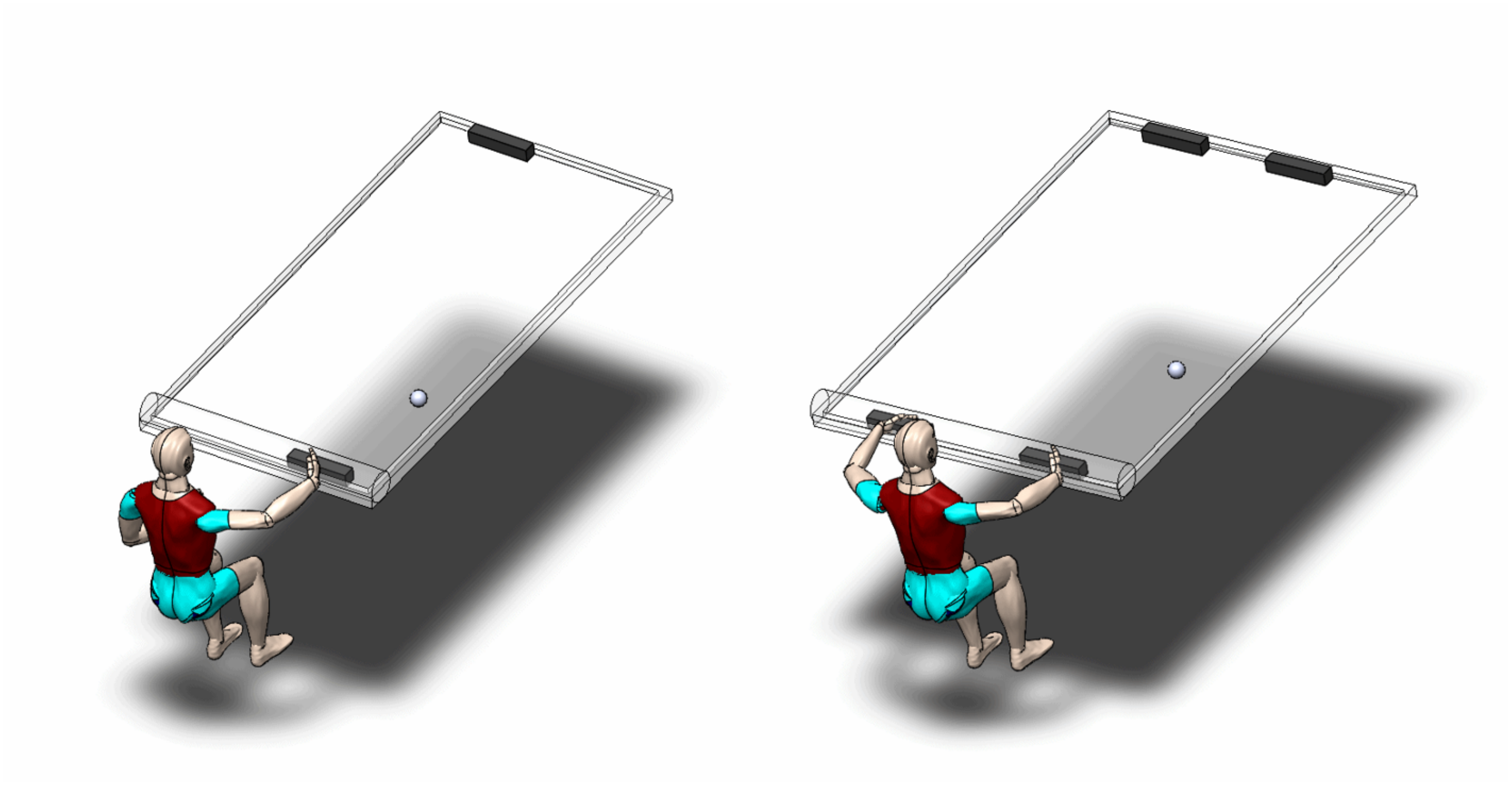

Figure 6.16: Game: “Pong Linear”. Left: unilateral mode; Right: bilateral mode.

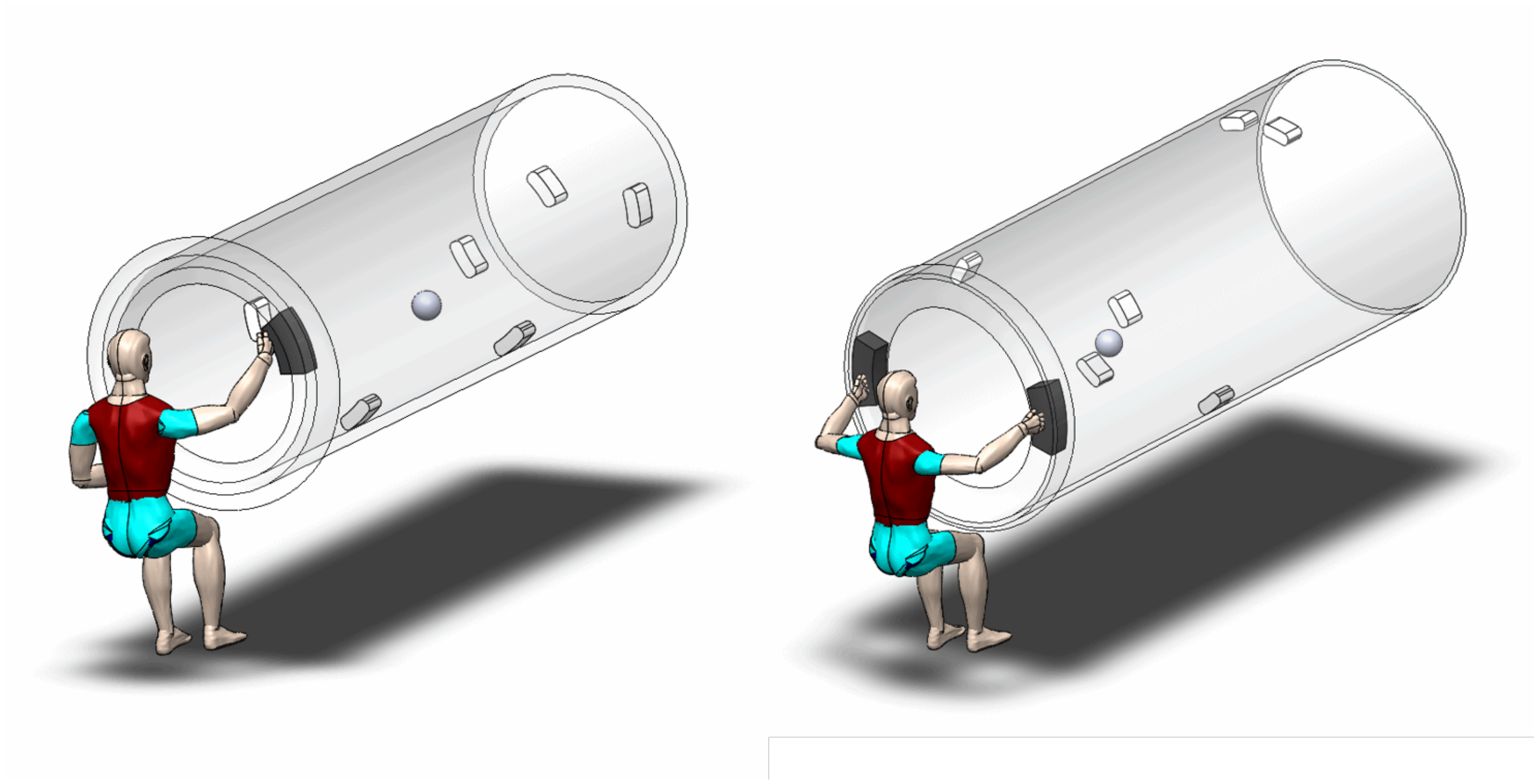

Figure 6.17: Game: “Pong Circular”. Left: unilateral mode; Right: bilateral mode.

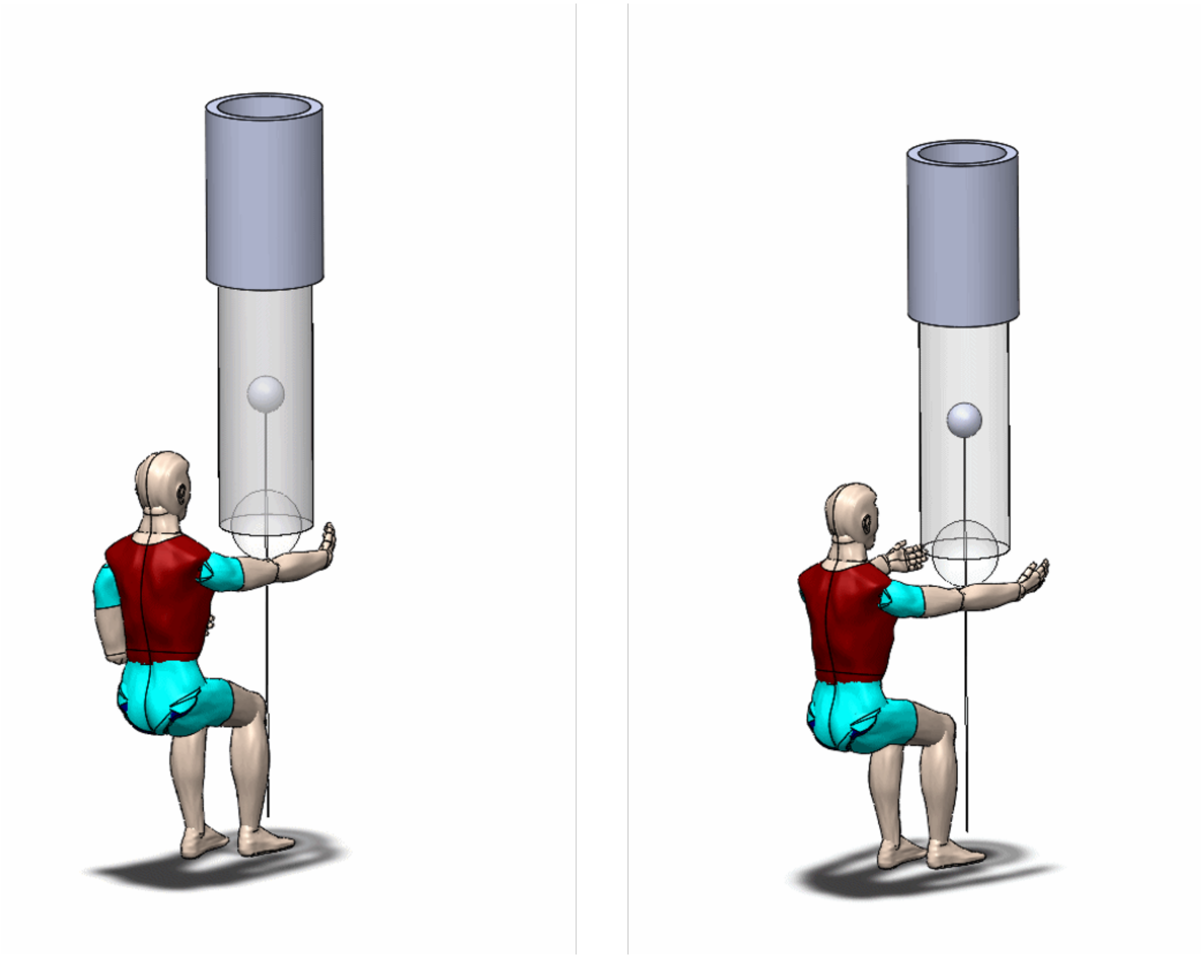

Figure 6.18: Game: “Catch Carry Drop”. Left: unilateral mode; Right: bilateral mode.

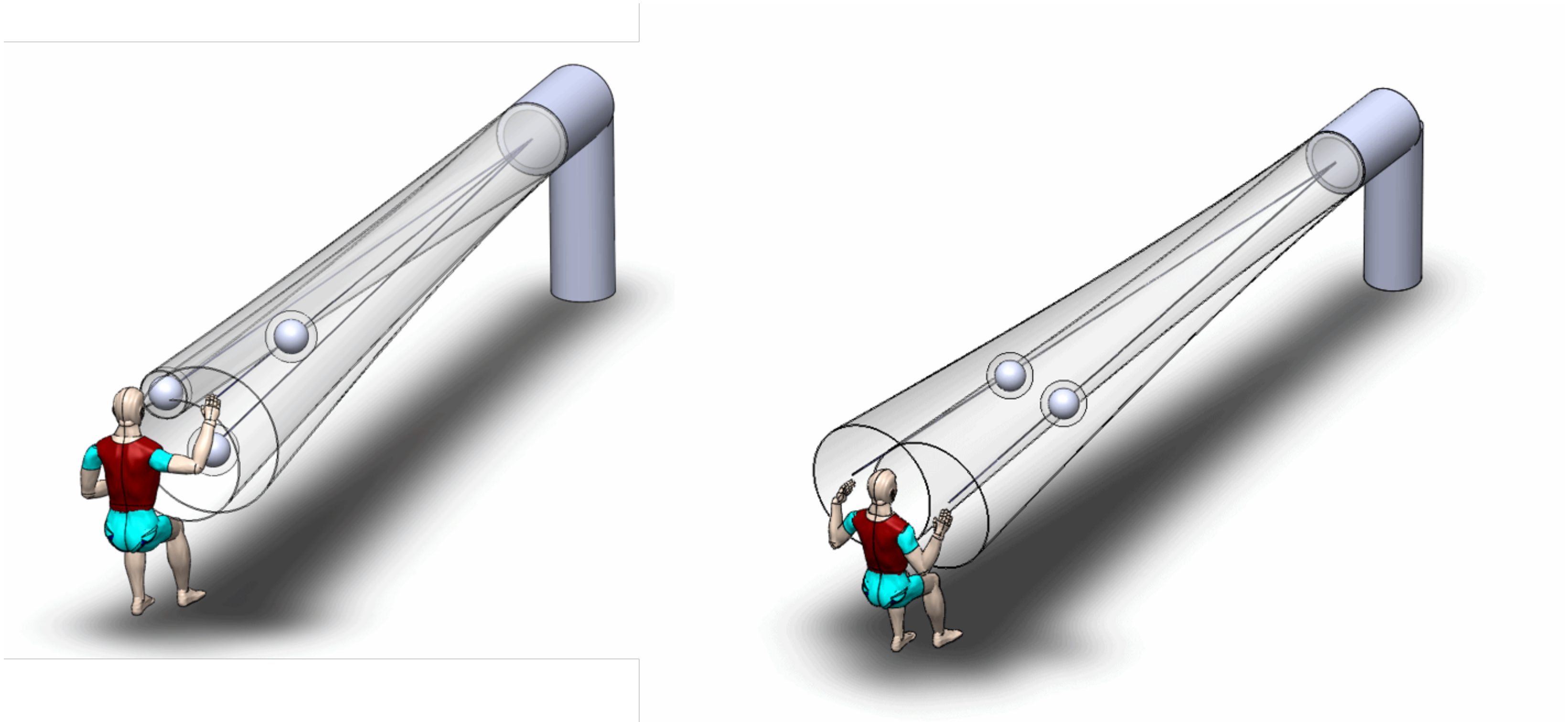

Figure 6.19: Game: “Cannon Ball”. Left: unilateral mode; Right: bilateral mode.

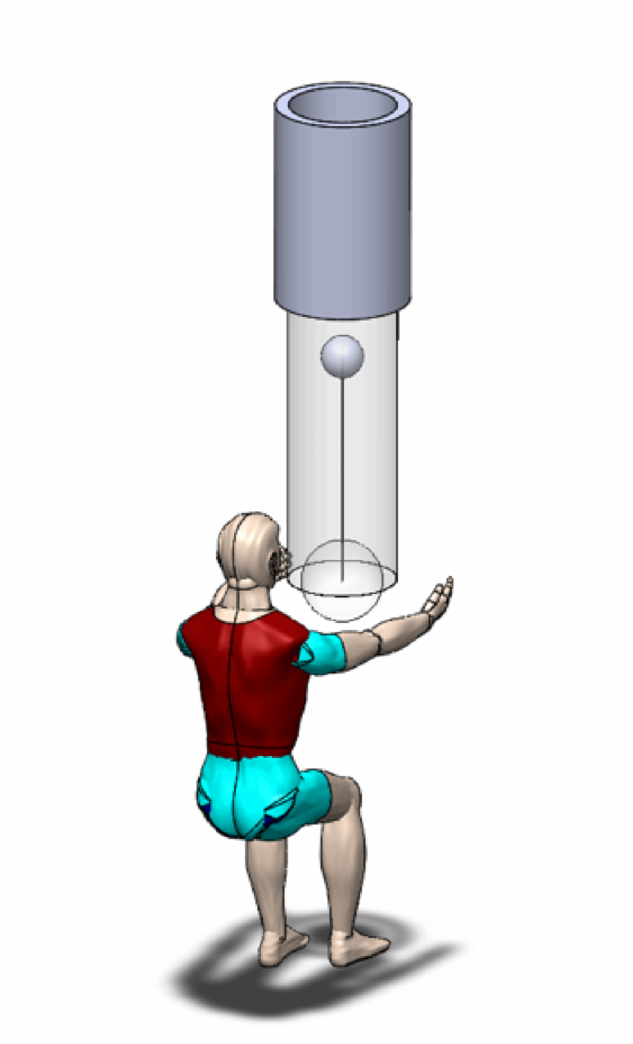

Figure 6.20: Game: “Pop Clap”. Left: unilateral mode; Right: bilateral mode.

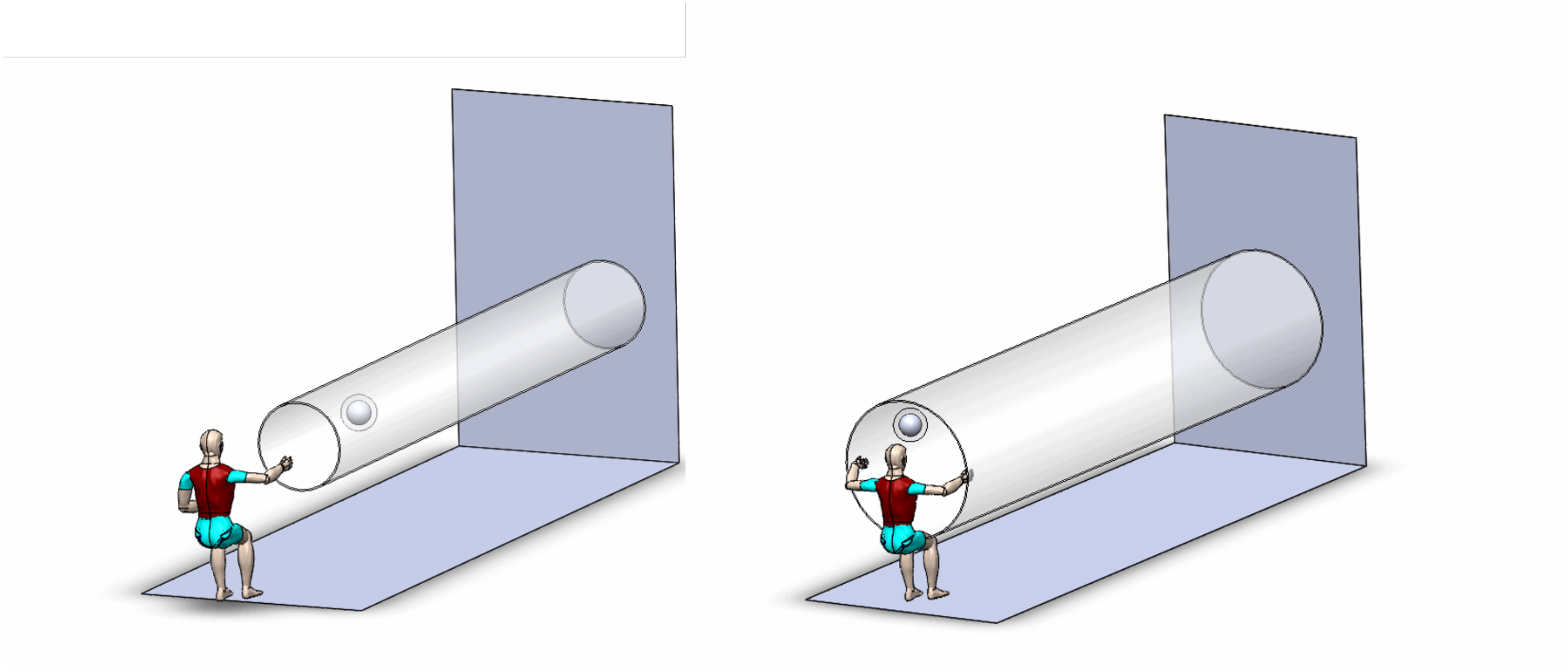

Figure 6.21: Game: “Hand Ball”. Left: unilateral mode; Right: bilateral mode.

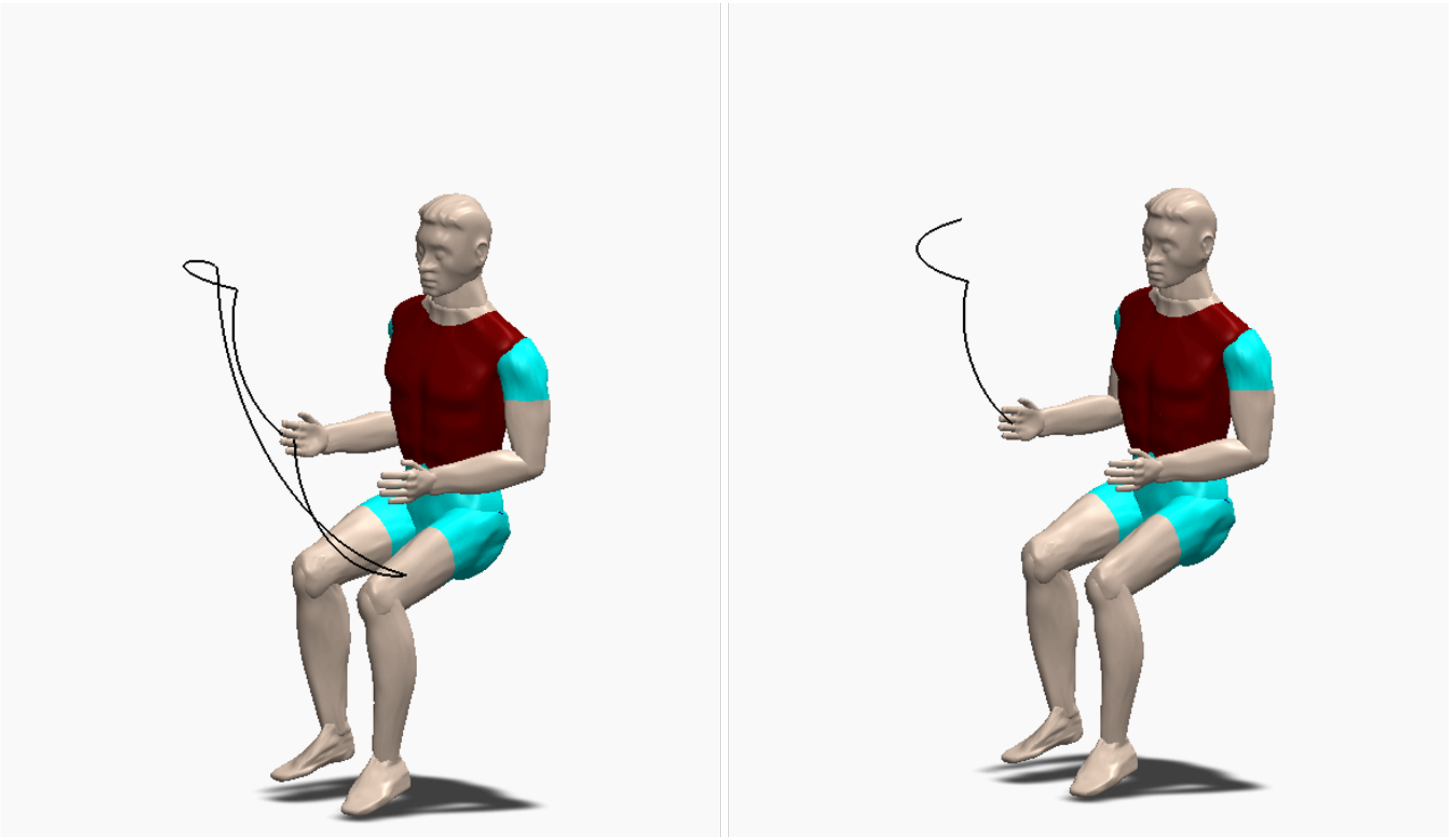

Figure 6.22: Game: “Motion Record/Playback”. Left: unilateral mode; Right: bilateral mode.

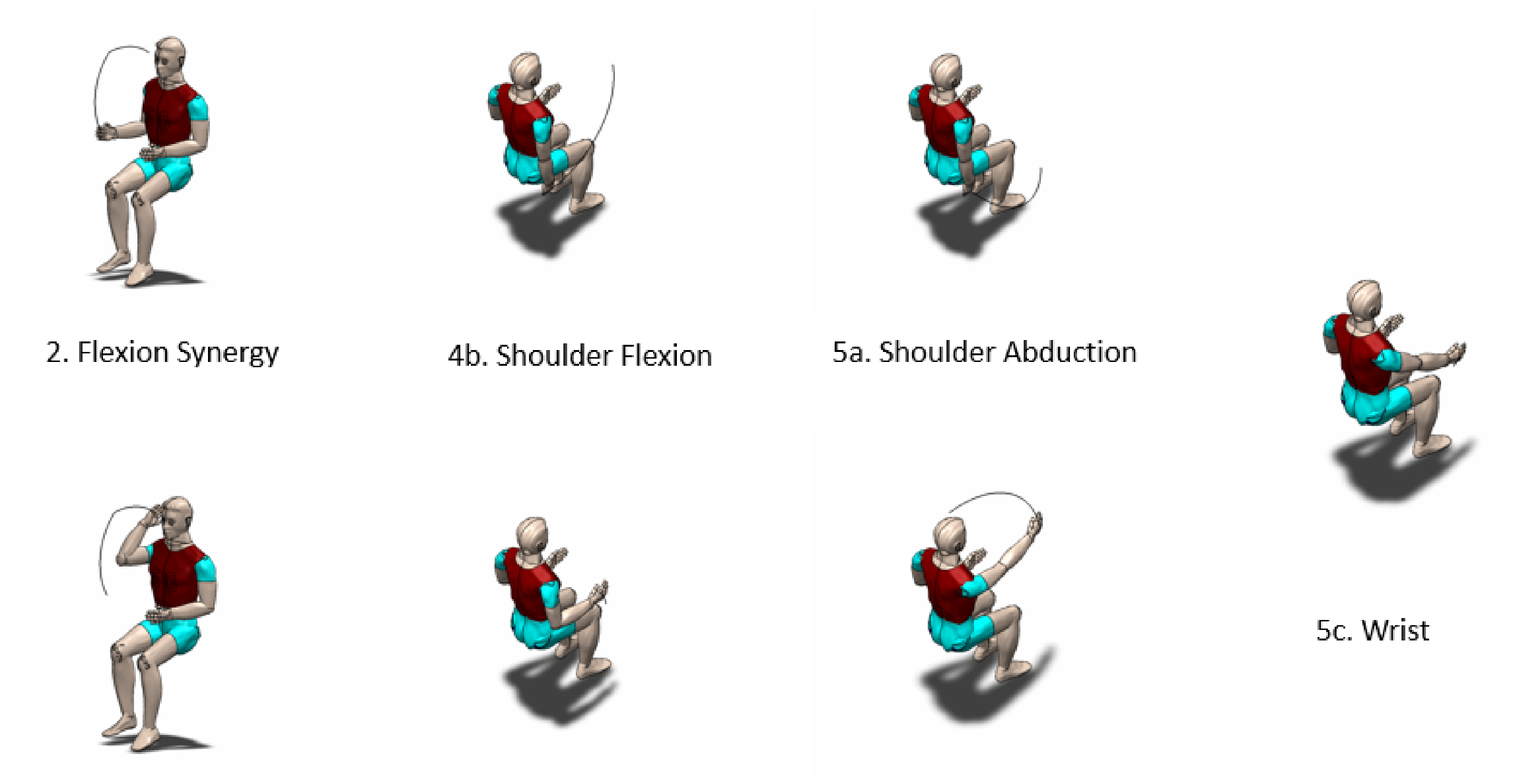

2. Flexion Synergy

4b. Shoulder Flexion

5a. Shoulder Abduction

5c. Wrist

3. Extension Synergy

4c. Pronation / Supination

5b. Shoulder Flexion

Figure 6.23: Game: “Fugl Meyer”. 2. Flexion Synergy; 3. Extension Synergy; 4b. Shoulder Flexion; 4c. Pronation / Supination; 5a. Shoulder Abduction; 5b. Shoulder Flexion; 5c. Wrist.

7a. Wrist

7c. Wrist

7e. Wrist Circling

7b. Wrist

7d. Wrist

9. Rapid Touching

Figure 6.24: Game: “Fugl Meyer”. 7a. Wrist; 7b. Wrist; 7c. Wrist; 7d. Wrist; 7e. Wrist Circling; 9. Rapid Touching.

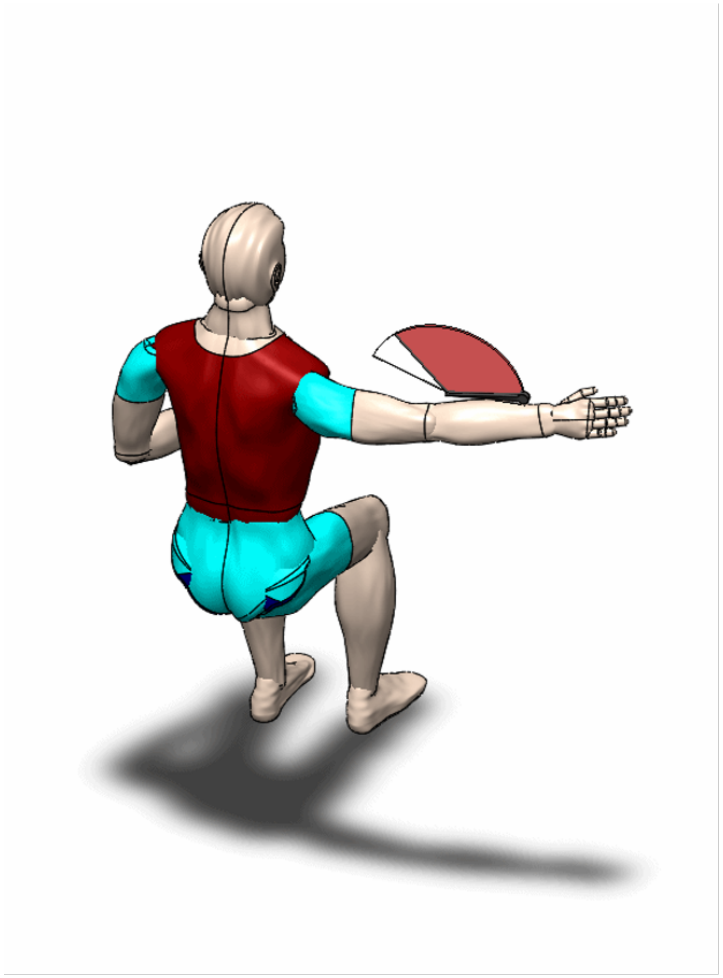

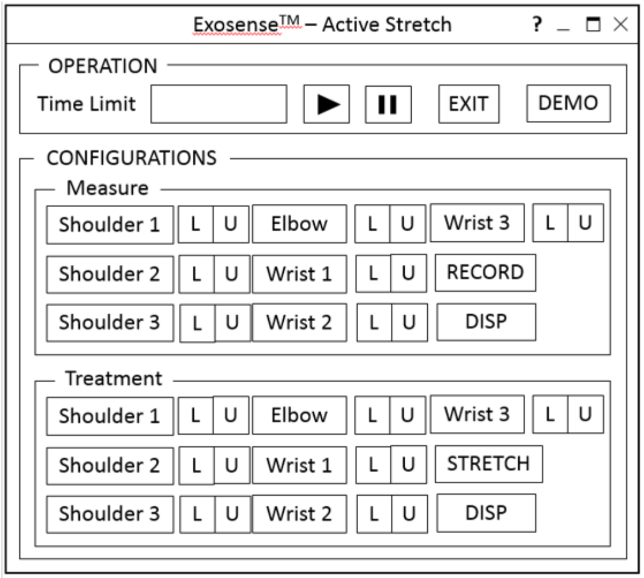

- 3D Dynamic
- Goal: increase motion range to alleviate spasm
- Assistive modes: None
- Swipe mode only
- Unilateral mode only

Figure 6.25: Game: “Active Stretch”.

CHAPTER 7

Asymmetric Bilateral Training - A Pilot Study

7.1 Overview

Unlike single-DOF rehabilitation devices (e.g., manipulanda), exoskeletons for rehabilitation often involve physical human-robot interaction (pHRI) at multiple limb locations [JPC14].

Control strategies for these exoskeletons include using surface electromyography (sEMG) signals, feedback from the force and inertial sensors, and detection of electroencephalography (EEG) signals to activate a motion. Understanding how a person physically interacts with rigid linkages becomes important, especially for exoskeleton devices controlled by interaction forces only. Lower limb exoskeletons are usually developed for assisting standing and for walking, which is cyclic movement constrained by the ground and repetitive, rather stereotyped stance and swing phases of gait [RWR16]. In contrast, arm rehabilitation training by upper limb exoskeletons must have more flexibility in protocol design to achieve reaching and grasping at a variety of locations in peripersonal space. The upper extremity exoskeletons must detect multi-joint movement intention as the person initiates a purposeful movement to an item. Hemiparetic persons are impaired by abnormal synergistic movements, hypertonicity, and variable motor control of flexor, extensor and rotator muscle groups. How they react to external assistance and resistance of an exoskeleton requires further study.

In addition, there is little or no research on robotic systems that train ecologically valid movements in which the hands asymmetrically converge to interact with an object (e.g., to open a jar, button a shirt, prepare a meal, dress). Other than exoskeletons that enslave the affected arm to movements of the other arm, most devices enable practice with only the affected arm. An important conceptual basis for an asymmetric bilateral practice approach to recovery from hemiplegia is that when either hand purposefully holds an item, bilateral attentional mechanisms for the integration of motor, visual, spatial, sensory, motivational, and other cognitive-motor nodes of the central nervous system are activated. This added drive may increase training-induced problem-solving and activation of spared, distributed motor networks that can further support the recovery of the paretic arm and hand. Thus, an important technological barrier to more effective UE rehabilitation that deploys robotic-assist systems is the absence of control mechanisms and rehabilitation strategies to use one arm to help train the other for daily activities. We have altered our original design of this bilateral robotic system to enable this.

To explore more in pHRI when stroke patients are wearing an exoskeleton, we conducted this very preliminary study. The majority of this chapter is adapted from the publication: **Shen, Y.**, Ma, J., Dobkin, B., Rosen, J. "*Asymmetric Dual Arm Approach for Post Stroke Recovery of Motor Functions Utilizing the EXO-UL8 Exoskeleton System: A Pilot Study*", 40^{th} Annual International Conference of the IEEE Engineering in Medicine and Biology Society (EMBC), Honolulu, HI, USA, 2018.

7.2 Previous Work: Mirror-Image Symmetric Bilateral Training

One of our exoskeleton system's distinct features is, dual-arm manipulation is enabled by inter-arm teleoperation (Chap 3.3). A pilot study on the effectiveness of mirror-image bilateral training has been done using the previous generation of exoskeleton system, EXO-UL7, and reported by [KMF13] and [BAP13]. While based on the preliminary study results, the mirror-image bilateral training is promising, asymmetric training seems to be able to provide more internal referential information to teach the patients themselves how to move their affected arm to the same target. The details of this newly proposed approach are provided below.

7.3 Asymmetric Bilateral Training

In a dual arm therapeutic regime aiming to rehabilitate motor functions post stroke, both the affected arm (paretic) and the unaffected (non-paretic) arm are involved. In this context, the leading idea is that motor functions of the affected arm during a reaching task may be improved if the unaffected arm has already reached the target. As part of this pilot study, one chronic post-stroke patient with weakness and spasticity on his right arm conducted reaching tasks to virtual targets arranged in a 5×3 matrix located parallel to his frontal plane, in two different configurations: (1) affected arm only (without assistance from the exoskeleton); (2) unaffected arm first followed by the affected arm (2a) without, and (2b) with assistance. A force field attracting the wrist of the affected arm to the target was used in the assistive mode. The data post-processing and analysis included task completion time, reachable task space, joint range of motion, human-robot interaction force/torque and power exchange at multiple sensors along the arm - visualized in a series of interaction maps. The data validated the robotic system's basic functionality in facilitating post-stroke unilateral and asymmetric bilateral training.

7.4 EXO-UL8 Upper Limb Exoskeleton System

7.4.1 Mechanical design

The new EXO-UL8, like its predecessor, the cable-driven EXO-UL7 [PR06], was designed to overlap with 95% of a healthy human arm workspace. The shoulder joint was designed to eliminate singular configurations within the workspace and was repositioned at the edge of the arm's workspace. Single-DOF hand grippers were added to increase the total number of DOFs from seven to eight for each arm and to enable reach-and-grasp motions that are critical to the recovery of the motor control system following a stroke. Furthermore, each link is adjustable in length in a telescopic fashion to accommodate a wide range of anthropometric arm dimensions (5% - 95%). Each joint includes mechanical limits preventing motion beyond anatomical limits. The cable driven mechanism embedded in the EXO-UL7 was replaced with servo unities mounted at each individual joint with two exceptions including the upper arm (J3) and forearm (J5) where belts were introduced. The servo system was selected to meet the combination of the following specs: (a) muscle strengths - provide joint torques that are comparable to a healthy individual; (b) gravity compensation - provide joint torques that compensate the weight of exoskeleton arm itself as well as that of the subject arm; (c) velocities/accelerations - provide angular velocities and accelerations comparable to those measured in activities of daily living; (d) payload - provide support of a payload of 5kg grasped by the hand. For each arm, three harmonic drive (Harmonic Drive Systems Inc., Japan) servo systems are equipped with encoders to facilitate movement for three out of the seven DOFs (J1, J2, J4 - Figure 2.2) at the shoulder and elbow joints, and with brakes that can freeze the arm configuration. The remaining five DOFs (J3, J5, J6, J7, J8 - Figure 2.2) are equipped with DC motors (Maxon Motor, Swiss). A set of four force/torque (F/T) sensors are placed at all the physical interaction points between the human operator and the exoskeleton system (Figure 2.4): three multi-axis F/T sensors (ATI mini 40) are located on the upper arm, forearm, and wrist, between a brace and the corresponding exoskeleton link; one single-axis force sensor is incorporated into the exoskeleton gripper for sensing grasping forces applied by the fingers. Anodized aluminum links are custom made and all cables are covered with 3D-printed shells.

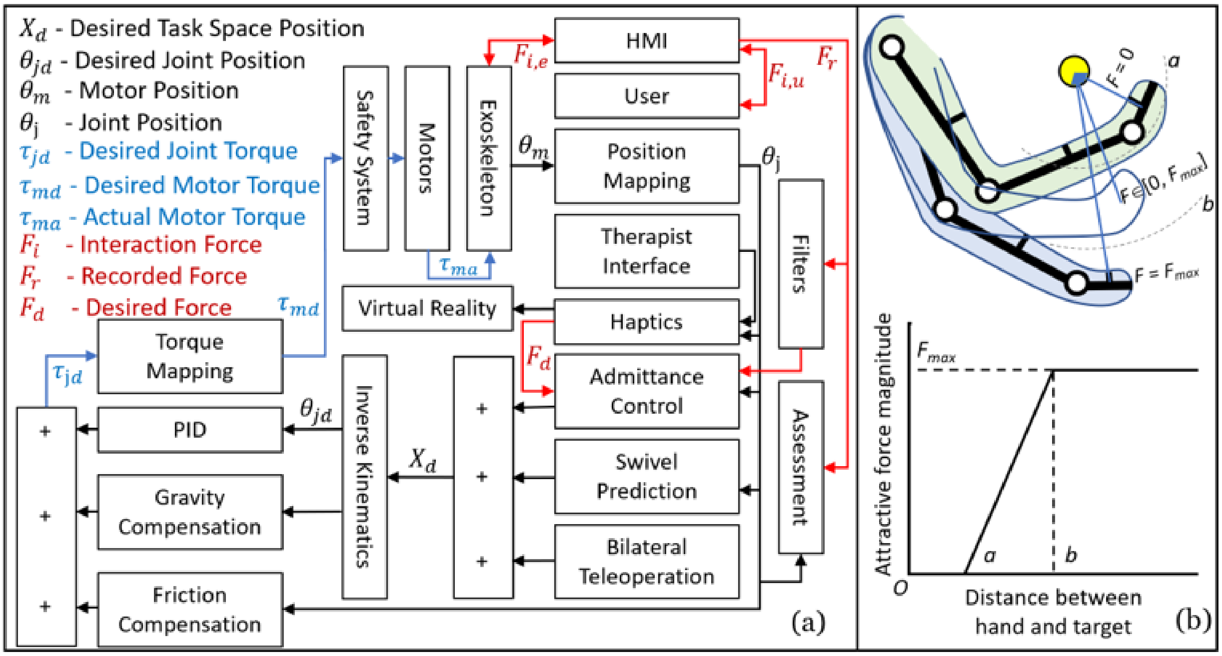

Figure 7.1: EXO-UL8 dual-arm upper limb exoskeleton system: (a) full view of the controller - the core is admittance control; (b) exoskeleton could provide spring-like force assistance attracting hand to the target (maximum and minimum values saturated).

7.4.2 Control

The exoskeleton system controller is illustrated in Figure 7.1(a), adopted from [Mil12]. The Jacobian matrices mapping the force/torque data collected by the sensors located on upper arm $J_{u(6\times3)}$, forearm $J_{f(6\times5)}$, and wrist $J_{w(6\times7)}$ to the base frame (center of shoulder joint) are calculated. From each sensor, force and torque signals ($F = [f_x, f_y, f_z, \tau_x, \tau_y, \tau_z]^T$) are picked up and transmitted to each joint in the form of joint torque command signals: $\Gamma_{j,u(3\times1)} = J^T_{u(3\times6)} F_{u(6\times1)}$, $\Gamma_{j,f(5\times1)} = J^T_{f(5\times6)} F_{f(6\times1)}$, and $\Gamma_{j,w(7\times1)} = J^T_{w(7\times6)} F_{w(6\times1)}$, respectively. Individual contributions are augmented with zero entries and summed up:

$$\Gamma_j = \Gamma_{j,u} + \Gamma_{j,f} + \Gamma_{j,w} \tag{7.1}$$

The desired torque signals are filtered and fed into a PD admittance controller:

$$\dot{\theta}_j = k_{j,p}\Gamma_j + k_{j,d}\dot{\Gamma}_j \tag{7.2}$$

with the joint angular velocity signals $\dot{\theta}_j$ as the output to a low-level motor PID controller. The proportional and derivative gains for each DOF are tuned such that the human's effort reaches minimum while the system stability is maintained. There are two sources of instability in the system due to the physical human-machine interfaces: (1) human arm is assumed to be rigid enough to have every movement detected, but since the arm's cross-sectional shape is close to a circle, with muscles and skin surrounded, motions like wrist pronation/supination and shoulder internal/external rotation cannot be easily sensed by the F/T sensors; (2) human arm cross-section profile varies among individuals and loose/tight cuffs change detection sensitivity. To address these uncertainties and non-linearities, hyper gains $\alpha_{j,s}, j \in \{1,2,...,7\}, s \in \{u,f,w\}$ were introduced to improve natural multi-joint coordination.

$$\Gamma_j = \alpha_{j,u}\Gamma_{j,u} + \alpha_{j,f}\Gamma_{j,f} + \alpha_{j,w}\Gamma_{j,w} \tag{7.3}$$

The hyper gains αs are manually tuned, and the exoskeleton's gravity and friction are separately compensated.

7.4.3 Assistance

A majority of upper limb post-stroke training tasks include reach and reach-to-grasp. Due to the redundancy in both the arm and the robotic exoskeleton, only the end effector (hand) is provided with a point-to-point attractive force field so that elbow flexibility is maximized and the user's pHRI preference could be assessed. Illustrated in Figure 7.1(b): when the distance between the hand and target (either virtual or real object) is within $[a, b]$, the exoskeleton provides a spring-like attractive force field, which is saturated to the maximum F_{max} if the distance is over b, and eliminated if below a to main system controller stability. In this study, one set of a, b, and F_{max} (50mm, 200mm, 10N) is used.

7.5 Experiment

One chronic post-stroke patient (male, 75 years, 79kg, 175cm) with weakness and spasticity in his right arm was recruited, and he served as the test subject following an approved IRB protocol (IRB #17-001646). This pilot study focuses on the validation of EXO-UL8's functionality in facilitating single-arm and dual-arm training for post-stroke patients. Previously the difference between dominant and nondominant arm movements without wearing exoskeletons was broadly studied (e.g., [HRG16]). We look more into the pHRI when post-stroke patients are wearing the upper limb exoskeleton system and the arms work separately as in real-world activities.

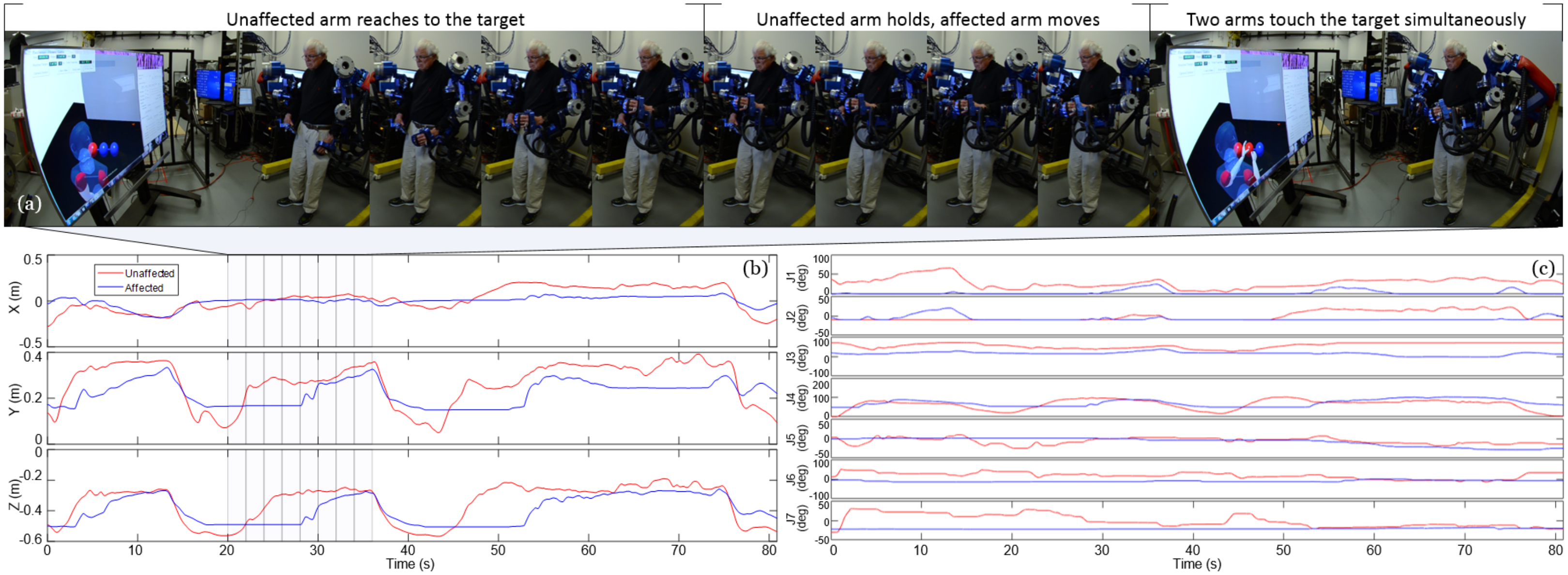

Figure 7.2: (a) Experiment photos taken every two seconds (marked in (b)): the subject wearing EXO-UL8 is reaching to the second target in Task 3 (dual-arm mode, with assistance) - Level 1, full level kinematic information of which is shown in (b) wrist position change in task space and (c) joint position change of unaffected (red) and affected (blue) arms versus time.

7.5.1 Setup

Figure 7.2(a), 7.3(a) and 7.3(b) together provide an overview of the experiment setup: facing towards a wide screen, the subject wearing the EXO-UL8 moved his arms to accomplish tasks in virtual reality while standing. The exoskeleton shoulder distance and arm link lengths are adjusted for the subject's comfort. The joint angle information is transmitted to the VR environment programmed with the open source haptic library Chai3D 3.0 via a UDP protocol [CBB03]. The subject could thus control the virtual avatar in real-time, with no movement scaling. The subject receives auditory instructions and visual feedback when accomplishing the tasks detailed below.

7.5.2 Tasks

Illustrated in Figure 7.3(a) and 7.3(b), based on the subject's reachable task space measured using a ten-camera motion capture system (Vicon, UK), the targets are symmetrically (about the subject's sagittal plane) positioned in a 5×3 matrix parallel to the subject's frontal plane (500mm distant). The horizontal distance between columns is 210mm (half the subject's shoulder width), and vertical distance between rows (levels) is 100mm. Note that the second row from the top (Lv4) is the same height as the subject's shoulder. While the subject could easily reach all the targets using his unaffected (left) arm, targets on the matrix's top row and right column are partially reachable by the subject's affected (right) arm. The subject is asked to operate the exoskeleton for assessment of the following three different tasks:

Task 1 (affected arm only, no assistance): First, only the lowest row (Lv1) of the target matrix is displayed, and the subject, wearing the exoskeleton, is asked to move his affected (right) arm to touch the left, center and right targets. Once touched the target changes color and the subject moves his arm back to the side. After all three targets are touched, the current task level disappears, the next higher level appears and the subtask continues. A short break is provided between each of the levels. A long break is provided after all five levels are attempted. The subject is asked to try his best to touch the target, and if he fails, relax the arm and move to the next. The exoskeleton does not provide any assistance.

Task 2 (unaffected → affected arm, no assistance): In this task, for each level (pattern and

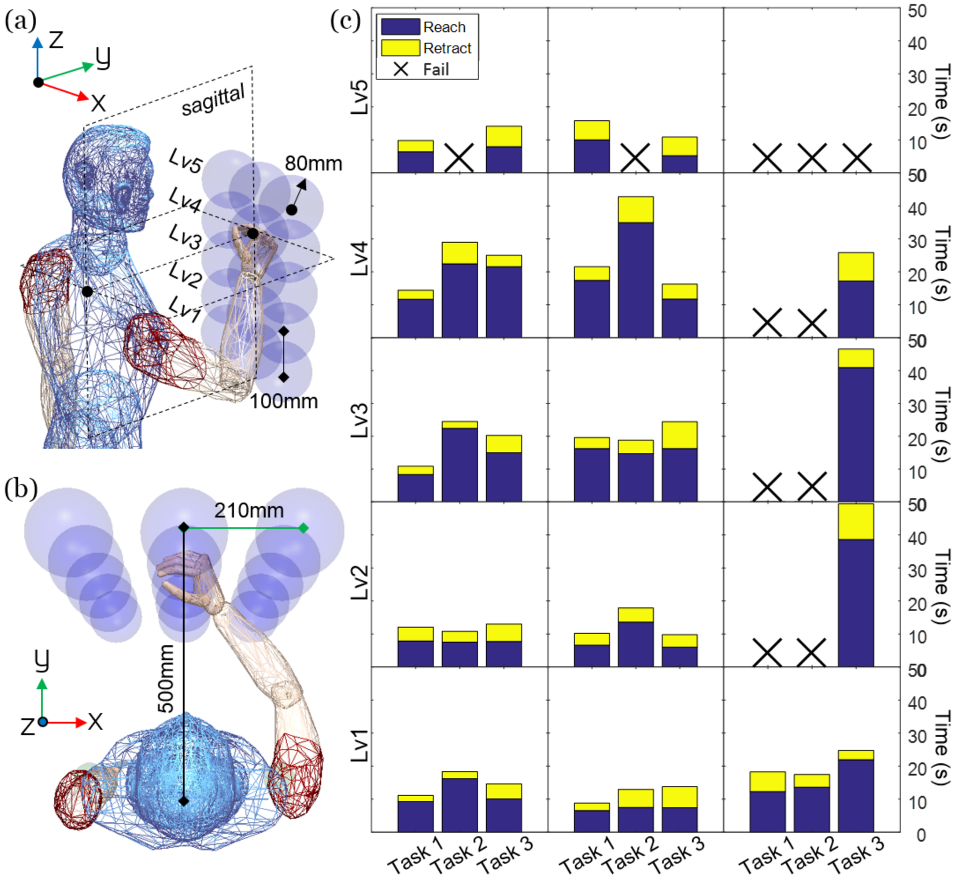

Figure 7.3: (a) Virtual targets are arranged in a 5×3 matrix parallel to the subject's frontal plane. Each row represents a level, assuming difficulty increases from Lv1 to Lv5 since it requires the patient to lift the arm up; (b) top view of the subject and targets in virtual reality; (c) task completion of the affected (right) arm: reach time and retract time for each target, under each task and level. Targets failed to touch are marked in '×'. All targets could be touched by the subject's unaffected (left) arm.

order same as Task 1) the subject moves the unaffected (left) arm to touch the target, which then changes to semi-transparent. While maintaining this position, he moves his affected arm to touch the same target. Once touched by two hands simultaneously, the target changes color. The subject retracts both arms back to his sides, then goes for the next target. No assistance provided by the exoskeleton.

Task 3 (unaffected → affected arm, with assistance): Similar to Task 2, except that once the unaffected (left) arm touches the target, the exoskeleton starts providing assistance in addition to voluntary movement, as illustrated in Figure 7.1(b), to bring the hand to the virtual target. Once the target is touched by two hands simultaneously, the attraction force field disappears. Figure 7.2 shows a sample target completion of Task 3 - Level 1.

7.5.3 Data collection

Both kinematic and force data are collected: joint position is recorded from the optical encoders at the seven motors on each exoskeleton arm at 100Hz; force/torque information $f_x, f_y, f_z, \tau_x, \tau_y, \tau_z$ is recorded from the three sensors on each exoskeleton arm at 100Hz as well. The data post-processing is done using MATLAB R2016b (MathWorks, USA). Figure 7.2(b) provides an example of wrist position change in task space while Figure 7.2(c) shows the joint space change, both with respect to time. The full experiment process including subject, exoskeleton and VR display is recorded using a hi-res video camera equipped with a fisheye lens.

7.6 Results & Discussion

Several aspects of the subject's physical interaction with EXO-UL8 are quantitatively analyzed and discussed below.

7.6.1 Kinematics

7.6.1.1 Task completion time

Unlike walking on the ground which is a cyclic movement with a relatively constant rhythm, the completion time of reaching tasks often depends on the spatial position of targets because of weakness and slower coordination. The observed spatial heterogeneity in reach time shown in Figure 7.3(c) (14.51 ± 9.07 second) reflects target-dependent task difficulty: a trend of increasing reach time from bottom-left to top-right indicates the spasticity, weakness and limited range of motion of the subject's affected arm. On the other hand, the retract time for different targets is much shorter and more concentrated (4.72 ± 2.06 second), due to the help from gravity and flexor synergy at the elbow and shoulder.

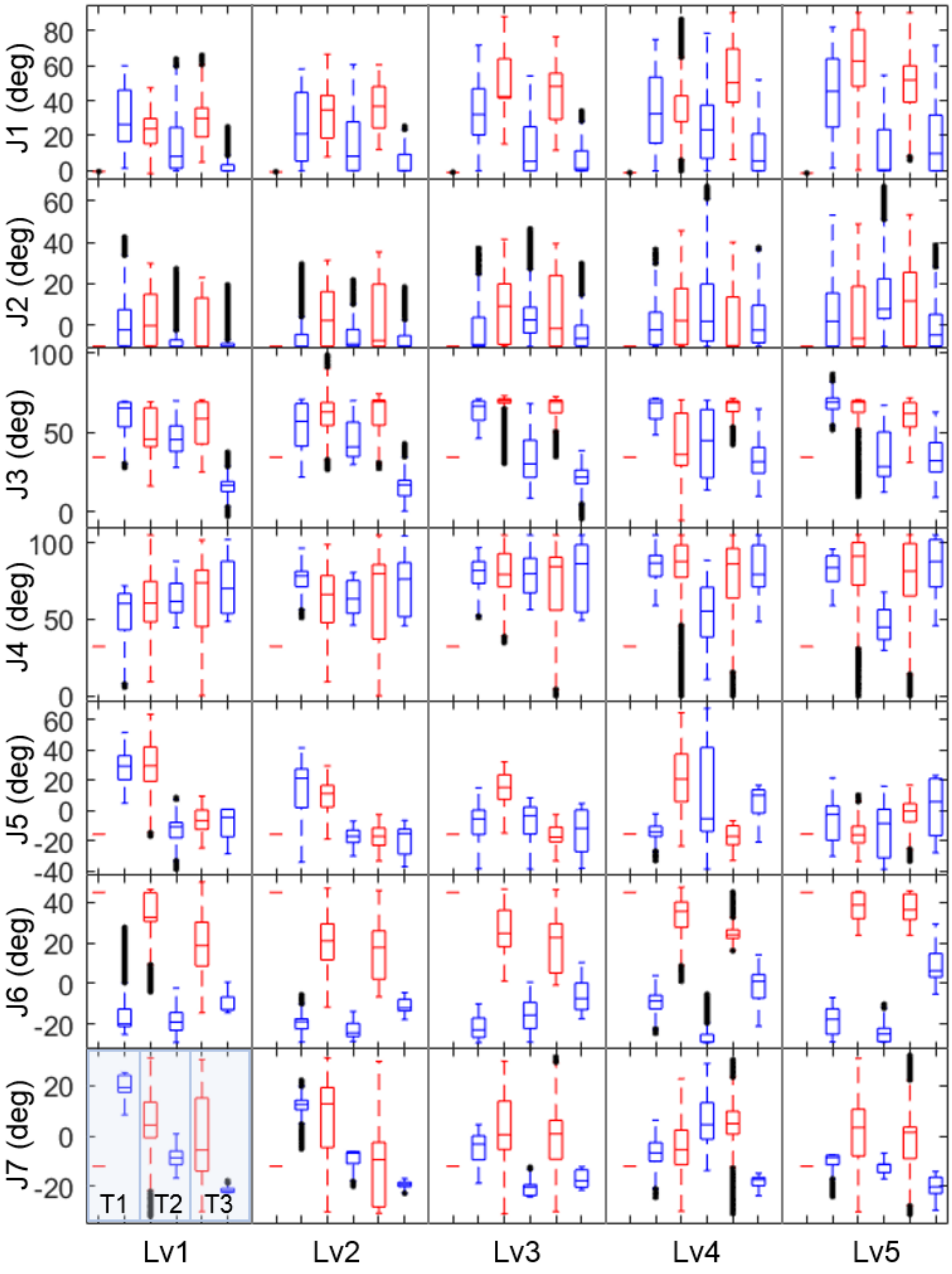

Figure 7.4: Individual joint range of motion (ROM) distribution ('J·'). For each level ('Lv·'), six (6) boxplots represent three (3) tasks ('T·'): unaffected arm (Task 1, null - no movement), affected arm (Task 1), unaffected and affected arm (Task 2), unaffected and affected arm (Task 3). All unaffected ones are colored in red and affected are in blue.

7.6.1.2 Reachable task space

Compared with single arm movement, dual-arm manipulation has a slightly reduced reachable workspace. As part of the validation test, the subject confirmed the receipt of assistance from the exoskeleton. With the external assistance, even in dual-arm task mode the subject could reach more targets which need coordinated shoulder flexion and elbow extension. This matches the results found in our previous research using a manipulability model [SHM17]. Another interesting observation (not plotted) is that without additional instructions, the subject tended to rest his right arm and wait for assistance instead of trying to initiate the reach (rest period is not included in time calculation). More experiments should be done to validate the importance of assist-as-needed (AAN).

7.6.1.3 Joint space

For each task and level, the individual joint ROM is plotted in Figure 7.4. The resultant rotation of J1-J3 is equal to that of the anatomical shoulder abduction(+) / adduction(-), shoulder flexion(+) / extension(-), and internal(+) / external(-) rotation; J4-J7 represent elbow flexion(+) / extension(-), forearm pronation(+) / supination(-), wrist extension(+) / flexion(-), radial(+) / ulnar(-) deviation. J8 is temporarily not included in this reach-only study (no grasp). Compared with the unaffected arm, the affected side is found to have more limited ROMs especially in forearm and wrist movements, possibly due to the subject's long-standing spasticity (Figure 7.2(c) provides another view versus time). Besides J4 (elbow flexion/extension), no significant difference in the affected arm due to exoskeleton's assistance is observed. Unaffected arm fluctuation (when held at the target) is reduced when assistance is provided to the affected arm. We conjecture that this is due to regained attention. In future investigation, more assistive protocols (even for unaffected arm) would be added to the system for quantitative comparison, e.g., using the exoskeleton to freeze the unaffected arm's posture once it touches the target.

7.6.2 Physical human-robot interaction

7.6.2.1 Interaction maps

In many cases of human movement description and understanding, researchers analyze time-variant quantities like interaction forces with respect to time. Due to the existence of multiple sensors and links in contact with human arm, and in order to better depict the possible stroke-induced motion symptoms, a series of maps are visualized - for the trajectory of each sensor in task space, the corresponding temporal order, sensor force, torque, force- and torque-induced power are incorporated with colors to show the pHRI intensity (Figure 7.5).

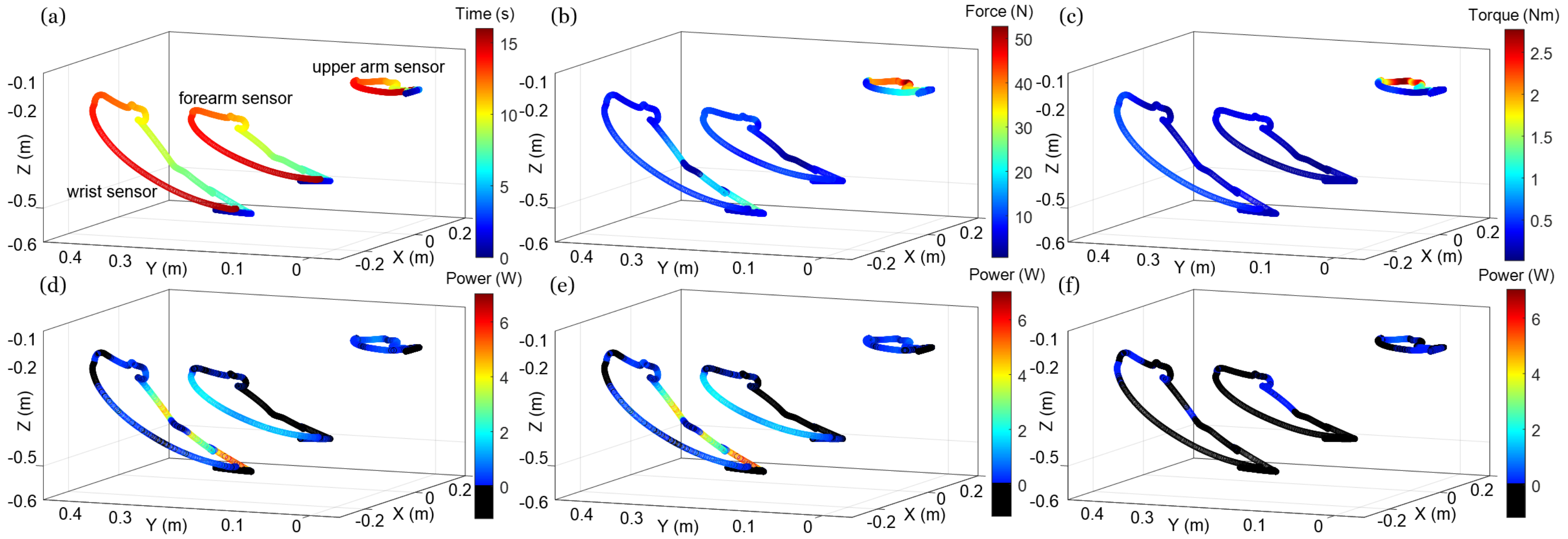

Figure 7.5: Interaction maps of the affected (right) arm (movement trajectory in Figure 7.2(a), Task 3-Level 1-Target 2, 20-36s) incorporated with colored information including: (a) temporal sequence; (b) interaction force ($\sqrt{f_x^2+f_y^2+f_z^2}$); (c) interaction torque ($\sqrt{\tau_x^2+\tau_y^2+\tau_z^2}$); (d) interaction power $p = p_f + p_\tau$; (e) force-induced interaction power p_f; (f) torque-induced interaction power p_τ. Note that negative interaction power is shown in black.

7.6.2.2 Forces and torques

High interaction forces and torques are observed in the upper arm sensor during reaching out movement (Figure 7.5(b) and 7.5(c)). The average forces and torques illustrated in Figure 7.6(a) and 7.6(b) indicate that the forearm sensor is less activated compared with the other two sensors, for both unaffected and affected arm. This is possibly due to the null contact when the elbow is flexed and shoulder flexes to reach out. This *preference* of anatomical part usage suggests a dynamic change of hyper gains $\alpha_{j,s}$ based on user's arm configuration may be needed.

7.6.2.3 Power exchange

Visualized in Figure 7.5(d-f), the interaction power consumed on each sensor includes force- and torque-induced (dominant) components, detailed calculation of which is provided in the Appendix. Since the admittance controller EXO-UL8 uses has, theoretically, a positive power exchange, the negative power (black) observed in part of Figure 7.5(a) trajectory indicates the exoskeleton links still have some inertia that needs to be compensated. We will fix this before further clinical trials. Note that the energy exchange (integral of power with respect to time) at the sensors is not the total energy consumed by the subject (e.g., isometric muscle contraction consumes energy as well). It is thus not plotted.

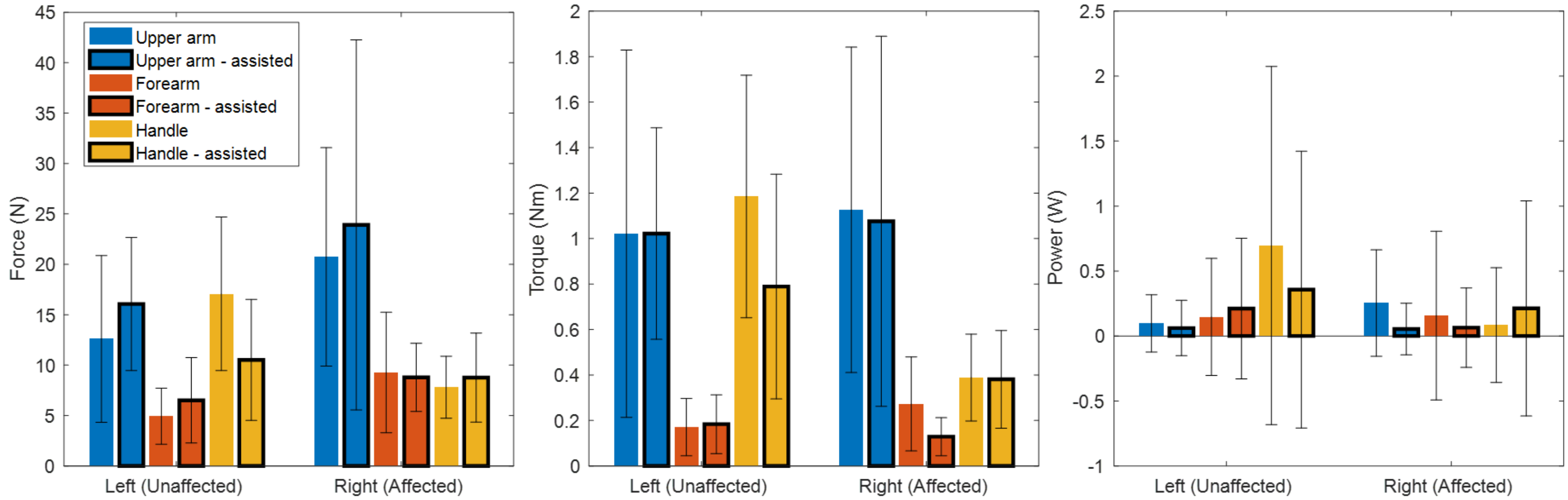

Figure 7.6: Comparison of sensors on both arms, without (Task 2-Level 1) and with (Task 3-Level 1) assistance from the exoskeleton: (a) interaction force magnitude (mean ± std), (b) interaction force magnitude (mean ± std), (c) power p (mean ± std). Targets are the same since levels are the same.

7.7 Conclusion & Future Plan

This pilot study discusses the mechanical and control of EXO-UL8, a dual-arm exoskeleton system for upper limb post-stroke rehabilitation. The device's functionality in facilitating single and dual-arm movement based on a chronic stroke patient's pHRI was validated while analyzing quantitative data such as task completion time, reachable workspace, joint ROMs, along with visualization of spacial interaction maps. Due to the force/torque distribution, the hyper gains αs may be further determined in dynamic movements, instead of being statically tuned. The proposed methodology will be further assessed with a larger pool of chronic post-stroke patients who will be recruited in future investigations.

7.8 Appendix: Calculation of Power Exchange

For readers' reference, the calculation of power exchange on distributed sensors $p_s, s \in \{u, f, w\}$ is provided below. The ss in sub- and superscripts have different meanings, e.g., ${}^{s}\mathbf{v}_s$ is the linear velocity of sensor s in its local coordinate system, while ${}^{0}\mathbf{v}_s$ represents that in the global coordinate system which is fixed to the shoulder center. First, find the instantaneous homogeneous transformation matrix at time t:

$${}^{0}_{s}T(t+\delta t)_{(4\times4)} = {}^{0}_{s}T(t)_{(4\times4)}\,{}^{t}_{t+\delta t}T_{(4\times4)} \tag{7.4}$$

$${}^{t}_{t+\delta t}T_{(4\times4)} = {}^{s}_{0}T(t)_{(4\times4)}\,{}^{0}_{s}T(t+\delta t)_{(4\times4)} \tag{7.5}$$

$${}^{t}_{t+\delta t}T_{(4\times4)} = \begin{bmatrix} {}^{t}_{t+\delta t}R_{(3\times3)} & {}^{t}_{t+\delta t}\mathbf{P}_{(3\times1)} \\ \mathbf{0}_{(3\times1)} & 1 \end{bmatrix} \tag{7.6}$$

The local linear and angular velocities are calculated:

$${}^{s}\mathbf{v}_s(t) = \lim_{\delta t\to 0} \frac{{}^{t}_{t+\delta t}\mathbf{P}_{(3\times1)}}{\delta t} \tag{7.7}$$

$$\begin{bmatrix} 0 & -{}^{s}\omega_{s,z} & {}^{s}\omega_{s,y} \\ {}^{s}\omega_{s,z} & 0 & -{}^{s}\omega_{s,x} \\ -{}^{s}\omega_{s,y} & {}^{s}\omega_{s,x} & 0 \end{bmatrix} = \lim_{\delta t \to 0} \frac{{}^{t}_{t+\delta t}R_{(3\times 3)}}{\delta t} \tag{7.8}$$

$${}^{s}\boldsymbol{\omega}_s(t) = [{}^{s}\omega_{s,x}, {}^{s}\omega_{s,y}, {}^{s}\omega_{s,z}]^T \tag{7.9}$$

Power exchange p_s (positive means energy flows from human arm to sensor) on each sensor s consists of force- and torque-induced components calculated locally:

$$p_{s,f} = \mathbf{f}^T({}^{s}\mathbf{v}_s) = [f_x, f_y, f_z][{}^{s}v_{s,x}, {}^{s}v_{s,y}, {}^{s}v_{s,z}]^T \tag{7.10}$$

$$p_{s,\tau} = \boldsymbol{\tau}^T({}^{s}\boldsymbol{\omega}_s) = [\tau_x, \tau_y, \tau_z][{}^{s}\omega_{s,x}, {}^{s}\omega_{s,y}, {}^{s}\omega_{s,z}]^T \tag{7.11}$$

$$p_s = p_{s,f} + p_{s,\tau} \tag{7.12}$$

CHAPTER 8

Conclusions

Using a multi-joint dual-arm/hand exoskeleton in post-stroke rehabilitation training is essentially challenging, due to the human-in-the-loop fact. Traditionally, part of this interdisciplinary topic has been empirical rather than quantitative. Having observed these, I mainly made contributions to the field in the following aspects during the years of my Ph.D. research:

(1) I first designed and developed a series of virtual reality games that could be used for interactive post-stroke rehabilitation training, the virtual reality environment, together with the exoskeleton robot, also provides a quantitative platform for human performance data collection.

(2) To provide better compliance control, my colleagues and I proposed and implemented two admittance controllers, based on the work done by previous research group alumni. Both the hyper parameter-based and Kalman Filter-based admittance controllers have good performance, and the latter is more promising in future adaptation.

(3) To provide better assist-as-needed control, I worked out a redundant version of a modified dynamic manipulability ellipsoid model to propose an Arm Postural Stability Index (APSI) to quantify the heterogeneity of the 3D Cartesian workspace. The theoretical model could be used to teach the exoskeleton where and when to provide assistance, and to guide the virtual reality where to add new minimal challenges to stroke patients. To the best of my knowledge, it is for the first time that human arm redundancy resolution was investigated with arm gravity considered.

(4) For the first time, I have done a pilot study on asymmetric dual-arm training using the exoskeleton system on one post-stroke patient, the exoskeleton on the healthy side could trigger assistance for that on the affected side, and validates that the current exoskeleton is eligible for asymmetric dual-arm training.

(5) My colleagues and I are proposing a dual-arm training framework (including classification of movements/assistance could be provided by exoskeleton, safety/reliability analysis, virtual reality games population). This is still an on-going research work.

Although the scope might still be limited, I hope that my research has brought inspirations and shed some lights to other researchers' work. I wish to see more stroke patients using our exoskeleton system and help make it available soon in rehabilitation centers.

REFERENCES

[AD13] Federico Augugliaro and Raffaello D'Andrea. "Admittance control for physical human-quadrocopter interaction." In *2013 Eur. Control Conf.*, pp. 1805–1810. IEEE, jul 2013.

[BAP13] Nancy N. Byl, Gary M. Abrams, Erica Pitsch, Irina Fedulow, Hyunchul Kim, Matt Simkins, Srikantan Nagarajan, and Jacob Rosen. "Chronic stroke survivors achieve comparable outcomes following virtual task specific repetitive training guided by a wearable robotic orthosis (UL-EXO7) and actual task specific repetitive training guided by a physical therapist." *J. Hand Ther.*, **26**(4):343–352, 2013.

[BBC17] Emelia J. Benjamin, Michael J. Blaha, Stephanie E. Chiuve, Mary Cushman, Sandeep R. Das, Rajat Deo, Sarah D. de Ferranti, James Floyd, Myriam Fornage, Cathleen Gillespie, Carmen R. Isasi, Monik C. Jiménez, Lori Chaffin Jordan, Suzanne E. Judd, Daniel Lackland, Judith H. Lichtman, Lynda Lisabeth, Simin Liu, Chris T. Longenecker, Rachel H. Mackey, Kunihiro Matsushita, Dariush Mozaffarian, Michael E. Mussolino, Khurram Nasir, Robert W. Neumar, Latha Palaniappan, Dilip K. Pandey, Ravi R. Thiagarajan, Mathew J. Reeves, Matthew Ritchey, Carlos J. Rodriguez, Gregory A. Roth, Wayne D. Rosamond, Comilla Sasson, Amytis Towfighi, Connie W. Tsao, Melanie B. Turner, Salim S. Virani, Jenifer H. Voeks, Joshua Z. Willey, John T. Wilkins, Jason HY. Wu, Heather M. Alger, Sally S. Wong, and Paul Muntner. "Heart Disease and Stroke Statistics-2017 Update: A Report From the American Heart Association." *Circulation*, **135**(10):e146–e603, mar 2017.

[BBS07] Stephen J. Ball, Ian E. Brown, and Stephen H. Scott. "MEDARM: a rehabilitation robot with 5DOF at the shoulder complex." In *2007 IEEE/ASME Int. Conf. Adv. Intell. mechatronics*, pp. 1–6. IEEE, sep 2007.

[BFP14] Amy A. Blank, James A. French, Ali Utku Pehlivan, and Marcia K. O'Malley. "Current Trends in Robot-Assisted Upper-Limb Stroke Rehabilitation: Promoting Patient Engagement in Therapy." *Curr. Phys. Med. Rehabil. Reports*, **2**(3):184–195, sep 2014.

[BLS00] Charles G. Burgar, Peter S. Lum, Peggy C. Shor, and H. F. Machiel Van der Loos. "Development of robots for rehabilitation therapy: the Palo Alto VA/Stanford experience." *J. Rehabil. Res. Dev.*, **37**(6):663–673, 2000.

[BWP08] Sivakumar Balasubramanian, H. Ruihua Wei, Mike Perez, Ben Shepard, Edward Koeneman, James Koeneman, Jiping He, Ruihua Wei, Mike Perez, Ben Shepard, Edward Koeneman, James Koeneman, and Jiping He. "RUPERT: An exoskeleton robot for assisting rehabilitation of arm functions." In *2008 Virtual Rehabil.*, pp. 163–167. IEEE, aug 2008.

[CAD10] Angela M. Coderre, Amr Abou Zeid, Sean P. Dukelow, Melanie J. Demmer, Kimberly D. Moore, Mary Jo Demers, Helen Bretzke, Troy M. Herter, Janice I. Glasgow, Kathleen E. Norman, Stephen D. Bagg, and Stephen H. Scott. “Assessment of upper-limb sensorimotor function of subacute stroke patients using visually guided reaching.” *Neurorehabil. Neural Repair*, **24**(6):528–541, 2010.

[CBB03] F. Conti, F. Barbagli, R. Balaniuk, M. Halg, C. Lu, D. Morris, L. Sentis, J. Warren, O. Khatib, and K. Salisbury. “The CHAI libraries.” In *Proc. Eurohaptics 2003*, pp. 496–500, 2003.

[CCL09] James H. Cauraugh, Stephen A. Coombes, Neha Lodha, Sagar K. Naik, and Jeffery J. Summers. “Upper extremity improvements in chronic stroke: Coupled bilateral load training.” *Restor. Neurol. Neurosci.*, **27**(1):17–25, 2009.

[CCS92] P. Chiacchio, S. Chiaverini, L. Sciavicco, and B. Siciliano. “Influence of Gravity on the Manipulability Ellipsoid for Robot Arms.” *J. Dyn. Syst. Meas. Control*, **114**(4):723–727, 1992.

[Chi88] Stephen L Chiu. “Task Compatibility of Manipulator Postures.” *Int. J. Rob. Res.*, **7**(5):13–21, 1988.

[Chi00] Pasquale Chiacchio. “A new dynamic manipulability ellipsoid for redundant manipulators.” *Robotica*, **18**(04):381–387, 2000.

[CJM10] Peter R. Culmer, Andrew E. Jackson, Sophie Makower, Robert Richardson, J. Alastair Cozens, Martin C. Levesley, and Bipin B. Bhakta. “A control strategy for upper limb robotic rehabilitation with a dual robot system.” *IEEE/ASME Trans. Mechatronics*, **15**(4):575–585, 2010.

[CKV05] Steven K. Charles, Hermano I. Krebs, Bruce T. Volpe, Daniel Lynch, and Neville Hogan. “Wrist rehabilitation following stroke: Initial clinical results.” In *Proc. 2005 IEEE 9th Int. Conf. Rehabil. Robot.*, pp. 13–16. IEEE, 2005.

[CRP05] Ettore Cavallaro, Jacob Rosen, J.C. Perry, Stephen Burns, and Blake Hannaford. “Hill-Based Model as a Myoprocessor for a Neural Controlled Powered Exoskeleton Arm - Parameters Optimization.” In *Proc. 2005 IEEE Int. Conf. Robot. Autom.*, pp. 4514–4519. IEEE, 2005.

[CRP06] Ettore E. Cavallaro, Jacob Rosen, Joel C. Perry, and Stephen Burns. “Real-time myoprocessors for a neural controlled powered exoskeleton arm.” *IEEE Trans. Biomed. Eng.*, **53**(11):2387–2396, 2006.

[CS05] James H. Cauraugh and Jeffery J. Summers. “Neural plasticity and bilateral movements: a rehabilitation approach for chronic stroke.” *Prog. Neurobiol.*, **75**(5):309–320, 2005.

[CTR09] Craig Carignan, Jonathan Tang, and Stephen Roderick. “Development of an exoskeleton haptic interface for virtual task training.” In *2009 IEEE/RSJ Int. Conf. Intell. Robot. Syst.*, pp. 3697–3702, 2009.

[Dob05] Bruce H. Dobkin. “Rehabilitation after Stroke.” *N. Engl. J. Med.*, **352**(16):1677–1684, 2005.

[End15] Hiroshi Endo. “Application of robotic manipulability indices to evaluate thumb performance during smartphone touch operations.” *Ergonomics*, **58**(5):736–747, 2015.

[ESM09] Michael D Ellis, Theresa M Sukal-moulton, Student Member, and Julius P A Dewald. “Impairment-Based 3-D Robotic Intervention Improves Upper Extremity Work Area in Chronic Stroke: Targeting Abnormal Joint Torque Coupling With Progressive Shoulder Abduction Loading.” *IEEE Trans. Robot.*, **25**(3):549–555, 2009.

[FBB08] A Frisoli, M Bergamasco, L Borelli, A Montagner, G Greco, C Procopio, M Carboncini, and B Rossi. “Robotic assisted rehabilitation in virtual reality with the L-EXOS.” In *Proc. 7th Int. Conf. Disabil. Virtual Real. Assoc. Technol. with Artabilitation (ICDVRAT 2008).*, pp. 253–260, 2008.

[FDS19] Peter Walker Ferguson, Brando Dimapasoc, Yang Shen, and Jacob Rosen. “Design of a Hand Exoskeleton for Use with Upper Limb Exoskeletons.” In Maria Chiara Carrozza, Silvestro Micera, and José L. Pons, editors, *Wearable Robot. Challenges Trends*, Biosystems & Biorobotics, pp. 276–280. Springer International Publishing, Cham, 2019.

[FGR98] Roberto Finotello, Tiberio Grasso, Giorgio Rossi, and A. Terribile. “Computation of kinetostatic performances of robot manipulators with polytopes.” *Proc. 1998 IEEE Int. Conf. Robot. Autom.*, pp. 3241–3246, 1998.

[FRM05] A. Frisoli, F. Rocchi, S. Marcheschi, A. Dettori, F. Salsedo, and M. Bergamasco. “A new force-feedback arm exoskeleton for haptic interaction in virtual environments.” *Proc. - 1st Jt. Eurohaptics Conf. Symp. Haptic Interfaces Virtual Environ. Teleoperator Syst. World Haptics Conf. WHC 2005*, pp. 195–201, 2005.

[GFM08] P. Garrec, J. P. Friconneau, Y. Méasson, and Y. Perrot. “ABLE, an innovative transparent exoskeleton for the upper-limb.” *2008 IEEE/RSJ Int. Conf. Intell. Robot. Syst. IROS*, pp. 1483–1488, 2008.

[GGJ15] Malin Gunasekara, Ruwan Gopura, and Sanath Jayawardena. “6-REXOS: Upper limb exoskeleton robot with improved pHRI.” *Int. J. Adv. Robot. Syst.*, **12**, 2015.

[GKL09] R. A. R. C. Gopura, Kazuo Kiguchi, and Yang Li. “SUEFUL-7: A 7DOF upper-limb exoskeleton robot with muscle-model-oriented EMG-based control.” In *Intell. Robot. Syst. 2009. IROS 2009. IEEE/RSJ Int. Conf.*, pp. 1126–1131, 2009.

[GOP08] A. Gupta, M. K. O’Malley, V. Patoglu, and C. Burgar. “Design, Control and Performance of RiceWrist: A Force Feedback Wrist Exoskeleton for Rehabilitation and Training.” *Int. J. Rob. Res.*, **27**(2):233–251, 2008.

[GWK09] Keith E Gordon, Ming Wu, Jennifer H Kahn, Yasin Y Dhaher, and Brian D Schmit. “Ankle load modulates hip kinetics and EMG during human locomotion.” *J. Neurophysiol.*, **101**(4):2062–2076, 2009.

[HHA98] K. Homma, S. Hashino, and T. Arai. "An upper limb motion assist system: experiments with arm models." *Proceedings. 1998 IEEE/RSJ Int. Conf. Intell. Robot. Syst. Innov. Theory, Pract. Appl. (Cat. No.98CH36190)*, **2**(October):758–763, 1998.

[HHS95] Patrick Haggard, Karen Hutchinson, and John Stein. "Patterns of coordinated multi-joint movement." *Exp. Brain Res.*, **107**(2):254–266, dec 1995.

[HHX15] Jian Huang, Weiguang Huo, Wenxia Xu, Samer Mohammed, and Yacine Amirat. "Control of Upper-Limb Power-Assist Exoskeleton Using a Human-Robot Interface Based on Motion Intention Recognition." *IEEE Trans. Autom. Sci. Eng.*, **12**(4):1257–1270, 2015.

[HKC92] N Hogan, H I Krebs, J Charnnarong, P Srikrishna, and A Sharon. "MIT - MANUS : A Workstation for Manual Therapy and Training." In *Proc. IEEE Int. Work. Robot Hum. Commun.*, pp. 161–165, 1992.

[HLD11] John Hu, Yi Je Lim, Ye Ding, Daniel Paluska, Aaron Solochek, David Laffery, Paolo Bonato, and Ronald Marchessault. "An advanced rehabilitation robotic system for augmenting healthcare." In *Int. Conf. IEEE Eng. Med. Biol. Soc. EMBS*, pp. 2073–2076, 2011.

[HRG16] Clint Hansen, Nasser Rezzoug, Philippe Gorce, and Brice Isableu. "Differences in the control of unconstrained three-dimensional arm motions of the dominant and the nondominant arm." *J. Appl. Biomech.*, **32**:311–315, 2016.

[HSK03] Stefan Hesse, Gotthard Schulte-Tigges, Matthias Konrad, Anita Bardeleben, and Cordula Werner. "Robot-assisted arm trainer for the passive and active practice of bilateral forearm and wrist movements in hemiparetic subjects." *Arch. Phys. Med. Rehabil.*, **84**(6):915–920, 2003.

[HYL17] Bo Huang, Zhifeng Ye, Zhijun Li, Wang Yuan, and Chenguang Yang. "Admittance control of a robotic exoskeleton for physical human robot interaction." In *2017 2nd Int. Conf. Adv. Robot. Mechatronics*, pp. 245–250, Hefei, 2017.

[JCP01] G R Johnson, D A Carus, G Parrini, SScattareggia Marchese, and R Valeggi. "The design of a five-degree-of-freedom powered orthosis for the upper limb." *Proc. Inst. Mech. Eng. Part H J. Eng. Med.*, **215**(3):275–284, mar 2001.

[JGR12] Julien Jacquier-Bret, Philippe Gorce, and Nasser Rezzoug. "The manipulability: a new index for quantifying movement capacities of upper extremity." *Ergonomics*, **55**(1):69–77, 2012.

[JM12] Nathanaël Jarrassé and Guillaume Morel. "Connecting a human limb to an exoskeleton." *IEEE Trans. Robot.*, **28**(3):697–709, 2012.

[JPC14] Nathanaël Jarrassé, Tommaso Proietti, Vincent Crocher, Johanna Robertson, Anis Sahbani, Guillaume Morel, and Agnès Roby-Brami. "Robotic exoskeletons: a perspective for the rehabilitation of arm coordination in stroke patients." *Front. Hum. Neurosci.*, **8**(December):947, dec 2014.

[Kim12] Hyunchul Kim. *Systematic Control and Application for 7 DOF Upper-Limb Exoskeleton.* PhD thesis, University of California, Santa Cruz, 2012.

[KMF13] Hyunchul Kim, Levi Makaio Miller, Irina Fedulow, Matt Simkins, Gary M. Abrams, Nancy Byl, and Jacob Rosen. "Kinematic Data Analysis for Post-Stroke Patients Following Bilateral Versus Unilateral Rehabilitation With an Upper LimbWearable Robotic System." *IEEE Trans. NEURAL Syst. Rehabil. Eng.*, **21**(2):153–164, 2013.

[KPG13] Atilla Kilicarslan, Saurabh Prasad, Robert G. Grossman, and Jose L. Contreras-Vidal. "High accuracy decoding of user intentions using EEG to control a lower-body exoskeleton." In *2013 35th Annu. Int. Conf. IEEE Eng. Med. Biol. Soc.*, pp. 5606–5609. IEEE, jul 2013.

[KSA08] J. Klein, S. J. Spencer, J. Allington, K. Minakata, E. T. Wolbrecht, R. Smith, J. E. Bobrow, and D. J. Reinkensmeyer. "Biomimetic orthosis for the neurorehabilitation of the elbow and shoulder (BONES)." In *Biomed. Robot. Biomechatronics, 2008. BioRob 2008. 2nd IEEE/RAS-EMBS Int. Conf.*, pp. 535–541, 2008.

[KTC06] S. Kousidou, N. Tsagarakis, D. G. Caldwell, and C. Smith. "Assistive exoskeleton for task based physiotherapy in 3-dimensional space." *Proc. First IEEE/RAS-EMBS Int. Conf. Biomed. Robot. Biomechatronics, 2006, BioRob 2006*, **2006**:266–271, 2006.

[KWS16] Elsa Andrea Kirchner, Niels Will, Marc Simnofske, Luis Manuel Vaca Benitez, Bertold Bongardt, Mario Michael Krell, Shivesh Kumar, Martin Mallwitz, Anett Seeland, Marc Tabie, Hendrik Wöhrle, Mehmed Yüksel, Anke Heß, Rüdiger Buschfort, and Frank Kirchner. "Recupera-Reha: Exoskeleton Technology with Integrated Biosignal Analysis for Sensorimotor Rehabilitation." *2. Transdisziplinäre Konf. "Technische Unterstützungssysteme, die die Menschen wirklich wollen". Transdisziplinäre Konf. "Technische Unterstützungssysteme, die die Menschen wirklich wollen", December 12-13, Hamburg, Ger.*, pp. 504–517, 2016.

[LAT03] Rui Loureiro, Farshid Amirabdollahian, Michael Topping, Bart Driessen, and William Harwin. "Upper Limb Robot Mediated Stroke Therapy — GENTLE/s Approach." *Auton. Robots*, **15**(1):35–51, 2003.

[LAV08] P. Letier, M. Avraam, S. Veillerette, M. Horodinca, M. De Bartolomei, A. Schiele, and A. Preumont. "SAM: A 7-DOF portable arm exoskeleton with local joint control." In *2008 IEEE/RSJ Int. Conf. Intell. Robot. Syst.*, pp. 3501–3506, 2008.

[LBK11] Peter Langhorne, Julie Bernhardt, and Gert Kwakkel. "Stroke rehabilitation." *Lancet*, **377**:1693–1702, 2011.

[LKS14] Joan Lobo-Prat, Peter N. Kooren, Arno Ha Stienen, Just L. Herder, Bart F.J.M. Koopman, and Peter H. Veltink. "Non-invasive control interfaces for intention detection in active movement-assistive devices." *J. Neuroeng. Rehabil.*, **11**(1), 2014.

[LL03] R.Q. Van Der Linde and P. Lammertse. "HapticMaster – a generic force controlled robot for human interaction." *Ind. Robot An Int. J.*, **30**(6):515–524, 2003.

[LWS14] Zhijun Li, Baocheng Wang, Fuchun Sun, Chenguang Yang, Qing Xie, and Weidong Zhang. "sEMG-Based Joint Force Control for an Upper-Limb Power-Assist Exoskeleton Robot." *IEEE J. Biomed. Heal. Informatics*, **18**(3):1043–1050, 2014.

[LWZ90] Philip Lee, Susanna Wei, Jianmin Zhao, and Norman I. Badler. "Strength guided motion." *ACM SIGGRAPH Comput. Graph.*, **24**(4):253–262, 1990.

[LX12] Ho Shing Lo and Sheng Quan Xie. "Exoskeleton robots for upper-limb rehabilitation: State of the art and future prospects." *Med. Eng. Phys.*, **34**(3):261–268, 2012.

[MB13] Soumya Kanti Manna and Subhasis Bhaumik. "A Bioinspired 10 DOF Wearable Powered Arm Exoskeleton for Rehabilitation." *J. Robot.*, **2013**:1–15, 2013.

[McM10] Don McMonagle. "Robotic Hands and Arms Developed by Raytheon SARCOS and SARCOS (Sterling)." Technical report, Raytheon Company, 2010.

[MFA05] Simone Marcheschi, Antonio Frisoli, Carlo Alberto Avizzano, and Massimo Bergamasco. "A Method for Modeling and Control Complex Tendon Transmissions in Haptic Interfaces." In *Proc. 2005 IEEE Int. Conf. Robot. Autom.*, pp. 1773–1778, Barcelona, 2005. IEEE.

[Mil06] Levi Makaio Miller. *Gravity Compensation for a 7 Degree of Freedom Powered Upper Limb Exoskeleton*. Master's thesis, University of Washington, 2006.

[Mil12] Levi Makaio Miller. *Comprehensive Control Strategies for a Seven Degree of Freedom Upper Limb Exoskeleton Targeting Stroke Rehabilitation*. PhD thesis, University of Washington, 2012.

[MKB13] Soumya Kanti Manna, Devendra Kumar, and Subhasis Bhaumik. "Design & Analysis of a Portable Exoskeleton Structure for Rehabilitation – A Mechatronic Approach." In *Proc. IEEE Int. Conf. Res. Dev. Prospect. Eng. Technol.*, pp. 214–220, 2013.

[MMS05] Michael Mistry, Peyman Mohajerian, and Stefan Schaal. "An exoskeleton robot for human arm movement study." In *Proc. 2005 IEEE/RSJ Int. Conf. Intell. Robot. Syst.*, pp. 4071–4076, 2005.

[MSC13] Marie-Hélène Milot, Steven J Spencer, Vicky Chan, James P Allington, Julius Klein, Cathy Chou, James E Bobrow, Steven C Cramer, and David J Reinkensmeyer. "A crossover pilot study evaluating the functional outcomes of two different types of robotic movement training in chronic stroke survivors using the arm exoskeleton BONES." *J. Neuroeng. Rehabil.*, **10**:112, 2013.

[MVA15] B. Morinière, A. Verney, N. Abroug, P. Garrec, and Y. Perrot. "EMY: a dual arm exoskeleton dedicated to the evaluation of Brain Machine Interface in clinical trials." In *2015 IEEE/RSJ Int. Conf. Intell. Robot. Syst.*, pp. 5333–5338, Hamburg, 2015.

[MWT15] Martin Mallwitz, Niels Will, Johannes Teiwes, and Elsa Andrea Kirchner. "the Capio Active Upper Body Exoskeleton and Its Application for Teleoperation." In *Proc. 13th Symp. Adv. Sp. Technol. Robot. Autom. ESA/Estec Symp. Adv. Sp. Technol. Robot. Autom.*, pp. 1–8. ESA, 2015.

[NGR09] Tobias Nef, Marco Guidali, and Robert Riener. “ARMin III - arm therapy exoskeleton with an ergonomic shoulder actuation.” *Appl. Bionics Biomech.*, **6**(2):127–142, 2009.

[NMK07] Tobias Nef, Matjaz Mihelj, Gabriela Kiefer, Christina Perndl, Roland Müller, and Robert Riener. “ARMin - Exoskeleton for arm therapy in stroke patients.” In *Proc. 2007 IEEE 10th Int. Conf. Rehabil. Robot.*, pp. 68–74, 2007.

[NTU14] Tomoyuki Noda, Tatsuya Teramae, Barkan Ugurlu, and Jun Morimoto. “Development of an upper limb exoskeleton powered via pneumatic electric hybrid actuators with bowden cable.” In *Intell. Robot. Syst. (IROS 2014), 2014 IEEE/RSJ Int. Conf.*, pp. 3573–3578, 2014.

[PCR16] Tommaso Proietti, Vincent Crocher, Agnes Roby-Brami, and Nathanael Jarrasse. “Upper-Limb Robotic Exoskeletons for Neurorehabilitation: A Review on Control Strategies.” *IEEE Rev. Biomed. Eng.*, **9**:4–14, 2016.

[PEA83] Stanley Plagenhoef, F. Gaynor Evans, and Thomas Abdelnour. “Anatomical Data for Analyzing Human Motion.” *Res. Q. Exerc. Sport*, **54**(2):169–178, 1983.

[Per06] Joel C. Perry. *Design and development of a 7 degree of freedom powered exoskeleton for the upper limb.* PhD thesis, University of Washington, 2006.

[PLB04] Carolynn Patten, Jan Lexell, and Heather E. Brown. “Weakness and strength training in persons with poststroke hemiplegia: Rationale, method, and efficacy.” *J. Rehabil. Res. Dev.*, **41**(3A):293–312, 2004.

[PNP16] Luka Peternel, Tomoyuki Noda, Tadej Petrič, Aleš Ude, Jun Morimoto, and Jan Babič. “Adaptive Control of Exoskeleton Robots for Periodic Assistive Behaviours Based on EMG Feedback Minimisation.” *PLoS One*, **11**(2):e0148942, feb 2016.

[PPR09] Joel C. Perry, Janet M. Powell, and Jacob Rosen. “Isotropy of an upper limb exoskeleton and the kinematics and dynamics of the human arm.” *Appl. Bionics Biomech.*, **6**(2):175–191, 2009.

[PR06] Joel C. Perry and Jacob Rosen. “Design of a 7 degree-of-freedom upper-limb powered exoskeleton.” In *Biomed. Robot. Biomechatronics, 2006. BioRob 2006. First IEEE/RAS-EMBS Int. Conf.*, pp. 805–810, Pisa, Italy, 2006.

[PR08] Joel C. Perry and Jacob Rosen. “Case Study: An Upper Limb Powered Exoskeleton.” In José L. Pons, editor, *Wearable Robot. biomechatronic exoskeletons*. John Wiley & Sons, 2008.

[PRB07] Joel C. Perry, Jacob Rosen, and Stephen Burns. “Upper-limb powered exoskeleton design.” *IEEE/ASME Trans. Mechatronics*, **12**(4):408–417, 2007.

[RBC16] David J Reinkensmeyer, Etienne Burdet, Maura Casadio, John W Krakauer, Gert Kwakkel, Catherine E Lang, Stephan P Swinnen, Nick S Ward, and Nicolas Schweighofer. “Computational neurorehabilitation: modeling plasticity and learning to predict recovery.” *J. Neuroeng. Rehabil.*, **13**(1):42, 2016.

[RBF01] Jacob Rosen, Moshe Brand, Moshe B. Fuchs, and Mircea Arcan. “A myosignal-based powered exoskeleton system.” *IEEE Trans. Syst. Man, Cybern. Part A Syst. Humans*, **31**(3):210–222, 2001.

[RFA99] Jacob Rosen, Moshe B. Fuchs, and Mircea Arcan. “Performances of hill-type and neural network muscle models-toward a myosignal-based exoskeleton.” *Comput. Biomed. Res.*, **32**(5):415–439, 1999.

[RGM05] Giulio Rosati, Paolo Gallina, Stefano Masiero, and Aldo Rossi. “Design of a new 5 d.o.f. wire-based robot for rehabilitation.” In *Proc. 2005 IEEE 9th Int. Conf. Rehabil. Robot.*, pp. 430–433, 2005.

[Ros97] Jacob Rosen. *Natural Integration of a Human Arm / Exoskeleton System*. PhD thesis, Tel-Aviv University, 1997.

[ROS15] Mohammad H Rahman, Cristobal Ochoa-Luna, Maarouf Saad, and Philippe Archambault. “EMG based control of a robotic exoskeleton for shoulder and elbow motion assist.” *J. Autom. Control Eng.*, **3**(4):270–276, 2015.

[RP07] Jacob Rosen and Joel C. Perry. “Upper Limb Powered Exoskeleton.” *Int. J. Humanoid Robot.*, **04**(03):529–548, 2007.

[RPM05] Jacob Rosen, J.C. Perry, Nathan Manning, Stephen Burns, and Blake Hannaford. “The human arm kinematics and dynamics during daily activities - toward a 7 DOF upper limb powered exoskeleton.” In *ICAR ’05. Proceedings., 12th Int. Conf. Adv. Robot. 2005.*, pp. 532–539. IEEE, 2005.

[RPZ09] Yupeng Ren, Hyung-Soon Soon Park, and Li-Qun Qun Zhang. “Developing a whole-arm exoskeleton robot with hand opening and closing mechanism for upper limb stroke rehabilitation.” In *2009 IEEE Int. Conf. Rehabil. Robot.*, pp. 761–765, 2009.

[RSD14] Joao Rebelo, Thomas Sednaoui, Emiel Boudewijn Den Exter, Thomas Krueger, and Andre Schiele. “Bilateral robot teleoperation: A wearable arm exoskeleton featuring an intuitive user interface.” *IEEE Robot. Autom. Mag.*, **21**(4):62–69, 2014.

[RWR16] Ashish Rathore, Matthew Wilcox, Dafne Zuleima Morgado Ramirez, Rui Loureiro, and Tom Carlson. “Quantifying the human-robot interaction forces between a lower limb exoskeleton and healthy users.” In *Eng. Med. Biol. Soc. (EMBC), 2016 IEEE 38th Annu. Int. Conf.*, pp. 586–589, 2016.

[SFM18] Yang Shen, Peter Walker Ferguson, Ji Ma, and Jacob Rosen. “Chapter 4 - Upper Limb Wearable Exoskeleton Systems for Rehabilitation: State of the Art Review and a Case Study of the EXO-UL8 Dual-Arm Exoskeleton System.” In Raymond Kai-Yu Tong, editor, *Wearable Technol. Med. Heal. Care*, pp. 71–90. Academic Press, 2018.

[SHM17] Yang Shen, Brandon Po-Yun Hsiao, Ji Ma, and Jacob Rosen. “Upper limb redundancy resolution under gravitational loading conditions: Arm postural stability index based on dynamic manipulability analysis.” In *2017 IEEE-RAS 17th Int. Conf. Humanoid Robot.*, pp. 332–338. IEEE, nov 2017.

[SIM10] Makoto Sasaki, Takehiro Iwami, Kazuto Miyawaki, Ikuro Sato, Goro Obinata, and Ashish Dutta. "Higher Dimensional Spatial Expression of Upper Limb Manipulation Ability based on Human Joint Torque Characteristics." In *Robot Manip. New Achiev.*, pp. 693–719. IntechOpen, 2010.

[SMD18] Yang Shen, Ji Ma, Bruce Dobkin, and Jacob Rosen. "Asymmetric Dual Arm Approach For Post Stroke Recovery Of Motor Functions Utilizing The EXO-UL8 Exoskeleton System: A Pilot Study." In *2018 40th Annu. Int. Conf. IEEE Eng. Med. Biol. Soc.*, volume 2018, pp. 1701–1707. IEEE, jul 2018.

[SSM19] Yang Shen, Jianwei Sun, Ji Ma, and Jacob Rosen. "Admittance Control Scheme Comparison of EXO-UL8 : A Dual-Arm Exoskeleton Robotic System." In *2019 Int. Conf. Rehabil. Robot.*, pp. 1–7. IEEE, 2019.

[TET12] Emanuel Todorov, Tom Erez, and Yuval Tassa. "MuJoCo: A physics engine for model-based control." In *2012 IEEE/RSJ Int. Conf. Intell. Robot. Syst.*, pp. 5026–5033. IEEE, oct 2012.

[TNY15] Yoshiyuki Tanaka, Kazuo Nishikawa, Naoki Yamada, and Toshio Tsuji. "Analysis of Operational Comfort in Manual Tasks Using Human Force Manipulability Measure." *IEEE Trans. Haptics*, **8**(1):8–19, 2015.

[Val09] Francisco J. Valero-Cuevas. "A Mathematical Approach to the Mechanical Capabilities of Limbs and Fingers." In D. Sternad, editor, *Prog. Mot. Control*, pp. 619–633. Springer US, 2009.

[WBX08] Ruihua Wei, Sivakumar Balasubramanian, Lihong Xu, and Jiping He. "Adaptive Iterative Learning Control design for RUPERT IV." In *Proc. 2nd Bienn. IEEE/RAS-EMBS Int. Conf. Biomed. Robot. Biomechatronics, BioRob 2008*, pp. 647–652, 2008.

[WCR08] Eric T. Wolbrecht, Vicky Chan, David J. Reinkensmeyer, and James E. Bobrow. "Optimizing compliant, model-based robotic assistance to promote neurorehabilitation." *IEEE Trans. Neural Syst. Rehabil. Eng.*, **16**(3):286–297, 2008.

[WPH06] Conor James Walsh, Kenneth Pasch, and Hugh Herr. "An autonomous, underactuated exoskeleton for load-carrying augmentation." In *IEEE Int. Conf. Intell. Robot. Syst.*, pp. 1410–1415, 2006.

[YL12] Yong Yu and Wenyuan Liang. "Design optimization for lower limb assistive mechanism based on Manipulability Inclusive Principle." *Proc. 2012 IEEE Int. Conf. Robot. Biomimetics*, pp. 174–180, 2012.

[Yos84] Tsuneo Yoshikawa. "Analysis and Control of Robot Manipulators with Redundancy." In *Robot. Res. First Int. Symp.*, pp. 735–747. MIT Press, Cambridge, MA, US, 1984.

[Yos85] T. Yoshikawa. "Manipulability and redundancy control of robotic mechanisms." *Proceedings. 1985 IEEE Int. Conf. Robot. Autom.*, **2**:1004–1009, 1985.

[YR10] Wen Yu and Jacob Rosen. “A novel linear PID controller for an upper limb exoskeleton.” In *Proc. IEEE Conf. Decis. Control*, pp. 3548–3553, 2010.

[YR13] Wen Yu and Jacob Rosen. “Neural PID control of robot manipulators with application to an upper limb exoskeleton.” *IEEE Trans. Cybern.*, **43**(2):673–684, 2013.

[YRL11] Wen Yu, Jacob Rosen, and Xiaoou Li. “PID admittance control for an upper limb exoskeleton.” In *2011 Am. Control Conf.*, pp. 1124–1129, 2011.

[ZPR07] Li-Qun Zhang, Hyung-Soon Park, and Yupeng Ren. “Developing an Intelligent Robotic Arm for Stroke Rehabilitation.” In *2007 IEEE 10th Int. Conf. Rehabil. Robot.*, pp. 984–993, 2007.